In-situ removal of iron and manganese from groundwater

Yasmina Ourradi

Master Thesis in Geosciences

Environmental Geosciences

Department of Geosciences

Faculty of Mathematics and Natural Sciences

UNIVERSITY OF OSLO

August 2021

2021

In-situ removal of iron and manganese from groundwater.

Yasmina Ourradi

http://www.duo.uio.no/

Print: Reprosentralen, Universitetet i Oslo

Abstract

Grindalsmoen waterworks is the main water supplier for Elverum town. The waterworks extract water from groundwater and utilize the Vyredox method as in-situ treatment system due to high concentrations of dissolved Fe and Mn in groundwater. The main objectives of this thesis were to determine the Mn adsorption capacities on different Fe-coated sand samples and to investigate the effect of pH on the oxidation of Mn with and without Fe-coated sand.

The initial solid material characterisation through a grain size analysis showed that the collected sediments presented a homogeneous distribution dominated by sand and the mineral composition obtained through an XRD coincided with the Holocene deposits in eastern Norway. The use of SEM confirmed the presence of Fe and Mn coatings on the sand grains.

The chemical characterization of Fe and Mn was based on two selected sand samples: dark-coloured sand (SD) and the light-coloured sand (SL). It was assumed that the SD sample might contain more Fe coating than the SL sample.

The Mn (II) sorption experiments showed that Mn (II) was up to two times more sorbed in the SD samples compared to the SL samples. It was therefore assumed that the presence of more crystalline and non-crystalline forms of Fe in the SD sample affected positively the amount of Mn (II) sorbed during the experiments. The sorption data for both samples (SD and SL) showed a very good fit to the Freundlich sorption isotherm with a better regression coefficient for the SL sample. In general, the Mn sorption capacity was higher on rich Fe-coated sand (SD) compared to less Fe-coated sand (SL).

The oxidation of Mn (II) was noticed to be more important for high pH ranges (8-10) compared to low pH levels (6-7). The rates of Mn (II) oxidation are therefore affected by the pH condition in solution as Mn (II) is oxidized faster at high pH conditions than at low pH levels. The oxidation of Mn (II) fits both a 1^{st} and 2^{nd} order reaction rates with slightly better regression coefficients for the 2^{nd} order reaction rate. The oxidation was observed to be more efficient in the sediment containing more Fe coating (SD sample). The results showed that the oxidation occurred during the first 20 hours of experiment where 80 % of the initial Mn (II) available in solution was lost.

Keywords: Iron, Manganese, oxidation, sorption, Vyredox method, Elverum.

Acknowledgement

Herewith, I would like to thank all people who have contributed to this master thesis.

In particular,

My supervisors Anja Sundal and Professor Per Aagaard for giving me the opportunity to work on this interesting topic and their great supervision. Thank you for your constant and constructive comments and suggestions during the development of this thesis which helped immensely in shaping this study. Thank you for your unflinching support and encouragements. Your insight, advices, and patience allowed this thesis to reflect not only on my efforts but also your own efforts.

My sincere thanks to Mufak Said Naoroz, Siri Simonsen, Magnus Kristoffersen and Ibrahim Omar Khaled for the technical support and assistance.

I would like to thank my family for always being there for me, for supporting me in every possible way. Thank you for your unconditional support and love through my whole life. It is thanks to your teaching and countless hours of guidance that instilled in me the love of learning that is still present with me to this day.

My heartfelt appreciation goes to you Luigi for your kindness, your presence and for always being there lifting me up with all the care of the world. Thank you for all the effort you made in order to understood what I am doing in science and all the hours you spent proofreading this thesis.

My gratitude to the smart and cheerful friends in room 217. You have made this challenging period memorable. A special thanks to Mats for always being there, thank you for the infinite attention you provided for my incessant questions.

Finally, special thanks are necessary to this beautiful land Norge. You welcomed me with such open and warm arms that I have never felt so much home than ever before. Your inner peace and strength made me aware of so many things I never considered. Tusen takk mitt vakre Norge.

Table of content

Abstract ..... **IV**

Acknowledgement ..... **V**

Table of content ..... **VII**

List of figures ..... **VIII**

List of tables ..... **IX**

1. Introduction **1**

1.1. Objectives 3

2. Background **4**

2.1. Study area 4

2.1.1. Geographical location 4

2.1.2. Regional Geology 4

2.1.3. Geological settings at Elverum 6

2.2. Groundwater in Norway 7

2.2.1. Elverum water supply 8

2.3. Iron and manganese in Groundwater 8

2.3.1. Sources and chemistry of iron in groundwater 9

2.3.2. Sources and chemistry of manganese in groundwater 12

2.4. Potential processes affecting Fe and Mn concentrations in Groundwater 14

2.4.1. Sorption processes 14

2.4.2. Redox processes 16

2.5. Vyredox method 24

2.5.1. Principle of the Vyredox method 24

2.5.2. Vyredox method application in Elverum 26

3. Methods and materials **28**

3.1. Geological sampling and weather condition 28

3.2. Solid material characterization 29

3.2.1. Grain size analysis 29

3.2.2. Microscopy analysis 30

3.2.3. X-ray Diffraction 32
3.3. Chemical analysis: trace elements analysis 34
3.4. Laboratory experiments 34
3.4.1. Iron extraction experiments 35
3.4.2. Manganese batch sorption experiments : 36
3.4.3. Mn catalytic aerobic oxidation 38
3.5. Geochemical modelling with PHREEQC 41
4. Results 43
4.1. Solid material characterisation 43
4.1.1. Grain size analysis and soil description 43
4.1.2. Mineral characteristics 45
4.2. Iron extraction 52
4.3. Manganese sorption experiments 53
4.4. Catalytic oxidation of Mn (II) 57
4.4.1. High pH: 8-9 57
4.4.2. Low pH value: 6-7 60
4.5. Geochemical modelling with PHREEQC 63
4.5.1. Manganese sorption 63
4.5.2. Manganese oxidation 66
5. Discussion 69
5.1. Iron extraction 69
5.2. Manganese sorption 70
5.3. Manganese oxidation 72
5.4. Oxidation kinetics 76
5.5. Solid material characterisation 80
5.6. Validity of the results 80
6. Conclusions 83
6.1. Recommendations for further studies 84
7. References 86
8. Appendices 103

List of figures

Figure 1: Geographic location of Elverum showing an overview location of the city (left) and the position of the water works in Grindalsmoen (right) (Google Earth). 4

Figure 2: The general outline of the glacial lake Nedre Glomsjø at the time of the flooding period with an approximate position of the ice sheet, the assumed drainage route and the flooded area. (modified from Longva, 1984, as cited in Høgaas & Longva, 2016)..... 5

Figure 3: Sediment mapping of Elverum area. The position of Grindalsmoen waterwork is pointed at with the black rectangle. Every color on the map represents a type of deposit. Moraine material is represented in different shades of green and reflects on the thickness of the deposit (ngu.no). 6

Figure 4: The use of groundwater and surface water for drinking water in the Nordic countries expressed by percentage (%). For instance, countries like Denmark and Iceland use mainly groundwater for their water supply (more than 95%) (Kløve et al., 2017). 7

Figure 5: Classification of the different forms of iron-bearing minerals depending on their mineral forms, solubility, and chemical nature (modified from Khatri et al., 2017). 9

Figure 6: Pourbaix diagram showing the dominant iron form for different pH and pE conditions (Buamah, 2009). Eh represents the activity of the electrons expressed in Volts. The lines, called phase-boundary lines indicate the stability field boundary where the activity of both adjacent dominant forms is equal. 11

Figure 7: Pourbaix diagram indicating which manganese form predominates under different pH and pE conditions (Martin, 2005). pE provides a nondimensional scale (as the pH) and expresses the activity of electrons in factors of 10. represents. The lines, called phase-boundary lines indicate the stability field boundary where the activity of both adjacent dominant forms is equal. 13

Figure 8: Sketch of the Freundlich (left) and Langmuir isotherms (right). X represents the solute concentration sorbed by the soil, C represents the solute concentration in solution and b is the maximum sorption capacity (g/g) (modified from Goldberg et al., 2007)..... 16

Figure 9: The rate laws and the reaction orders for the reaction A→B. A and B represent the reactant and product of the reaction respectively. The rate is given a negative sign because the slope is negative as the reactant decreases during the reaction. K is the rate constant and is equal to the reaction rate when all the reactant compounds are present at unit concentrations (Appelo & Postma, 2005)..... 17

Figure 10: Schematic drawing showing the two pathways through which manganese ions precipitates on iron-oxides (pathway A) and on albite (pathway B) (modified from Junta & Hochella, 1994). 23

Figure 11: The disposition of the production and aeration wells for iron and manganese oxidation (Ahmed, 2012). 24

Figure 12: Vyredox method application and precipitation zone for iron and manganese during the treatment. The zones colored in red and in brown represent the precipitation zone of iron and manganese, respectively (modified from Hallberg & Martinell, 1976). 25

Figure 13: The setting of the production wells in Grindalsmoen waterworks. The pumping wells are pointed at with the yellow dot. Each production well is composed of 9 satellite wells and are shown in black dots. 27

Figure 14: Position of the sampling point where the sand samples were collected in comparison with the location the four producing wells in Grindalsmoen waterworks (norgeskart.no). 28

Figure 15: Schematic representation designed to illustrate the setup applied during the ferrihydrite precipitation treatment of the SD and SL sand samples for SEM analysis. In the first step, the iron is precipitated under constant stirring while adding a solution of NaOH to increase the pH of the solution. When a pH range of 7-8 is obtained the solution is washed with Milli-Q water until a conductivity of 21 µs/cm or less is reached. The samples are freeze dried and analyzed with SEM..... 31

Figure 17: the Teflon cup and agate pellets used during the wet milling of the samples. The sample and ethanol are poured on top of the pellets and the cup is firmly closed before inserting it in the micronizing mill. 33

Figure 17: An example of the sample holders used during the XRD analysis. The white circle in the middle represents the sand sample in powder that were softly flattened by a glass plate. 33

Figure 18: Sorption experimental setup designed for the sorption experiments carried out in the laboratory. The sample are prepared by adding a volume of a solution of $NaHCO_3$ to which is added 1 gr (or 2 gr) of the sand sample and a volume of a solution of $(MnNO_3)_2$. The samples then are centrifuged and analyzed by ICP-MS..... 38

Figure 19: A) A model set-up for the catalytic oxidation of manganese. B) the experimental set-up for the oxidation experiments. The sample containing the sand sub-samples and the blank are connected to the air pump by tubes during the whole period of oxidation. 40

Figure 20: A- Grain size distribution for the collected samples. B- Soil textural triangle for the collected samples. The colored circles dots represent the different soil depth: Red for 0-15 cm, blue for 15-40 cm, green for 40-50 cm, orange for 50-70 cm, black for 70-80 cm and yellow dot for 80-100 cm. 44

Figure 21: A representative backscatter image of all the samples: 0-15 cm (1), 15-40 cm (2), 40-50 cm (3), 50-70 cm (4), 70-80 cm (5) and 80-100 cm (6). Some of the main minerals are highlighted in the images. 46

Figure 22: Cumulative element spectra for sample 70-80 cm. Different minerals can be deduced from the graph such as ilmenite ($FeTiO_3$) and titanomagnetite ($Fe^{2+}(Fe^{3+}, Ti)_2O_4$). Mn is also present in this sample as coating on top of mica and ilmenite. 47

Figure 23: Mapping of the SL sample, showing the distribution of Si, Fe, P, Na, Mg, Al, K, Ca and Ti. Top left: Si and Fe. Top right: mix of different elements: Na, Mg, Al, K, Ca and Ti. Bottom left: Fe. Bottom right: P..... 49

Figure 24: Mapping of the SD sample, showing the distribution of different elements as Si, Fe, P, Na, Mg, Al, K, Ca and Ti. 50

Figure 25: The mineral content detected by XRD for all the samples. The mineral content in percentage is given in the x axis. The Y axis represents the depth at which the samples were collected. 51

Figure 26: Results of the Manganese sorption experiments. Top: the total distribution for Mn sorption experiments 1 and 2 where both data sets were combined. Bottom Left represents the results of the first sorption experiments and the figure on the right represents the results of the second experiment. [Mn] solution is the concentration of Mn left in solution after sorption while [Mn] sorbed is the concentration of Mn sorbed onto the soil. The green and red markers represent the SD and SL samples, respectively. 55

Figure 27: The Freundlich isotherm for the total manganese sorption experiments. The data of the first and second sorptions are combined in one graph. The replicas are also plotted instead of the average of the replicas results. The green and red markers represent the SD and SL samples, respectively. 56

Figure 28: Evolution of the manganese (II) concentration in solution in the SD sample and in the blank for high pH values over time. The marker in green represents the sample containing the SD sand sub-sample while the purple marker is the blank sample free of sand sub-sample. 58

Figure 29: Evolution of manganese (II) concentration in the SL sample and the blank at high pH value over time. Left: concentrations of Mn (II) and right represents the pH. The marker in red represents the sample containing the SL sand sub-sample while the purple marker is the blank sample free of sand sub-sample. 59

Figure 30: pH evolution in the SD and SL samples during the manganese (II) oxidation experiments over time. Left: the pH in the SD sample. Right: the pH in the SL sample for high pH levels (8-10). The marker in green represents the sample containing the SD sand sub-sample, the red markers represent the sample containing the SL sand sub-samples and the purple markers are used for the blank sample free of sand sub-sample. 60

Figure 31: Evolution of manganese (II) concentration in the SD sample and the blank at low pH value over time. The marker in green represents the sample containing the SD sand sub-sample while the purple marker is the blank sample free of sand sub-sample. 61

Figure 32: Evolution of mnganese (II) concentration in the SL sample and the blank at low pH value. The red and purple markers represent the SL and blank samples, respectively. 62

Figure 33: pH evolution in the SD and SL samples during the manganese (II) oxidation experiments over time. Left: the pH in the SD sample. Right: the pH in the SL sample for high pH levels (8-10). The marker in green represents the sample containing the SD sand sub-sample, the red marker represents the sample containing the SL sand sub-samples and the purple marker is the blank sample free of sand sub-sample. 63

Figure 34: Results of the sorption experiments (1 and 2) compared to the sorption modelling with PHREEQC. [Mn] sorbed reflects on the Mn (II) sorbed onto the sand sub-samples and

[Mn] solution reflects on the concentration of Mn (II) remaining in solution. The markers (in green and red) represent the measured sorption results while the solid lines (in green and red) represent the sorption of manganese resulting from PHREEQC. 64

Figure 35: The Freundlich isotherm for the computed manganese sorption. The green and red markers represent the SD and SL samples respectively. 65

Figure 36: Results of manganese sorption on hydrous ferric oxide and organic matter resulting from PHREEQC modelling. The Mn_Hfo represents the part of Mn sorbed on Fe oxides (blue line) and Mn_organic.matter represents the Mn sorbed onto the organic matter (green line). The Total sorption (black line) is the sum of both Mn_Hfo and Mn_organic.matter. 66

Figure 37: Evolution of manganese (II) and pH during the modelling of the oxidation reaction with PHREEQC at high pH range. Mn-1st (blue solid line) represents the manganese (II) concentrations obtained from the oxidation reaction simulated with the 1st order reaction rate constants resulting from the laboratory experiments (same for Mn-2^{nd,} orange solid line). pH-1st represents the pH values obtained from the oxidation reaction simulated with the 1st order reaction rate constants resulting from the laboratory experiments (same for pH-2nd). The pH is shown in dotted lines and the concentrations of manganese (II) in a solid line. 67

Figure 38: A comparison between the modelling and the experimental results obtained for the oxidation of manganese (II) for high pH levels. The experimental results are represented by the SD (green markers) and SL (red markers) samples. The modelling results are presented in a solid line. Mn-1st (blue solid line) represents the manganese (II) concentrations obtained from the oxidation reaction simulated with the 1st order reaction rate constants resulting from the laboratory experiments (same for Mn-2nd, orange solid line). 68

Figure 39: Percentage of manganese sorption for various manganese concentrations in solution for the SD and SL samples in the first sorption experiment. 71

Figure 40: The effect of pH on the oxidation of manganese with time in the SD and SL samples. The figure on the left represents the results of the oxidation experiment for the SD sample for high pH level (dark green markers) and low pH level (light green markers). The results of the oxidation experiments run on the SL sample is represented in the figure on the right. The dark red markers reflect on the experiments at high pH levels and the light red markers reflect on the experiments run at low pH levels. 75

Figure 41: Manganese (II) oxidation kinetics on the SD and SL sand sub-samples at high (left) and low pH (right) ranges. The figures on the top represents the 1st order kinetics and the figures in the bottom represents the 2nd order kinetics. The profiles are divided into two parts: the parts highlighted with a dashed-line bracket where the oxidation rate decreases, and the part highlighted with a solid-line bracket and representing heterogenous reactions occurring in solution. 77

Figure 42: Oxidation kinetics resulting from the manganese (II) oxidation experiments. The figure on the top represents the 1st order reaction rate for high pH (left) and low pH (right) levels. The figures in the bottom represents the 2nd order reaction rate at high pH level (left) and low pH level (right). The green triangle markers and the red lozenge markers represents the SD and SL sand sub-samples, respectively. 79

List of tables

Table 1: List of some manganese minerals and their chemical formula (Bricker, 1965; Post, 1999)..... 12

Table 2: An example for the sample's preparation method for the manganese sorption experiments. The numbers in SD10, SL20, B80 and so on, represent the volume of $MnNO_3$ used during the preparation in µl. B represents the blank while SD and SL reflects respectively on the dark and light sand sample. 37

Table 3: Soil characteristics resulting from the grain size analysis of the sand samples collected in Elverum. 45

Table 4: Description of the treated SD and SL samples with a solution of 0.01 M and 0.001 M of $Fe(NO_3)_3$. 47

Table 5: Results of the iron and manganese extraction experiments. Mn_d and Fe_o reflect to the manganese and iron extracted by the DCB method, while Mn_o and Fe_o express the extraction by oxalate. 52

Table 6: The iron activity index (indicates the degree of crystallinity of the soil) for SD and SL samples. 52

Table 7: Sorption results for the SD and SL samples for sorption experiment 1. The [Mn] solution represents the concentration of Mn (II) left in solution after sorption and [Mn] sorbed represents the sorbed Mn (II). 53

Table 8: Sorption results for the SD and SL samples for sorption experiment 2. The [Mn] solution represents the concentration of Mn (II) left in solution after sorption and [Mn] sorbed represents the sorbed Mn (II). 54

Table 9: The Freundlich isotherm properties for the total sorption experiment for the SD and SL samples. K_F is Freundlich coefficient, n is a measure of the adsorption intensity and reflects on the slope of the curve and R^2 is the regression coefficient. 56

Table 10: Results of the manganese oxidation at high pH levels for the SD and SL samples. 57

Table 11: Manganese oxidation results for the SD and SL samples at low pH values. 60

Table 12: Freundlich Isotherm parameters resulting from the modelling investigation. K_F is Freundlich coefficient, n is a measure of the adsorption intensity and reflects on the slope of the curve and R^2 is the regression coefficient. 65

1. Introduction

Under natural conditions, groundwater quality depends on the atmospheric inputs, water-rock interaction in the soil-bedrock interface and on the long-term reactions occurring along the flow paths in the saturated zone (Edmunds & Shand, 2008). Sometimes groundwater may contain excessive amounts of iron (Fe) and manganese (Mn) and in some cases the content of these two ions is so high, that the water needs to be purified before being used (Hallberg & Martinell, 1976). The aquifer located in Elverum, which constitutes the area examined for this master's thesis, is also rich in Fe and Mn. Therefore, the groundwater needs to be filtrated before being distributed to the municipality.

Because Fe and Mn are chemically similar; and display similar chemical behaviour (Penrose, 1893; Hem, 1972; Davidson, 1993; Fitsanakis et al., 2009), they usually cause similar problems (Seelig et al., 1992). Fe is known for causing reddish-brownish stains on clothes, dishes, and utensils while Mn causes brownish-black stains on the same cited materials (Hem, 1989). More importantly, during the ultraviolet (UV) disinfection of water, bacteria have proved to be protected by particles having a diameter larger than 7-10 μm (Emerick et al., 2000; Jolis et al., 2001; Wright et al., 2002). Among many examples, Fe precipitates play a significant role in the survival of coliform bacteria during UV disinfection due to the absorbance of UV light by the Fe (Cairns et al., 1993, as cited in Templeton et al., 2006).

Field observations showed that at concentrations of around 1mg/l, dissolved Mn can cause toxic effects in aquatic organisms (Howe et al., 2004). Similar events were observed in 2007, 2015 and 2016 in Risa River in Gardermoen area where several brown trout were found dead in the river. A mucous coat was observed in the trout gills, analysis showed that the death of these fish was probably due to respiration problems caused by the precipitation of Fe, Mn and aluminium (Al) oxides at the surface of the gills (Frogner & Almhjell, 2019; Hagen, 2020).

Fe and Mn may naturally be present in water due to weathering processes and dissolution of rocks and Fe-bearing minerals (such as magnetite and pyrite) (Appelo & Postma, 1992), Mn-bearing minerals (lithiophorite and manganosite) (Taylor et al., 1964; Golden et al., 1993) but also from ferromagnesiosillicates (Fe-Mg silicates) (Appelo & Postma, 2005). The presence of Fe and Mn in groundwater can be either in the dissolved form as ions (Fe (II), Mn (II)) or in the solid form as $Fe(OH)_3$ and Mn $(OH)_4$. The form in which Fe and Mn are found depends on different environmental factors such as: redox potential, presence of organic and inorganic

substances, solubility of Fe and Mn, pH value and oxygen concentrations (Schwertmann, 1991; Ehrlich, 1998; Barloková & Ilavský, 2009; Buamah, 2009). For instance, the solubility of Fe and Mn is strongly dependent on the redox conditions; High positive value of redox potential (Eh) can lead to the precipitation of Fe and Mn oxides and hydroxides as coating on aquifer sediments while low values of Eh will results in the dissolution and the release of Fe (II) and Mn (II) in the water (Figure 6, 7) (Stokes et al., 1988; Lazerte & Burling, 1990; McMahon et al., 2009; Rosecrans et al., 2017).

Some groundwaters tend to be poorly oxygenated as the oxygen is rapidly consumed by microbial uptake, the biodegradation of organic matter, reactions with reduced mineral phases and groundwater age (Winograd & Robertson, 1982; Malard & Hervant, 1999; Rosecrans et al., 2017). Therefore, Fe and Mn in this type of environment are relatively soluble thus the concentrations of dissolved Fe and Mn are high.

In recognition of the various problems caused by both ions, several methods have been designed and conceived through the years to mitigate the toxic effects of Mn and Fe in excess and to provide a safe supply of drinking water. The principle on which most of these methods rely on entails the transformation of dissolved Fe and Mn into undissolved compounds (Barloková & Ilavský, 2009). These methods are separated in ex-situ and in-situ techniques.

Ex-situ methods: the water is treated on the surface through different processes such as oxidation-filtration processes (aeration-filtration, chemical oxidation-precipitation and filtration etc.), removal through softening by lime or zeolite and ion exchange (Mouchet, 1992; Buamah, 2009).

In-situ methods: consist of introducing oxygenated water into the aquifer through wells which will create a treatment area around the main pumping well (Mouchet, 1992). The Vyredox method is one of the methods used in the in-situ removal techniques, its principle is based on the creation of highly oxidized zone around the producing well through the injection of water rich in oxygen (Hallberg & Martinell, 1976).

1.1.Objectives

This Master research project concerns the redox processes occurring in the aquifer at the Elverum Water Works, where the Vyredox method has been applied for more than 30 years. This method removes Fe and Mn from groundwater through the injection of oxygenated water which will oxidize the Fe and Mn. However, the exact mechanisms behind the oxidation and co-precipitation of Fe and Mn remain unclear so far (Mettler, 2002, Sparrow & Uren, 2014). Currently, the biotic mechanism that involves the Fe and Mn oxidizing microorganism and the chemical mechanisms through an oxidation-precipitation pathway are considered. Therefore, it is important to carry out additional research studies in order to expand the already existing knowledge in relation to these processes. Hence, in light of what was exposed above, the objectives of the present study are:

- To determine Mn adsorption capacities on different Fe-coated sand samples.
- To determine the effect of pH on the oxidation and adsorption of Mn with and without Fe-coated sand, consequently investigating the oxidation kinetics of adsorbed Mn.

To address these research questions laboratory experiments were conducted and tested by a geochemical modelling tool (PHREEQC). The experiments are restricted to abiotic reactions as conducting biotic experiments was not possible due to time constraints.

Answering these questions is crucial as there has been a limited understanding of the reaction kinetics and mechanisms of the redox reactions of Fe and Mn in general and also during the application of the Vyredox method. It is also important because it may help understand the distribution of the different precipitates during the oxidation of Fe and Mn and their role in clogging and reducing the available pore volume which will affect the transmissivity of the aquifer and the capacity of the production well over a long term.

2. Background

2.1. Study area

2.1.1. Geographical location

Elverum is situated on the bank of Glomma River, the longest river of Norway, in Hedmark County, Southeast of Norway. The study site, Grindalsmoen, lies on the West side of the Glomma River and is the main source of water supply for Elverum municipality (Figure 1).

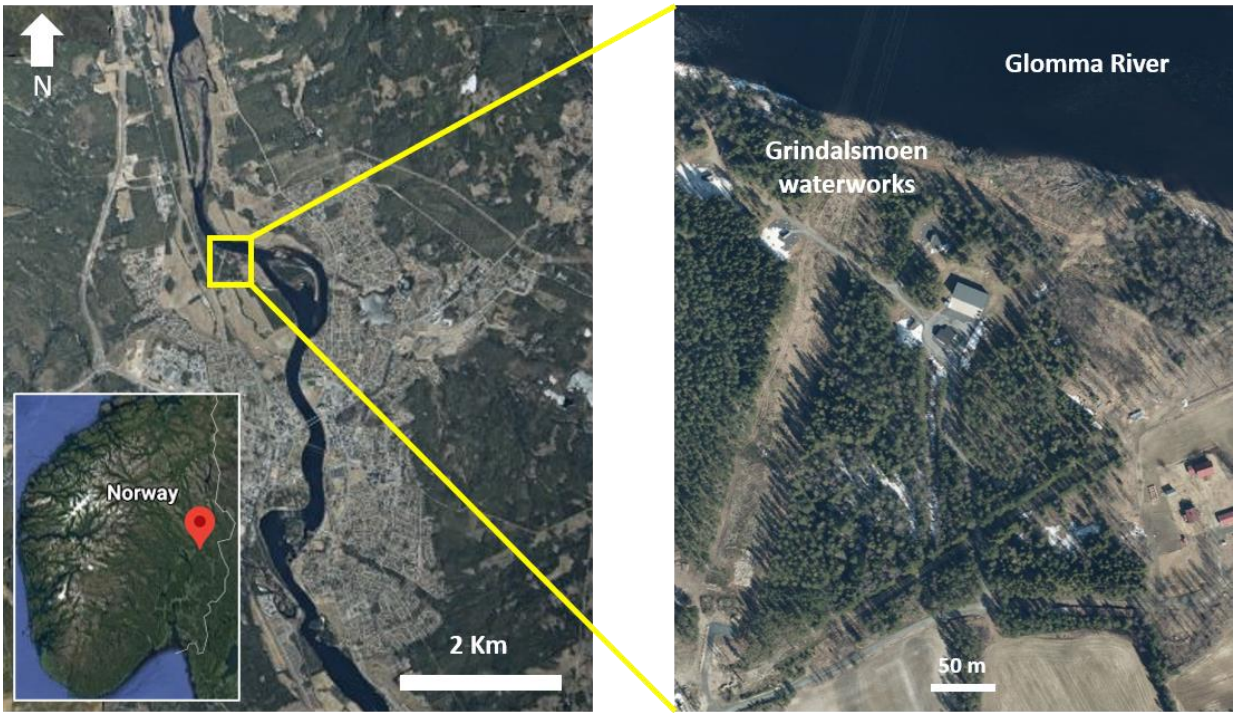

Figure 1: Geographic location of Elverum showing an overview location of the city (left) and the position of the water works in Grindalsmoen (right) (Google Earth).

2.1.2. Regional Geology

The Quaternary period has been characterized by repeated climatic oscillations between cold glacial and warm interglacial events (Pillans & Gibbard, 2012). The current Norwegian landscape is the result of geological surface processes during these numerous glaciations episodes and interglacial periods. The movement of ice sheets and glaciers has contributed enormously to the formation of deep glacial fjords, long U-shaped valleys and many lakes in bedrock basins (Fredrin et al., 2013; Olsen et al., 2013).

Towards the end of the last deglaciation in Norway, the glacial lake Nedre Glomsjø was confined between the water divide in the North and the receding ice sheet in the South (Holmsen, 1915 as cited in Høgaas & Longva, 2016) (Figure 2). The lake drained due to the establishment of a passage through the receding ice sheet around 10-10.4 cal Ka years BP (calibrated years before the present. Ka refers to kilo annum or thousand years) (Longva, 1994). This ice sheet margin was situated around 15 km North of Elverum during the flood period (Høgaas & Longva, 2016) and provoked a considerable erosion and deposition of vast slackwater deposits in the regions South of the ice sheet (1994; Høgaas & Longva, 2016, 2019). The valley floors of this area are dominated by till, glaciofluvial or fluvial sediments connected to the drainage of the glacial Nedre Glomsjø Lake (Bargel, 1983; Høgaas & Longva, 2016).

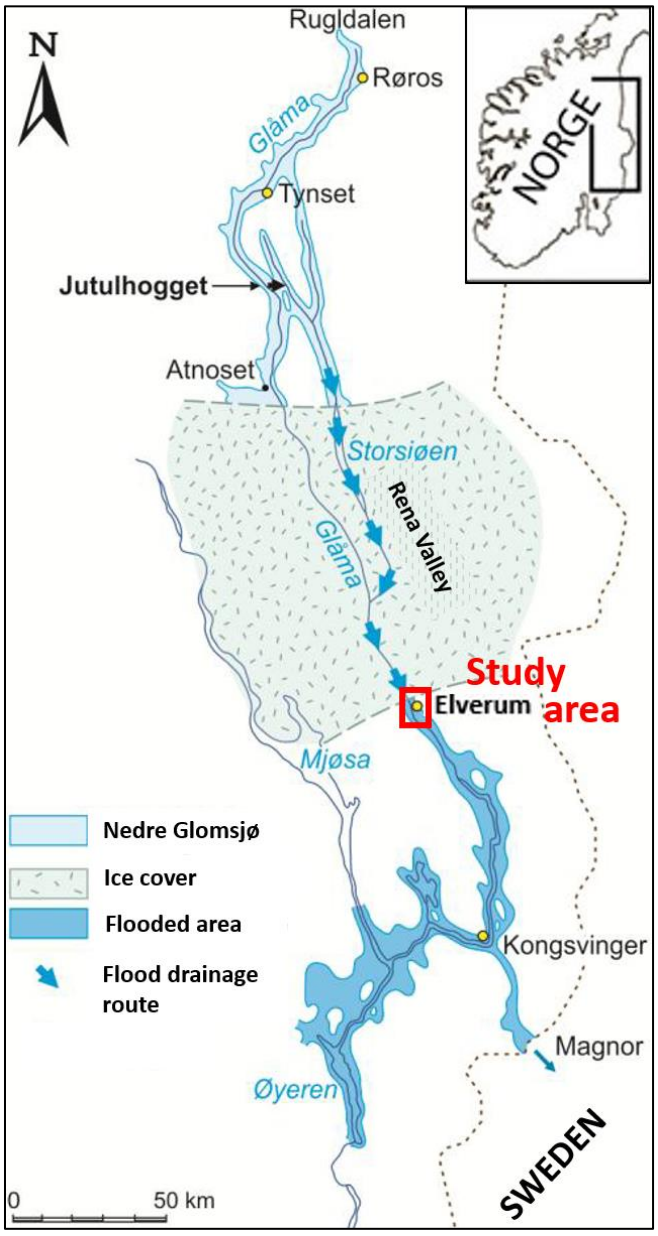

Figure 2: The general outline of the glacial lake Nedre Glomsjø at the time of the flooding period with an approximate position of the ice sheet, the assumed drainage route and the flooded area. (modified from Longva, 1984, as cited in Høgaas & Longva, 2016).

2.1.3. Geological settings at Elverum

Overall, Norway is characterized by large areas of exposed bedrock or bedrock covered by Quaternary sediments. However, in Østlandet region where Elverum is located, most areas have a continuous cover of sediments as illustrated in figure 3.

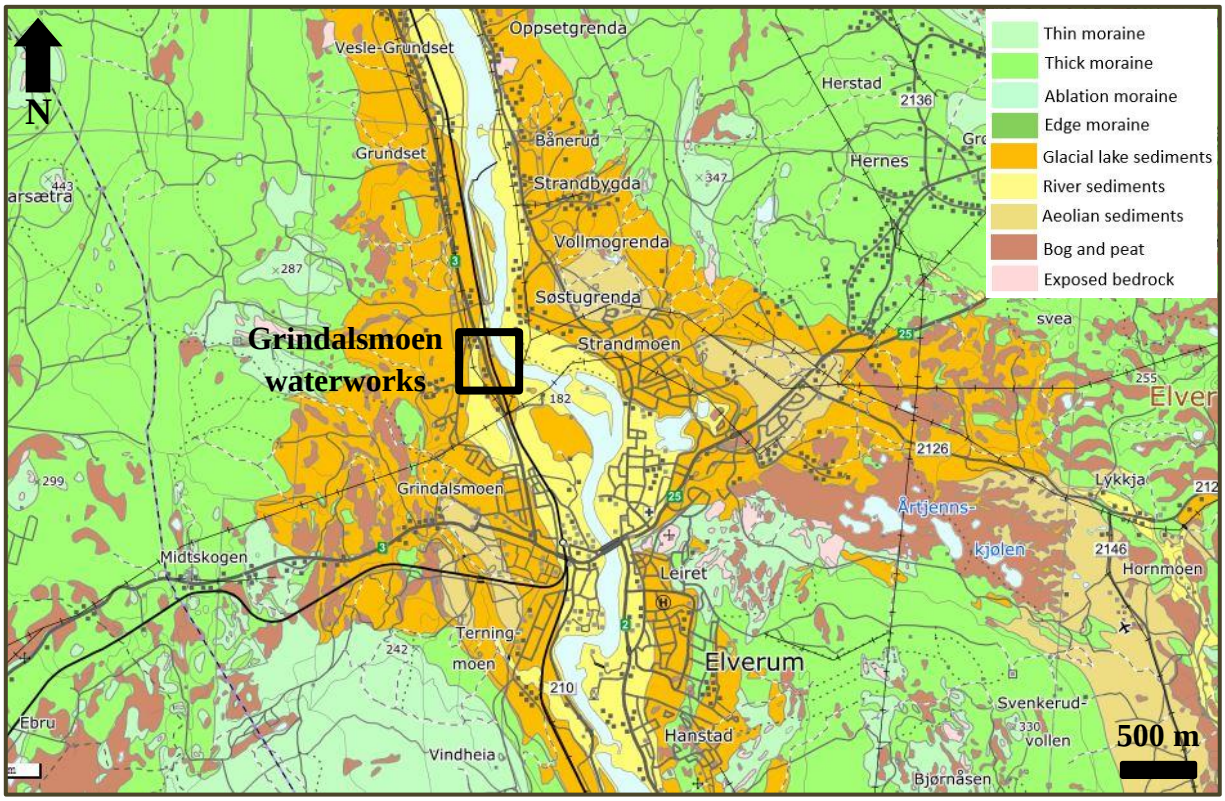

Figure 3: Sediment mapping of Elverum area. The position of Grindalsmoen waterwork is pointed at with the black rectangle. Every color on the map represents a type of deposit. Moraine material is represented in different shades of green and reflects on the thickness of the deposit (ngu.no).

Till deposits are represented by light green color for thin sediment cover. Thicker deposits are represented in dark green (Olsen et al., 2017).

Glaciofluvial deposits are dominantly sandy in Elverum (Klemsdal, 2010). The deposits are mostly located along the watercourses (Olsen et al., 2017). On the map, the glaciofluvial deposits are illustrated by the orange color.

The fluvial deposits: the area along the Glomma River is dominated by modern fluvial material and is represented by a thin yellow strip. This material, which lays on both sides of the river, is flanked by important glaciofluvial deposits.

Aeolian deposits are usually associated with large glaciofluvial deposits where fossil dunes are possibly present like in Elverum (Bargel, 1983). The aeolian deposits are represented by light brown on the map.

Peat and bog are naturally rich in organic acids and include all types of natural accumulations of organic matter. These deposits play an important role in controlling the fate of Fe and Mn as these two elements show a high degree of mobility in peats (Novak et al., 2011). Peats and Bogs are a very common type of deposits in Norway (Moen, 1998) and are shown with dark brown color on the map.

Both aeolian deposits and peat and bog are distributed on top of glaciofluvial and till deposits however, they are rarely found near the river with the modern fluvial material.

2.2. Groundwater in Norway

Norway predominantly uses fresh surface water instead of groundwater (15%) as opposed to many European countries (NGU, 2017). Indeed, 75 % of European inhabitants depends on groundwater for their drinking water supply (European commission, 2009) (Figure 4). This is due to the abundance and the ease-of-use of this fresh water. However, the use of groundwater is becoming more important in rural areas, where sanitation is a source of concern (NGU, 2017).

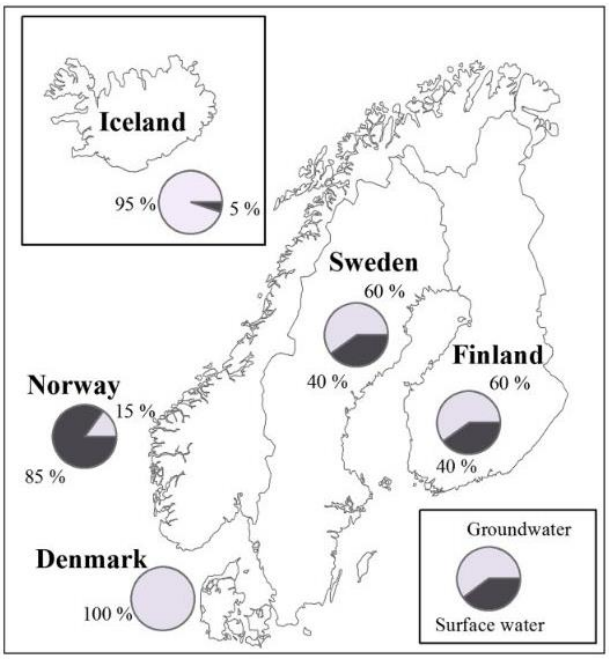

Figure 4: The use of groundwater and surface water for drinking water in the Nordic countries expressed by percentage (%). For instance, countries like Denmark and Iceland use mainly groundwater for their water supply (more than 95%) (Kløve et al., 2017).

There are two main types of aquifer in Norway: Porous and fractured aquifers (European Environmental Agency, 2008). The porous aquifers are mainly found in unconsolidated Quaternary sediments while the fractured aquifers are found within igneous and metamorphic bedrock. As stated in Banks et al. (1988), there is a limited number of studies on the chemistry of groundwater from Quaternary unconsolidated-deposit aquifers in Norway compared to fractured aquifers. However, some key differences in terms of water quality between

these two aquifers have been established. Indeed, drinking water from porous aquifers (which comprise siliciclastic material, mainly silicate minerals) contains higher concentrations of Aluminum (Al), Copper (Cu) and Zinc (Zinc). The water in this type of aquifer is generally less mature with lower pH values. According to the same study, the porous aquifers are more oxidizing than the fractured aquifers as the latter exceeds Fe and Mn concentration norms more frequently than the Quaternary aquifers (Banks et al., 1988).

2.2.1. Elverum water supply

Elverum municipality is equipped with two waterworks: Grindalsmoen and Kirkekretsen waterworks. The latter is located in Sørskogbygda and covers the water supply of this area. Grindalsmoen waterworks on the other hand, is the main water supplier for Elverum town. The waterwork extracts water from 4 groundwater wells and utilizes an in-situ treatment system.

Due to high concentrations of dissolved Fe and Mn in the groundwater, the Vyredox method is applied in the Grindalsmoen waterworks in order to remove the Fe and Mn from the water before its distribution to the municipality.

2.3. Iron and manganese in Groundwater

Unpolluted groundwater has generally a good quality as the water is filtered when it is percolating down from the surface. However, some groundwater may naturally contain high amounts of dissolved trace elements from the aquifer matrix such as Fe and Mn, which limits its use (Edmunds & Smedley, 1996). This excess of Fe and Mn in groundwater is probably due to a combination of many factors. Indeed, the soil strata and the bedrock can vary over a distance of just few meters, thus the groundwater quality and its composition will change spatially as well. Rainwater, melted snow and ice will bring an important amount of dissolved oxygen when they infiltrate the soil and percolate into the groundwater. This will result in a groundwater poor in Fe and Mn. However, surface water infiltration can be limited due to the low permeability of the strata; consequently, the oxygen content of groundwater is reduced whereas the Fe and Mn content increase. These hydrological and geological conditions are not the only factors controlling the groundwater quality, but also biological, physical and chemical factors play an important role (Hallberg & Martinell, 1976; Stumm & Morgan, 1996; Appelo & Postma, 2005).

The concentration of Fe and Mn in groundwater varies from 0-40 mg/l and 0 to 10 mg/l, respectively (Buamah, 2009). However, the Environmental Protection Agency (EPA) established a secondary maximum contaminant levels (SMCL), which represents the maximum allowable amount of contaminant in drinking water, of 0.3 mg/l for Fe and 0.05 mg/l for Mn (EPA, 2006;

WHO, 2007). Above these concentrations, the water might present some problems for water consumers as excessive amount of Fe and Mn will negatively affect the aesthetic value of drinking water (color, taste and odor) and will cause damage to the water equipment (EPA, 2016).

2.3.1. Sources and chemistry of iron in groundwater

Fe is a natural constituent of the earth's crust and is one of the most abundant elements in sedimentary and igneous rocks (Hem, 1989). Fe in groundwater may originate from the weathering of different type of Fe-bearing minerals. These minerals are classified depending on their solubility, chemical nature, and mineral form into four groups (Figure 5): oxides, silicates, carbonates and sulfides (Khatri et al., 2017).

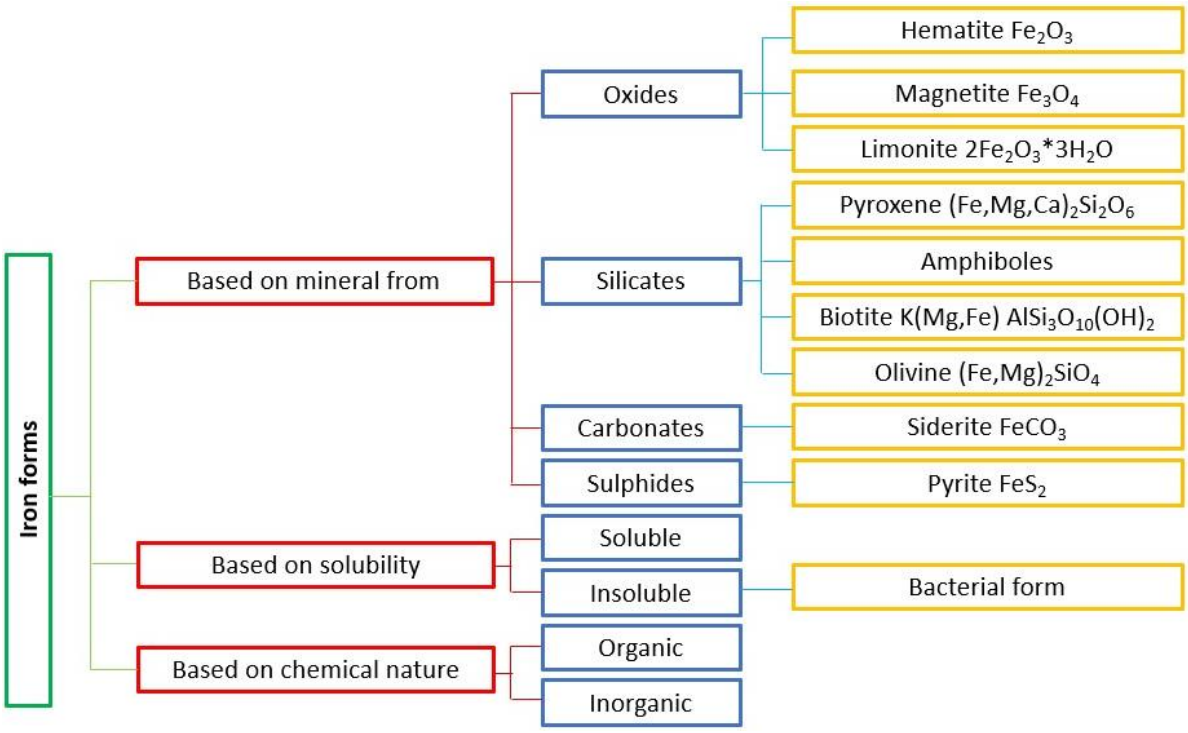

Figure 5: Classification of the different forms of iron-bearing minerals depending on their mineral forms, solubility, and chemical nature (modified from Khatri et al., 2017).

The initial source of Fe is related to the weathering of Fe-rich minerals such as Fe-Mg silicates and pyrite. During the oxidation process of pyrite in presence of organic matter reduced groundwater, the amount of Fe (II) and the water acidity increases as below (Equation 1) (Sracek et al., 2001; Appelo & Postma, 2005):

$$FeS_2 + \frac{7}{2}O_2 + H_2O \rightarrow Fe^{2+} + 2SO_4^{2-} + 2H^+ \qquad \text{(Eq. 1)}$$

Subsequently, the released Fe (II) is oxidized by oxygen and the produced Fe (III) precipitates according to:

$$Fe^{2+} + \frac{1}{4}\,O_2 + H^+ \rightarrow Fe^{3+} + \frac{1}{2}H_2O \qquad \text{(Eq. 2)}$$

$$Fe^{3+} + 3H_2 \rightarrow Fe(OH)_3 + 3H^+ \qquad \text{(Eq. 3)}$$

Therefore, the overall oxidation process of pyrite is described by the reaction:

$$FeS_2 + \frac{15}{4}O_2 + \frac{7}{2}H_2O \rightarrow Fe(OH)_3 + 2SO_4^{2-} + 4H^+ \quad \text{(Eq. 4)}$$

The weathering of silicates minerals like hornblende or biotite may also release Fe (II) to the groundwater under anoxic conditions. However, under oxic conditions the released Fe (II) precipitates as an Fe oxyhydroxide coating. During these weathering reactions, carbonic acid and organic acids are used as sources of protons and bicarbonates are produced which increases the pH. The following equations portray the weathering reaction of biotite (mica) where kaolinite is used as an example of the weathering product (Appelo & Postma, 2005):

$$Biotite + 10H^+ + \frac{1}{2}O_2 + 7H_2O \rightarrow$$

$$Kaolinite + 2K^+ + 4Mg^{2+} + 2Fe(OH)_3 + 4H_4SiO_4 \quad \text{(Eq. 5)}$$

$$CO_2 + H_2O \rightarrow H^+ + HCO_3^- \qquad \text{(Eq. 6)}$$

Where biotite is given by $2K\,(Mg_2\,Fe)(AlSi_3)\,O_{10}\,(OH)_2$ and kaolinite by $Al_2Si_2O_5(OH)_4$.

The dissolution of the different metals and minerals in the water will depend on the availability of carbon dioxide (CO_2). The CO_2 is exhausted in the water due to the interaction between water and minerals (Allen & Suchy, 2001). The released protons H^+ (Equation 3) have a strong impact on the water pH thus increasing the acidity of the water, which will in return affect the Fe oxidation state.

In groundwater, Fe is either in the form of reduced soluble ferrous iron (Fe (II)) or oxidized insoluble ferric iron (Fe (III)) (Hem, 1989; Ngah & Nwankwoala, 2013). The oxidation of Fe (II) to Fe (III) is made possible by an exchange of electrons between the two states (Equation 7). In environments rich in dissolved oxygen, the produced Fe (III) reacts with hydroxyl groups and form a solid precipitate such as ferric hydroxide or oxyhydroxide (Equation 8).

$$Fe^{2+} \leftrightarrows Fe^{3+} + e^{-} \qquad \text{(Eq. 7)}$$

$$Fe^{3+} + 3OH^{-} \leftrightarrows Fe(OH)_3 \qquad \text{(Eq.8)}$$

The general oxidation-reduction reaction (Equations 7 and 8) is given in equation 9:

$$Fe^{2+} + 3H_2O \leftrightarrows Fe(OH)_3 + 3H^{+} + e^{-} \qquad \text{(Eq. 9)}$$

The stability of the reaction described in equation 9 does not only depend on pH but also on the activity of electrons which can be represented by a redox potential Eh (Hem, 1989). The redox potential, expressed in volts, indicates if the environment is oxidizing and where Fe is most likely insoluble (high values of Eh) or if the environment is reducing (low values of Eh) where Fe is in solution. The stability between the oxidized and reduced forms of Fe as a function of pH and Eh is shown in Pourbaix diagram (Figure 6)

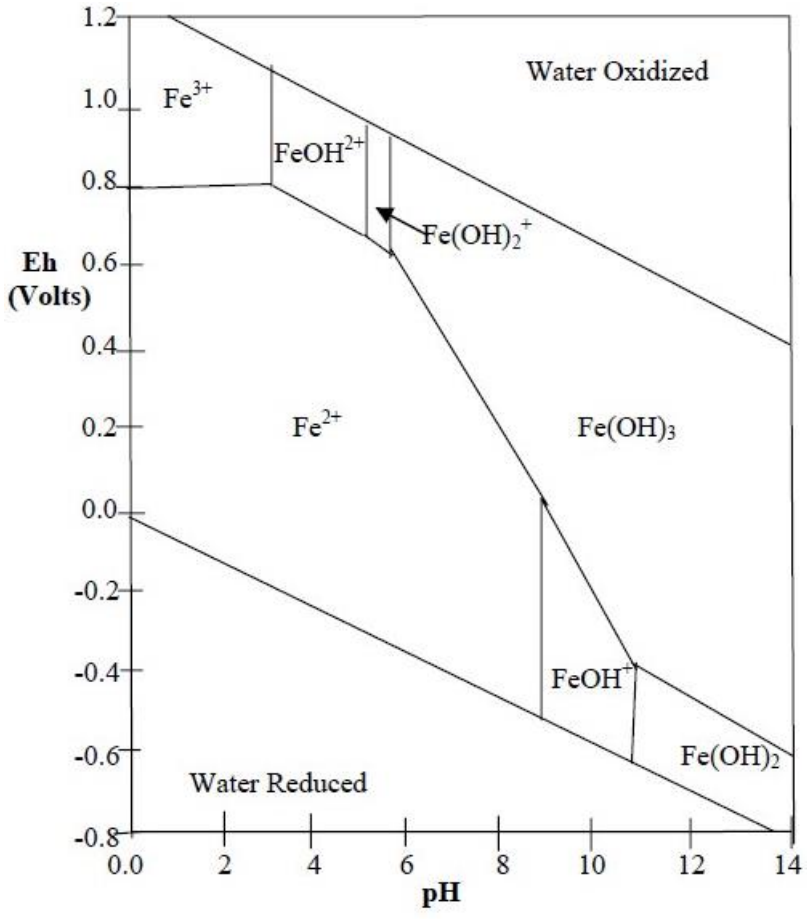

Figure 6: Pourbaix diagram showing the dominant iron form for different pH and pE conditions (Buamah, 2009). Eh represents the activity of the electrons expressed in Volts. The lines, called phase-boundary lines indicate the stability field boundary where the activity of both adjacent dominant forms is equal.

2.3.2. Sources and chemistry of manganese in groundwater

Mn is the eleventh most abundant constituent in the earth's crust and the third most abundant transition metal (Taylor, 1964). Under natural conditions, the Mn present in groundwater probably results from the weathering of Mn-bearing minerals (Hem, 1989; Huang et al., 2015). Additionally, Mn may be substituted in various Fe-Mg silicates (Bray et al., 2015). In the table below is a short list of some Mn minerals and their chemical formulas.

Table 1: List of some manganese minerals and their chemical formula (Bricker, 1965; Post, 1999).

Mineral	Chemical formula
Manganosite	MnO
Ramsdellite	MnO_2
Pyrolusite	β-MnO_2
Birnessite	$(Na, Ca)_4Mn_7O_{14}$ x $2.8H_2O$
Manganite	γ–MνOOH
Rhodochrosite	$MnCO^3$
Hausmannite	Mn^{2+} Mn^{3+} O_4 or Mn_3O_4
Pyrochroite	Mn $(OH)^2$

In addition, both Fe and Mn, as many other metals, can have anthropogenic sources due to direct emission of wastewater, leaching of solid waste and contaminated surface water (Huang et al., 2015; Brindha et al., 2020). As for Fe, Mn is also not present as a free metal in nature, but it is found in the form of oxides, sulfides, carbonates and silicates, adsorbed on Fe oxide, and organic compounds (Penrose, 1893; Post, 1999).

This abundance of Fe and Mn means that these two elements are frequently found in soils and aquifers (Zhang et al., 2020) and will dissolve and migrate to groundwater when the latter percolates and flows though rich organic soil (Weng et al., 2007). The decomposition of the organic matter released into the groundwater will deplete the dissolved oxygen, resulting in a more reductive environment and the groundwater gradually shifts from oxic to reductive with the increase of residence time (Weng et al., 2007). Consequently, the reductive dissolution of Fe and Mn oxides increases the concentration of dissolved Fe and Mn in the water (Brown et al., 1999; Luzati et al., 2016).

Mn can occur in different oxidation states ranging from – III to + VII, although the following oxidation states +II, +III and +IV dominates in natural environments (Bricker, 1965; Buamah, 2009). Mn (III) is a strong oxidant and in the absence of complexing ligands, it converts to Mn (II) and MnO_2 (Yamaguchi & Sawyer, 1985). The Mn (II) is the most stable state in solution and can oxidize easily into MnO_2 and many other Mn oxide and hydroxide minerals (Table 1) (Hem, 1989; Post, 1999; Buamah, 2009; Khozyem et al., 2019).

The thermodynamic stability of these oxides and hydroxides is determined by the pH, temperature, and the redox conditions. In natural waters, at low pH and low redox potential, Mn is mainly present as Mn (II) while at pH above 8 with high redox potential, MnO_2 is usually dominant (Figure 7). The Mn (III) ions are thermodynamically instable in aqueous solutions but at high pH, these ions can be stabilized in the form of MnOOH. The Mn (IV) ions are generally present in the solid form as Mn oxides (Buamah, 2009).

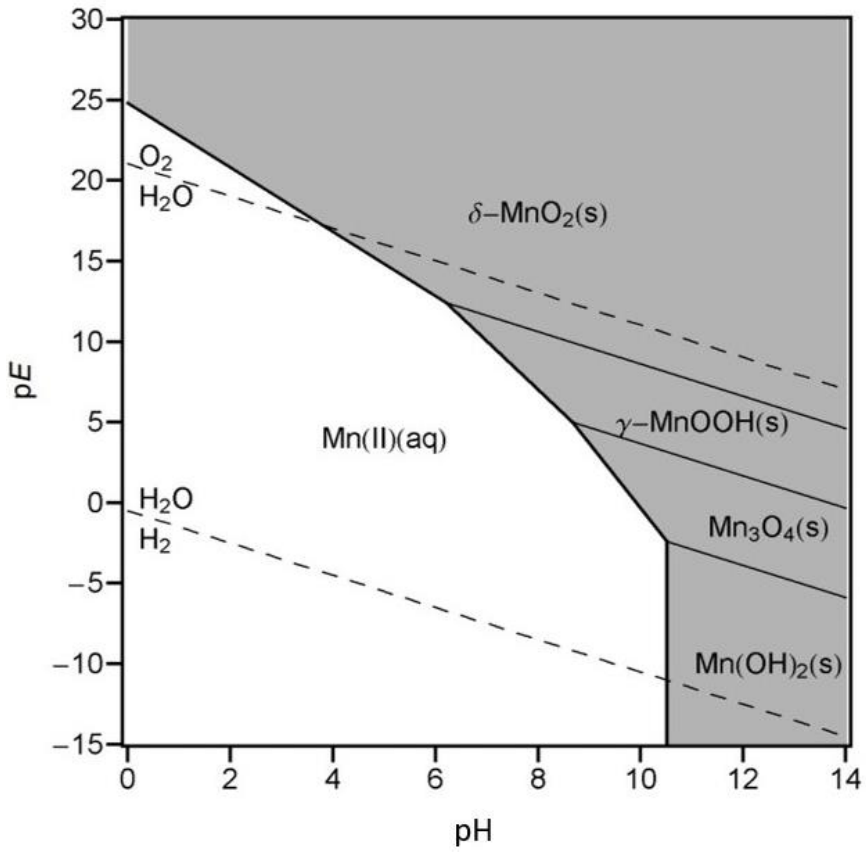

Figure 7: Pourbaix diagram indicating which manganese form predominates under different pH and pE conditions (Martin, 2005). pE provides a nondimensional scale (as the pH) and expresses the activity of electrons in factors of 10. represents. The lines, called phase-boundary lines indicate the stability field boundary where the activity of both adjacent dominant forms is equal.

The oxidation of Mn (II) is due to the change in redox conditions in the environment through the production and release of acids or oxidants or bases by microorganisms (Ghiorse, 1984; Nealson et al., 1989). These microorganisms will oxidize Mn (II) through enzymatic reactions to Mn (III) that will be transformed into Mn (IV) which will then precipitate as MnO_2 (Ehrlich, 1996):

$$2Mn^{2+} + 1/2\,O_2 + 2H^+ > 2Mn^{3+} + H_2O \quad \text{(Eq. 10)}$$

$$2Mn^{3+} + 1/2\,O_2 + 3H_2O > 2MnO_2 + 6H^+ \quad \text{(Eq. 11)}$$

2.4. Potential processes affecting Fe and Mn concentrations in Groundwater

2.4.1. Sorption processes

Sorption is the generic term that groups the ion exchange, sorption and adsorption. The ion exchange process is an exchange of ions between solid and liquid phases (Harland,1994), absorption takes place when the ion is incorporated into a solid structure. Adsorption is the reaction between adsorbent and adsorbate that results in the change of the chemical form of the adsorbate and occurs when an ion is bound to a solid surface (Appelo & Postma, 2005, Buamah, 2009).

Sorption isotherms describe the mathematical relation between the amount of substance sorbed (X) and its composition in the solution at equilibrium condition (C) (Buamah, 2009; Thompson & Goyne, 2012; Bharat, 2017). The two most commonly used sorption models are the Freundlich's and Langmuir models (Appelo & Postma, 2005; Buamah, 2009).

1. **Freundlich sorption isotherm**

Freundlich isotherm is a mathematical expression for the adsorption equilibrium between a liquid (or gas) and a solid. The Freundlich equation (Equation 12) is an empirical expression that represents the isothermal variation of adsorption of a liquid (or gas) onto the surface of a solid (Van der Bruggen, 2014), it is defined as follows (Appelo & Postma, 2005):

$$X=K_F*C^n \quad \text{(Eq.12)}$$

X is the solute concentration sorbed by the soil (mol/kg, µg/g, etc.), C is the solute concentration in solution (mol/l, µg/ml). K_F is Freundlich coefficient and indicates the adsorption capacity while n is a measure of the adsorption intensity and reflects on the slope of the curve whether plotted on an arithmetic or logarithmic scale (Faust & Aly, 1998).

When the Freundlich equation is written in a logarithmic form, a linear relation between log X and log C is obtained (Equation 13). The slope is given by the value of n and the intercept is equal to log K_F.

$$\text{Log } X = \log K_F + n*\log C \qquad \text{(Eq.13)}$$

The above-mentioned linear equation can be used to assess whether the adsorption process satisfies the Freundlich isotherm and to identify the constants. If the adsorption results indicate a good linearity, the adsorption process may be considered to follow the Freundlich isotherm (Chung et al., 2015).

A major limitation of the Freundlich isotherm is represented by the fact that it does not describe a limit in adsorption capacity (Figure 8); that is, the amount of adsorbed may be infinite if the solute concentration increases (Suzuki, 1990).

2. Langmuir sorption isotherm

This isotherm was developed by Langmuir and is used to describe the equilibrium between the adsorbate and adsorbent in a monolayer surface coverage condition. It is considered to be an oversimplified model for numerous processes occurring in the environment. Nonetheless, this isotherm is considered as the foundation of most of the sorption theory and so provides important conceptual basis to understand this process (Ballantine et al., 1996).

The Langmuir isotherm model assumes a maximum sorption capacity (Figure 8) which means that the sorption is limited by the available sorption sites on the solid phase (Bharat, 2017). Additionally, it also considers a homogeneous sorption with a similar sorption activation energy for each site (Ballantine et al., 1996; Kundu & Gupta, 2006; Jin et al al., 2017; Al-Ghouti & Da'Ana, 2020). The Langmuir isotherm is defined as follows (Goldberg et al., 2007):

$$X = \frac{K_L * b*C}{1 + K_L*C} \qquad \text{(Eq.14)}$$

Where X is the solute concentration sorbed by the soil, b is the maximum sorption capacity (g/g) and C is the solute concentration in solution. K_L is the constant of Langmuir representing the strength at which the solute is bound to the subsurface (L/meq) (Goldberg et al., 2007).

Equation 14 can be rearranged into a linear equation as shown below (Rezakazemi & Zhang, 2018):

$$\frac{C}{X} = \frac{1}{b*K_L} + \frac{C}{b} \qquad \text{(Eq.15)}$$

A graph of C/X against C results in a straight line which determines the maximum sorption capacity from the slope (1/b) and the constant of Langmuir from the intercept ($1/b*K_L$).

The Freundlich isotherm is widely used for describing non-ideal and reversible sorption (Bharat, 2017). Unlike the Langmuir model, the Freundlich model is not limited to monolayer sorption, it is also applicable for heterogenous surfaces such as sediments. It is for this reason that the Freundlich isotherm model was considered for this Master thesis work, since the Langmuir isotherm, which assumes a homogeneous adsorbent surface, would not be appropriate to study the sorption on heterogenous formations (Jin et al., 2017).

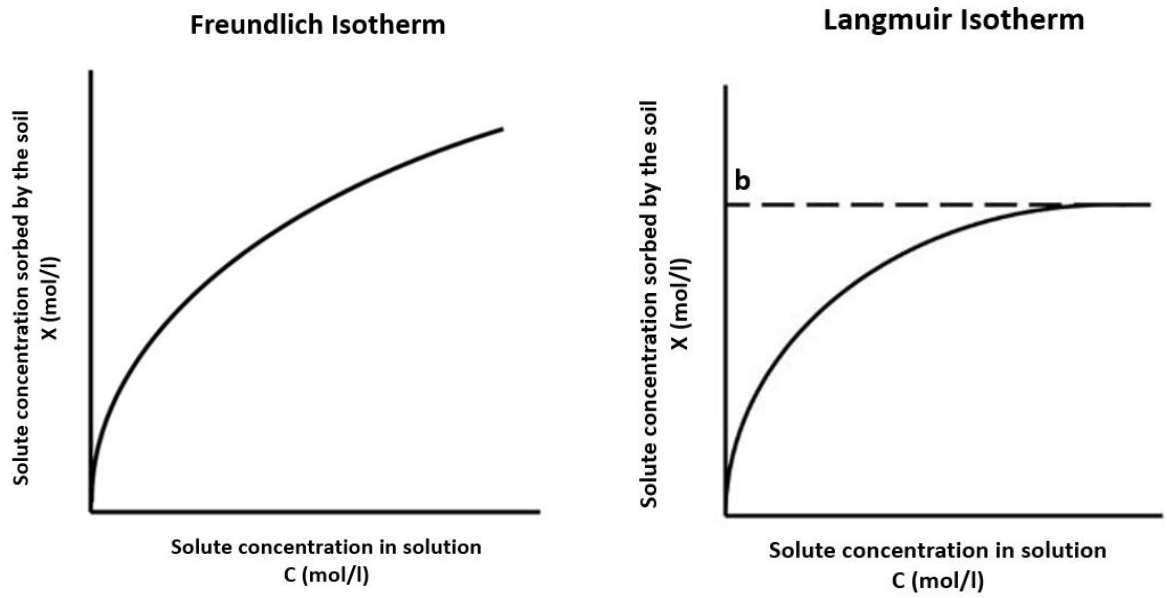

Figure 8: Sketch of the Freundlich (left) and Langmuir isotherms (right). X represents the solute concentration sorbed by the soil, C represents the solute concentration in solution and b is the maximum sorption capacity (g/g) (modified from Goldberg et al., 2007).

2.4.2. Redox processes

Reduction and oxidation reactions have a significant control on the concentrations and fate of O_2, Fe (II), Mn (II), etc. These processes are the results of electron transfer (from one atom to another) which usually is very slow and may only proceed at important rates when mediated by bacterial catalysis (Appelo & Postma, 2005).

The redox processes can proceed through two paths, a homogeneous and a heterogeneous path. The homogeneous system refers to reactions where the reactants and products are in one phase, such as the liquid phase. In contrast to the homogeneous path, the heterogeneous system reflects

to the presence of catalyst and substrate in one or more phases, such as a liquid and a solid phase (Schwartz, 1985).

The rate of a reaction can be determined by measuring the change in the concentration of a reactant with time as expressed in the following equation (Appelo & Postma, 2005):

$$Rate = \frac{\Delta concentration}{\Delta time} \qquad \text{(Eq. 16)}$$

In which Δconcentration represents the difference between the concentration of the reactant between a time interval t_2-t_1 (Δtime).

The determination of the reaction rate is crucial to establish the order of reaction which enables the classification of chemical reactions in zero, first or second order kinetics (Figure 9) (Appelo & Postma, 2005).

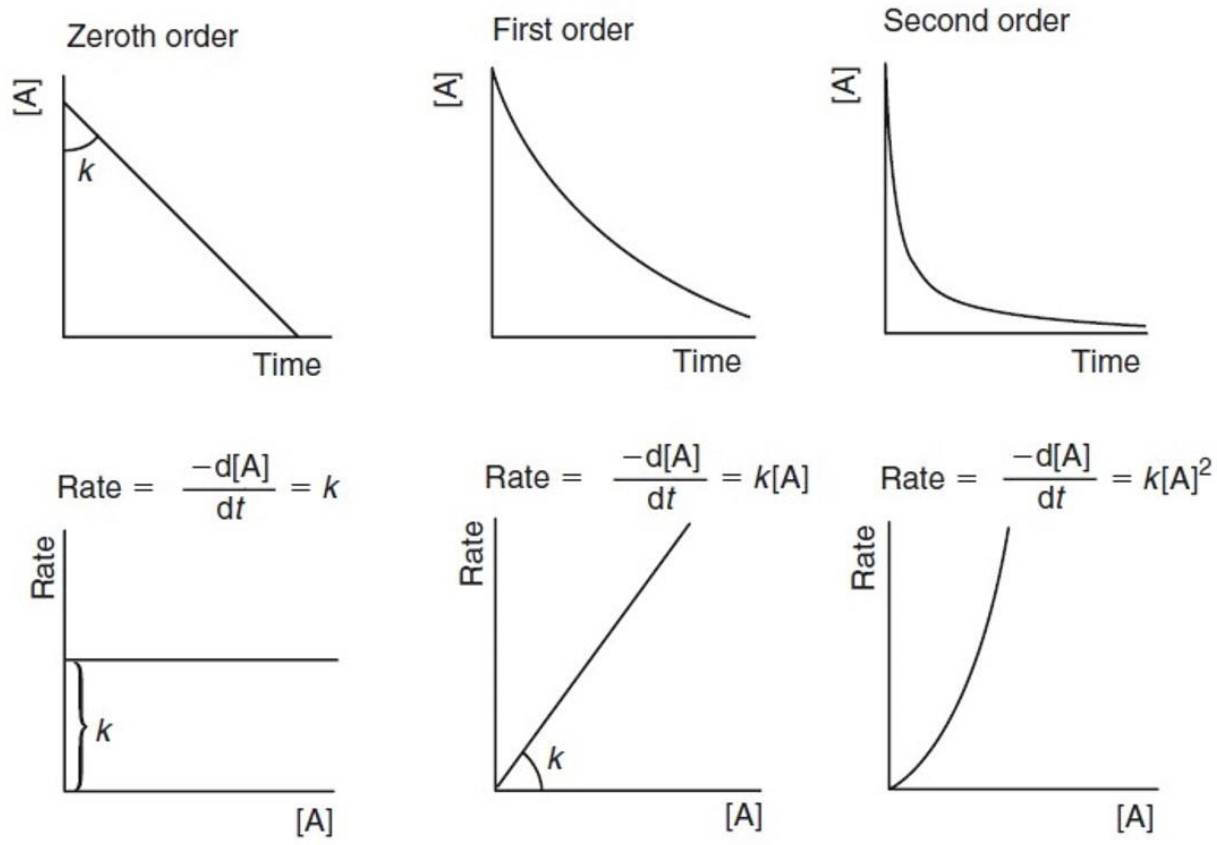

Figure 9: The rate laws and the reaction orders for the reaction A→B. A and B represent the reactant and product of the reaction respectively. The rate is given a negative sign because the slope is negative as the reactant decreases during the reaction. K is the rate constant and is equal to the reaction rate when all the reactant compounds are present at unit concentrations (Appelo & Postma, 2005).

a. Iron oxidation kinetics

The oxidation of Fe (II) to Fe (III) by O_2 is a perplex process that involves many partially oxidized Fe intermediate species that are complicated to characterize or predict during the oxidation reaction. These Fe intermediate forms evolve into more stable Fe oxide end-products such as goethite and lepidocrocite (Morgan & Lahav, 2007). The environmental conditions during the oxidation of Fe (II), in particular the pH, temperature, organic matter, the solution composition and the oxidation rate (Stumm & Lee, 1961; Theis & Singer, 1974; Sung & Morgan, 1980; Morgan & Lahav, 2007) will control the exact end-products of the process (Morgan & Lahav, 2007).

The oxidation of Fe (II) at low pH in the environment has long been acknowledged as biologically remediated process while in abiotic conditions the oxidation is kinetically very slow (Colmer & Hinkle, 1947; Baker & Banfield, 2003). Although, at approximately neutral pH levels under constant pressure of oxygen, the abiotic oxidation of Fe (II) is generally fast as Fe (II) is able to form redox-active hydrolysis species (Stumm & Morgan, 1996). The rate law applicable with such conditions and with O_2 as the electron acceptor is expressed as follows (Stumm & Lee, 1961; Tamura & Nagayama, 1976; Singer & Stumm, 1970; Stumm & Morgan, 1996):

$$-\frac{d[Fe^{2+}]}{dt} = k[Fe^{2+}][O_2][OH^-]^2 \qquad \text{(Eq. 17)}$$

Where $d[Fe^{2+}]/dt$ represents the rate of Fe (II) oxidation in mol/l/mn. K is the reaction rate constant and is equal to 8.0 (+/- 2.5) * 10^{13} $L^2/mn/atm/mol^2$ at 25° C. $[O_2]$ is the partial pressure of oxygen, $[OH^-]$ is the concentration of hydroxide ion in mol/l and $[Fe^{2+}]$ is the concentration of Fe (II) in mol/l.

From the rate equation (Equation 17), the oxidation of Fe (II) may be considered as a first order reaction with respect to Fe (II) and oxygen but second order with respect to the hydroxide ion. The oxidation of Fe (II) is also considered to follow a pseudo first-order kinetic as presented below (Millero et al., 1987):

$$-\frac{d[Fe^{2+}]}{dt} = k_1[Fe^{2+}] \qquad \text{(Eq. 18)}$$

Where k_1 is the pseudo-first order rate constant and is strongly dependent on pH.

Millero (1985) discussed the pH dependency of the speciation of Fe (II) which is described in the following hydrolysis equilibria:

$$Fe^{2+} + OH^- \rightarrow Fe(OH)^+ \qquad \text{(Eq. 19)}$$

$$Fe^{2+} + 2OH^- \rightarrow Fe(OH)_2^0 \qquad \text{(Eq. 20)}$$

$$Fe^{2+} + 3OH^- \rightarrow Fe(OH)_3^- \qquad \text{(Eq. 21)}$$

This implies that more than one oxidation reaction is occurring in solution contrary to what is considered for the rate equation presented in equation 17. Consequently, the oxidation reaction of Fe (II) includes various parallel reactions involving different Fe (II) species:

$$Fe^{2+} + O_2 \xrightarrow{\mathbf{K_{Fe}}} Products \qquad \text{(Eq. 22)}$$

$$Fe(OH)^+ + O_2 \xrightarrow{\mathbf{K_{FeOH}}} Products \qquad \text{(Eq. 23)}$$

$$Fe(OH)_2 + O_2 \xrightarrow{\mathbf{K_{Fe(OH)_2}}} Products \qquad \text{(Eq. 24)}$$

$$Fe(OH)_3^- + O_2 \xrightarrow{\mathbf{K_{Fe(OH)_3}}} Products \qquad \text{(Eq. 25)}$$

Considering all these reactions, the overall Fe (II) oxidation rate includes the sum of the oxidation rates of individual Fe (II) species is expressed as (Millero 1990, 1992):

$$-\frac{d[Fe^{2+}]}{dt} = k_{app}[Fe^{2+}][O_2] \qquad \text{(Eq. 26)}$$

Where $k_{app} = 4(K_1\alpha_{Fe^{2+}} + K_1\alpha_{FeOH} + K_1\alpha_{Fe(OH)_2} + \ldots\ldots K_n\alpha_n)$ and α represents the molar fractions of the Fe species.

In addition to the pH and the above-mentioned factors, the Fe (III) hydroxide precipitates also influence the oxidation rate of Fe (II) (Tamura & Nagayama, 1976; Tüfekci & Sarikaya, 1996). Indeed, it has been showed that Fe (II) oxidation rate linearly increases with Fe (III) concentrations up to 600 mg/l (Tamura & Nagayama, 1976; Tüfekci & Sarikaya, 1996), although no noticeable catalytic effect was observed past this concentration (Tüfekci & Sarikaya, 1996). Therefore, with the presence of Fe (III) the oxidation reaction of Fe (II) will proceed along two processes. The first process is a homogeneous reaction that takes place in solution while the second process, a heterogeneous reaction, occurs on the surface of ferric hydroxide precipitates (Tüfekci & Sarikaya, 1996). The rate equation expressing these two reactions under constant O_2 concentration and pH is given as (Tamura & Nagayama, 1976; Sung & Morgan, 1980; Tüfekci & Sarikaya, 1996):

$$\frac{-d[Fe(II)]}{dt} = (k + k'[Fe(III)])[Fe(II)] \qquad \text{(Eq. 27)}$$

Where k is the rate constant for the homogeneous reaction and is equal to $K_o[O_2][OH^-]^2$. k' is the rate constant for the heterogenous reaction and is determined by $k_{s,o}[O_2]K_{Fe} / [H^+]$.

K_o and $K_{s,o}$ are the real rate constant and K_{Fe} represents the equilibrium constant for the adsorption of Fe (II) on Fe (III) hydroxide.

The oxidation rate of Fe (II) increases in the presence of Mn (II) as was observed in Luo et al. (2018) but the presence of Mn oxides can also enhance the Fe (II) oxidation and the formation of Fe oxides (Postma, 1985) through the adsorption-oxidation process of Fe (II) on the negatively charged surfaces of Mn oxides (Luo et al., 2018). However, laboratory investigations of Fe (II) adsorption on oxides and hydroxides are highly challenging due to the high oxidation rate of Fe (II) by O_2 (Morgan & Lahav, 2007; Piasecki et al., 2019). Therefore, to deepen the knowledge about these processes, all the experiments require to be conducted in anaerobic conditions and where even the prepared solutions have not had any contact with oxygen. This is what makes the experiments very complicated (Piasecki et al., 2019).

The adsorption of Fe (II) is believed to have a different mechanism depending on the type of oxides, ferric or non-ferric oxides (Hiemstra & Riemsdijk, 2007). The globally accepted hypothesis is that the adsorption of Fe (II) on Fe oxides (such as Fe_2O_3) can be easily oxidized through the transfer of an electron from the adsorbed Fe (II) to the solid phase creating a Fe (III) ion that will hydrolyze (Tronc et al., 1992; Stumm & Sulzberger, 1992; Coughlin & Stone, 1995; Hiemstra & Riemsdijk, 2007). Whereas the adsorbed Fe (II) bounds without electron transfer on non-ferric oxides, such as titanium dioxide (Hiemstra & Riemsdijk, 2007). However, the recent findings of Piasecki et al. (2019) indicates that the mineral composition of soils or rocks does not control the fate of Fe (II). Indeed, the latter is mostly dependent on the solution properties such as pH, temperature, redox potential and aerobic or anaerobic conditions.

b. Manganese oxidation kinetics

The Mn (II) oxidation process is expected to be more complex than the Fe (II) oxidation as Mn can be oxidized in more than one form: Mn (III) and Mn (IV) (Hem, 1963). Mn (II) is thermodynamically instable in the pH range of natural waters in presence of O_2 as expressed by the following equations (Diem & Stumm, 1984):

$$Mn^{2+} + \frac{1}{4}O_2 + \frac{3}{2}H_2O \rightarrow MnOOH + 2H^+ \qquad \text{(Eq. 28)}$$

However, Mn (II) remains in oxic conditions as a result of its sluggish oxidation kinetics (Diem & Stumm, 1984) in addition to the reduction of Mn (IV) and Mn (III) by organic compounds

(Sunda et al., 1983). The oxidation of Mn (II) consists of a homogeneous and a heterogeneous process. This oxidation process by O_2 is an autocatalytic reaction induced by the adsorption of Mn (II) onto the surface areas of Fe-oxides or onto the reactive sites of newly formed sites (Morgan, 1964 as cited in Davies & Morgan, 1989). The Mn (II) oxidation and its kinetics have been the center of attention of many studies (e.g. Hem, 1963; Diem & Stumm, 1984; Ren et al., 2013; Huang & Zhang, 2020). Under pseudo first order conditions (excess of oxidant), the rate law for the Mn (II) oxidation by O_2 in an aqueous solution is formulated as follows (Diem & Stumm, 1984):

$$-\frac{d[Mn(II)]}{dt} = k_1[Mn(II)] + k_2[Mn(II)][MnO_x] \qquad \text{(Eq. 29)}$$

Where K_1 is the homogeneous reaction rate constant and is equal to $K_1'[O_2][OH^-]^2$ (in $l^2/mol^2.atm.mn$). K_2 is the heterogeneous reaction rate constant and is equal to $K_2'[O_2][OH^-]^2$ (in $l^2/mol^2.atm.mn$). $[MnO_x]$ is considered as $[Mn\ (II)]_0 - [Mn\ (II)]$, with $[Mn\ (II)]_0$ referring to the initial concentration of Mn (II).

From the K_1 and K_2 equations, it can be observed that the oxidation reaction is highly influenced by the O_2 concentrations in the solution and strongly pH dependent. The rate equation (Equation 29) expresses the physico-chemical oxidation of Mn (II) and entails that the homogeneous oxidation of Mn (II) involves a simple first order reaction (k_1) and is enhanced by the heterogenous autocatalytic activity of the Mn solid phase present in solution (Stumm & Morgan, 1996). In their article Diem & Stumm (1984) mentioned that this equation may still be used even if the initial oxidation of Mn (II) is homogeneous.

In the absence of Mn solid phase, the abiotic oxidation of Mn (II) by O_2 is kinetically very slow at pH levels below 9, consequently Mn (II) cannot be removed from drinking water (as the pH of most drinking water lies between 6.5 – 8.5 (WHO, 2007)) by only aeration and precipitation. Therefore, a Mn solid phase is needed to autocatalyze the Mn (II) oxidation process (Diem & Stumm, 1984; Luo et al., 2018). The presence of Mn (III) oxides and hydroxides are not the only solid phases that may influence the Mn (II) oxidation, indeed many other solid phases such as Fe oxides and silicates can catalyze the Mn (II) oxidation process (Junta & Hochella, 1994). Contrary to the abiotic oxidation of Mn (II), the biotically mediated oxidation is less pH dependent (Bruins et al., 2015.) as biological Mn removal was observed at a pH of 6.5 (Burger et al., 2008a, 2008b) and as low as 6.3 by Hoyland et al. (2014).

The rate equation model (Equation 30), widely used, considers firstly that the reactive surface area of a mineral is directly proportional to the total surface area (Steefel & Van Cappellen, 1990)

and secondly it assumes a homogeneous distribution of these reactive sites across the mineral (Steefel & Van Cappellen, 1990; Junta & Hochella, 1994). Based on these two assumptions, the rate model predictions are perceived as an oversimplification of a more complex crystal growth processes (Coughlin & Matsui, 1976; White & Peterson, 1990; Dove & Hochella, 1993) due to the possibility that the density of growth sites at the mineral surface may change with time (Steefel & Van Cappellen, 1990).

As mentioned, the Mn (II) oxidation rate is increased as a result of heterogeneous reactivity due to the presence of mineral surfaces in the environment (Hem, 1963; Coughlin & Matsui, 1976; Stumm & Morgan, 1996). The onset of this heterogeneous oxidation starts on the surfaces of the minerals present in solution or in the environment. With the adsorption process, one or more of the H_2O ligands is replaced (through the loss of protons) on the hydrated Mn ions which increases the rate of electron transfer from Mn (II) to O_2 (Coughlin & Matsui, 1976; Junta & Hochella, 1994). The following equation summarizes the process (Coughlin & Matsui, 1976):

$$[Mn(H_2O)_x]^{2+} \rightarrow [Mn(H_2O)_{x-y}(OH)_y]^{2-y+} + yH^+ \qquad \text{(Eq. 30)}$$

Where x expresses the number of ligands bonded to Mn.

With this reaction occurring, the charge of the ions is lowered, and the polymerization of the complex Mn ions arises. In the case other cations (including oxygen) are present in solution, they may as well be assimilated during the polymerization process which constitutes the precursor of Mn oxides that are formed upon oxidation at high pH levels. As shown in equation 31, the Mn oxides precipitates are generally hydrated, non-stoichiometric, and negatively charged due to the loss of protons during polymerization and oxidation. It is this negatively charged characteristic that allows the sorption of cations and play the role of catalyst for the oxidation process (Coughlin & Matsui, 1976).

A direct relation between the initial Mn (II) concentration adsorbed on the mineral surface and the oxidation rate with respect to the oxygen concentration was demonstrated by Davis and Morgan (1989). According the same study, two types of surface species were suggested by the adsorption models, a monodentate and bidentate complex. It was based on this speciation that Davis and Morgan (1989) were able to show that it is the Mn (II) bidentate surface complex that is reactive and not the monodentate complex.

Following the initial oxidation of the adsorbed Mn (II) at the surface of the mineral, the recently created site grows into the most reactive site for the continuation of the adsorption-oxidation process. Although the newly formed site will not control where the next adsorption-oxidation

reaction will happen, it will be dependent on the type of surface. For instance, in the presence of goethite or hematite, the adsorption-oxidation of Mn (II) continues at the new reactive site/solution interface resulting in a thin layer of precipitates that coat the whole mineral surface. Additional adsorption-oxidation reactions occur at the precipitate/solution interface which results in the creation of surface coating of microcrystallites that covers the entire surface of the mineral with precipitates (Figure 10 A). In comparison with the Fe oxides, the adsorption-oxidation reaction at the surface of albite for instance is different. Indeed, the early precipitation on albite is described by ridge development at the initial adsorption-oxidation site and where the ridge develops in both vertical and horizontal directions (Junta & Hochella, 1994). In the study carried out by Junta and Hochella (1994), the Mn (II) adsorption-oxidation experiment run on albite showed that even after months in solution, the albite surface was never entirely covered with precipitates as was observed for the Fe oxides (Figure 10 B).

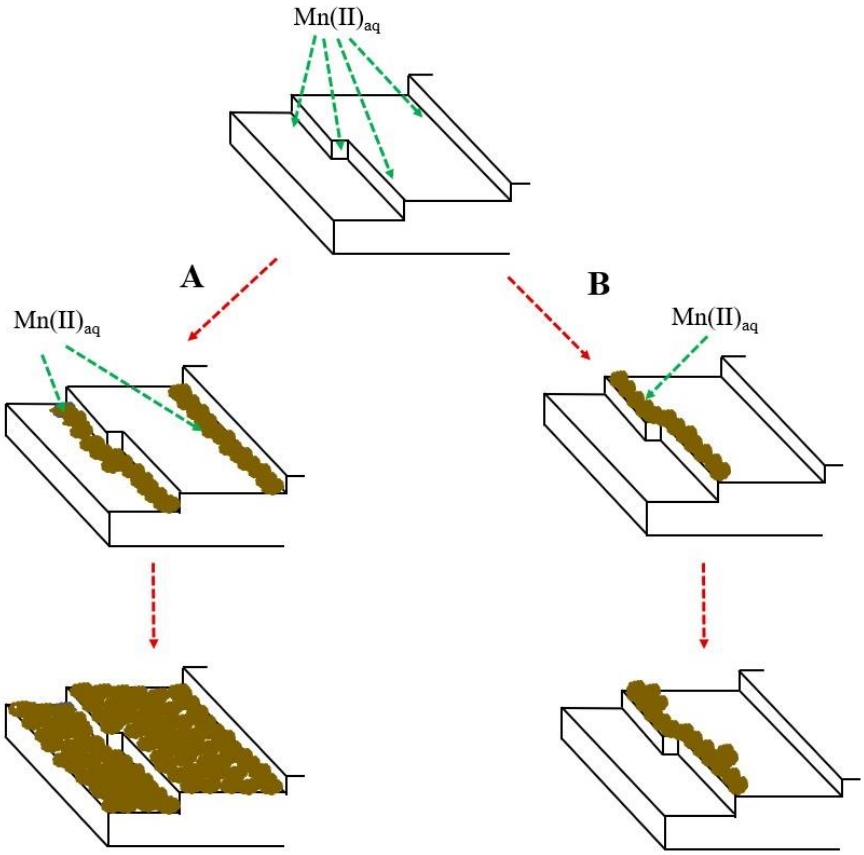

Figure 10: Schematic drawing showing the two pathways through which manganese ions precipitates on iron-oxides (pathway A) and on albite (pathway B) (modified from Junta & Hochella, 1994).

At low pH levels, Mn (II) is stable owing to its high charge which confers its repulsive force preventing the polymerization of the Mn ions (Coughlin & Matsui, 1976) therefore the adsorption-oxidation of Mn (II) is limited.

2.5. Vyredox method

2.5.1. Principle of the Vyredox method

The Vyredox method was developed in Finland by Veli and Yrjo Reijonen in the late 1960's (Seppanen, 1992).

The principle of this method is to oxidize the soluble Fe (II) and Mn (II) into Fe (III) and Mn (IV) (Figure 11). This method will oxidize the zone around the supply well by injecting oxygenated waters through injection wells surrounding the supply well. This oxidized zone will keep the pH and Eh high enough to precipitate the Fe and Mn in the sediments and will ensure that these metals will be retained by it; namely, the water that will enter the supply well is purified from Fe and Mn.

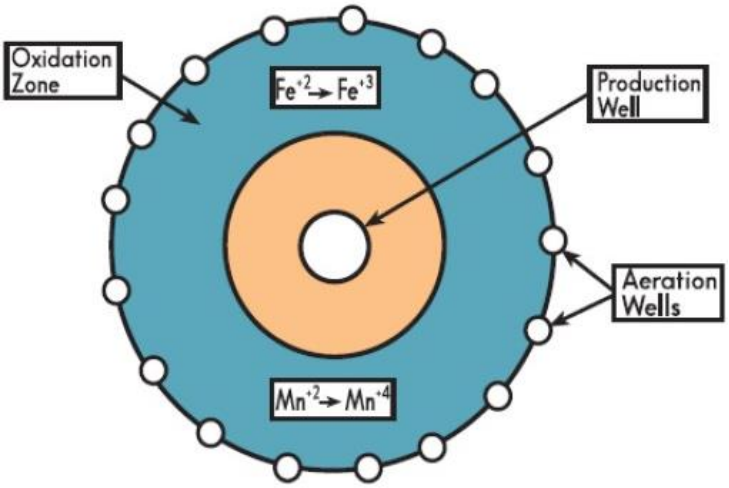

Figure 11: The disposition of the production and aeration wells for iron and manganese oxidation (Ahmed, 2012).

The application of the Vyredox method is illustrated in figure 12. The figure shows the redox gradient between the reduced and oxidized zones and where the Eh increases towards the supply well from – 100 mV to + 600 mV. Consequently, Fe precipitates first at the outer boundary of the oxidation zone which will results in an increase of Fe preferring bacteria, and so does the number of dead bacteria. The organic matter contained in the dead bacteria becomes a source of

carbon for the bacteria responsible for the Mn oxidation (Hallberg & Martinell, 1976). As the Fe and Mn precipitate, the boundary between the reduced and oxidized zones moves in the direction of the supply well allowing a distribution of the precipitates around the supply well. This results in a spatial separation between the formation of Fe oxides and Mn oxides, with the latter closer to the well (Figure 12) (Hallberg & Martinell, 1976).

In general, Fe is easier to remove from water than Mn, as Mn has a slower oxidation rate and has the tendency to form colloidal solids when rapidly oxidized (Morgan & Stumm, 1964). It is important to emphasize that abiotic oxidation of Fe (II) and Mn (II) might occur. However, in natural environments the oxidation of Mn (II) is mainly mediated by microorganisms (Butterfield et al., 2013) while the biotic oxidation of Fe (II) by microorganisms is responsible for up to 50 % of the Fe oxidation at circumneutral pH (Emerson et al., 2010).

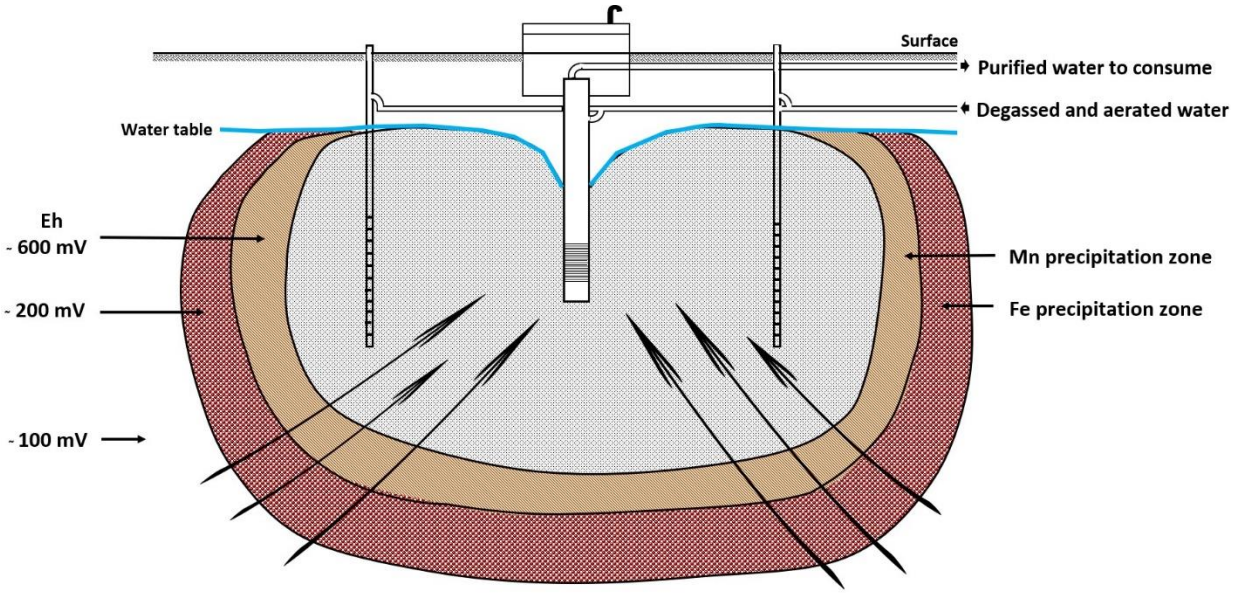

Figure 12: Vyredox method application and precipitation zone for iron and manganese during the treatment. The zones colored in red and in brown represent the precipitation zone of iron and manganese, respectively (modified from Hallberg & Martinell, 1976).

2.5.2. Vyredox method application in Elverum

There are 4 main pumping wells at Grindalsmoen water works. Each well has a production capacity of 60 l/s which means 6 million liters of water are produced every day for more than 16 000 people and the industry in the area (Elverum Municipality). A ring of 9 aeration wells is installed around every pumping well to inject and extract water from the aquifer. These wells are referred to as satellite aeration wells and are named from SB 1 to SB 9 (Figure 13).

The principle of this process is explained in the following steps (Jaudon et al., 1989):

- First, the pumping is stopped in the production well which will be treated.
- Water is pumped from two satellite wells e.g., SB1 and SB8 (Figure 13) at a rate of 6 l/s for two hours (h) (Papadimitrakis, 2019) then atmospheric air is incorporated to aerate the water in these two wells.
- The next step is to degas the aerated water in a tank to eliminate the non-dissolved oxygen and the oxygen-saturated water returns to the aquifer due to gravity through the well located between the above-mentioned wells (in this case, it is well SB9). This operation takes approximately 20 h and is repeated for all the other wells.
- The process is halted for about 4 h to achieve a high pH and redox potential in the aquifer. This is accomplished during the injection of the aerated water which helps maintaining a population of oxidizing bacteria that contributes to the precipitation of the metals by their activities. As a result, a high redox potential is upheld.
- Finally, the water is treated by UV light to ensure that the water is clean and safe. The water can be pumped from the treated supply well and directed towards the different facilities.

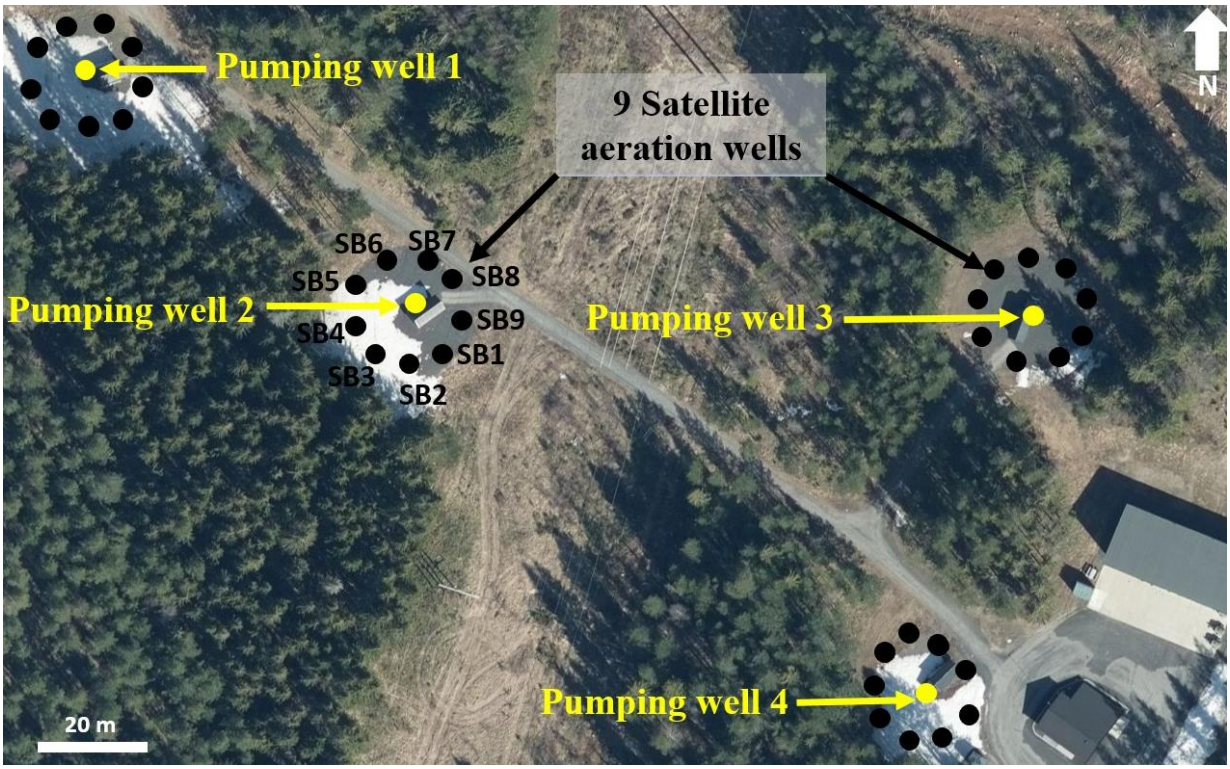

Figure 13: The setting of the production wells in Grindalsmoen waterworks. The pumping wells are pointed at with the yellow dot. Each production well is composed of 9 satellite wells and are shown in black dots.

3. Methods and materials

3.1. Geological sampling and weather condition

The samples were collected on the 17th of February 2020 between 11 am and 12 pm with temperatures ranging between 2° C to 7° C. The area surrounding the well stations, including the sampling point was covered in snow. The soil surface was to some extent frozen due the cold temperatures and snow therefore, the uppermost part of the soil was dismissed and not sampled.

The sampling was not carried out exactly where the wells are, but at close distance, around a hundred meters. Because the aquifer material from depth around the production wells was not available for sampling, therefore analogue sand samples close to the wells were used instead. The sampling point is situated South-West of the waterworks near the construction zone of the new road (Figure 14).

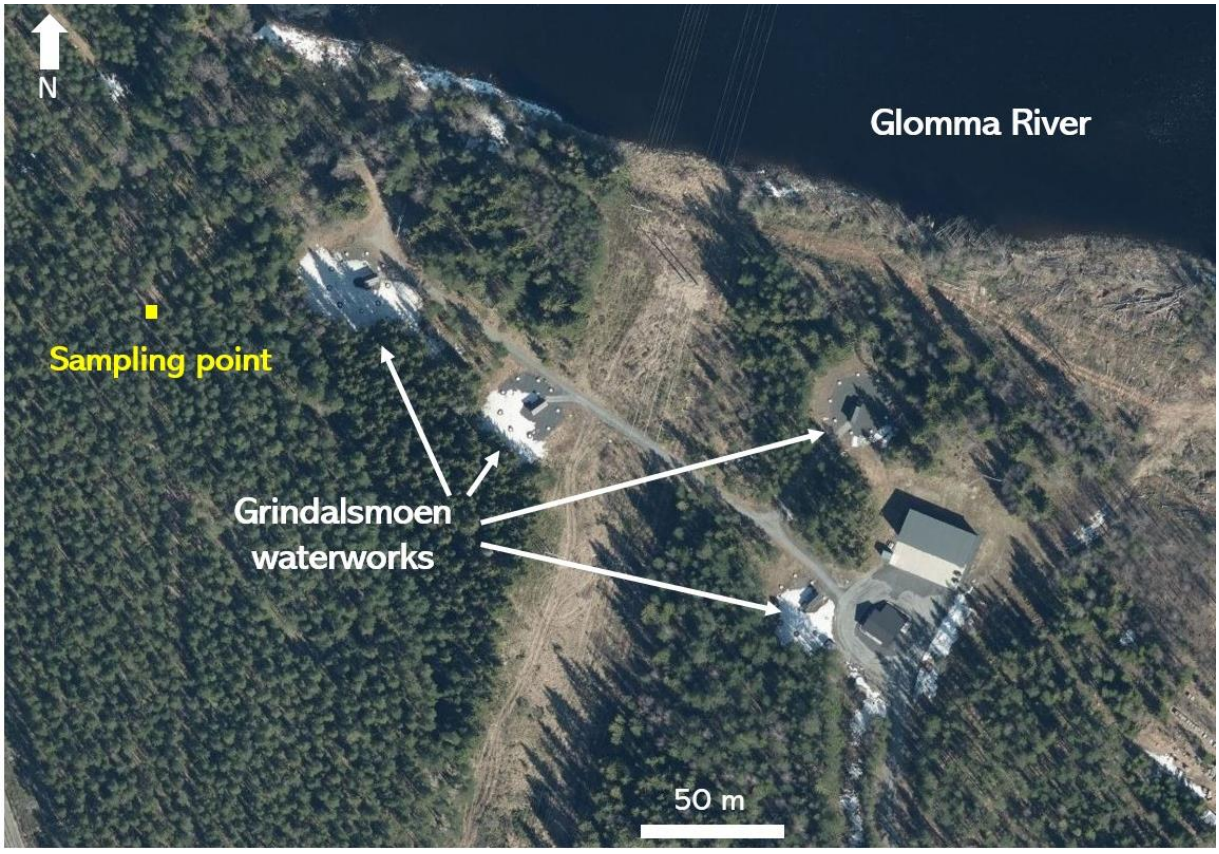

Figure 14: Position of the sampling point where the sand samples were collected in comparison with the location the four producing wells in Grindalsmoen waterworks (norgeskart.no).

The sampling was conducted at only one location but at different depths: 0-15 cm, 15-40 cm, 40-50 cm, 50-70 cm, 70-80 cm and 80-100 cm deep with a 120 cm long manual auger. This division was realized in accordance with the color and the texture of the sediment. The collected soil was stored in plastic boxes and brought to the sediment laboratory at the Department of Geology at the University of Oslo for treatment.

Immediately upon returning from the study area, all the sediment samples were oven dried in an Electrolux Intuition dryer and in a Heraeus dryer at 50° C – 60° C for at least 24 h. It is necessary to dry the soil before starting any treatment to remove the moisture from the soil as well as to avoid the aggregation of the particles.

3.2. Solid material characterization

3.2.1. Grain size analysis

The grain size analysis was performed manually, and each sample was analyzed twice. Each sample was mixed in order to be as homogenous as possible before starting the sieving process, also to dismiss any sources of variation in the results related with samples themselves. The material of the weighed portion is separated through a series of sieves with progressively smaller openings from 8000 µm to < 63 µm.

From the grain size distribution, the uniformity coefficient (Cu), the curvature coefficient (Cc) and the effective sizes (D10, D30 and D60) are calculated. The D10 or the effective grain size means that 10 % of the particles are finer and the rest 90 % of the particles are coarser than D10 size. D30 and D60 are defined in a similar way. The Cu and Cc represents a measure of a soil gradation. They are used to classify the soil as well or poorly graded (Lambe & Whitman, 1969). The Cu and Cc are defined as fellow:

$$Cu = D60/D10 \qquad \text{(Eq. 31)}$$

$$Cc = (D30)^2/D60 * D10 \qquad \text{(Eq. 32)}$$

For a soil to be well graded, the value of Cu must be higher than 6 and the value of Cc must be between 1 and 3. When Cu is less than 4, the soil is classified as poorly graded (Lambe & Whitman, 1969).

For the characterization of the sand sub-samples collected from Elverum and for the laboratory experiments, the solid material used was restricted to the grain size interval 250-125 µm. Therefore, all the sand sub-samples used for this thesis is between 250 and 125 µm.

3.2.2. Microscopy analysis

Scanning Electron Microscopy (SEM) was conducted to investigate the external morphology, the chemical composition and the structure of the material characterizing the collected samples. The objective was to identify the elemental composition at selected specific locations on the surface of the grains searching for Fe and Mn coating.

The SEM analysis was performed at the Geosciences Department, University of Oslo, with the collaboration of Senior Engineer Siri Simonsen. A Scanning Electron Microscope Hitachi SU5000 FE-SEM (Schottky FEG) with dual EDS (Energy Dispersive Spectroscopy), High resolution EBSD (Electron Backscatter Diffraction) and cathodoluminescence (CL) system was used.

The SEM uses high-energy electrons instead of light to form an image. These electrons are produced and directed towards the sample, where it interacts with the atoms in the sample and generates backscattered electrons (BSE) and secondary electrons (SE). These newly formed electrons are collected by a detector and converted into a signal that is sent to a computer monitor, thus producing an image. The secondary electrons are mostly used to show details of the morphology and surface topography of the grains, the backscattered electrons are used to illustrate contrasts in the sample composition (Nesse, 2000).

Sample preparation

- **Non-treated samples**

Samples from all the different depths were analyzed by SEM. The 6 specimens were not treated prior to the scanning but underwent the standard procedure preparation for SEM. Some grains were sprinkled on a sticky carbon tab then coated with carbon in order to reduce beam penetration and to generate sharper images (Vos et al., 2014). Carbon was chosen as coating material instead of other materials such as gold and tungsten, because carbon's X-ray peak does not interfere with the peak of other elements (Mukhopadhyay, 2003).

- **Treated samples**

After analyzing all the samples by SEM, only 2 samples were considered for the rest of the experiments. The samples from 0-15 cm and from 40-50 cm depth were selected for further studies as their distinctive colors (lightest and darkest soil color respectively) reflects the presence and amount of Fe oxides and hydroxides in the soil (Schwertmann & Cornell, 2000).

The treatment consists of synthesizing ferrihydrite according to the method described in Schwertmann and Cornell (2008). Ferrihydrite is the initial precipitation product, in goethite synthesis, resulting from the rapid hydrolysis of Fe (III) (Villacis- Garcia et al., 2015).

The method consists of adding relatively slowly a 1 M (molar) sodium hydroxide (NaOH) solution to 250 ml of 0.1 M iron nitrate ($Fe(NO_3)_3*9H_2O$) solution with constant and vigorous stirring until reaching a pH between 7 and 8. The resulting precipitate is repeatedly washed with Milli-Q water until reaching a conductivity of 20 µS/cm or below. Subsequently, the samples were freeze-dried and prepared for SEM analysis in the same way the untreated samples were. The experiment setup is portrayed below in figure 15.

The same experiment was repeated for different concentrations of $Fe(NO_3)_3*9H_2O$: 0.01 M and 0.001 M, to observe how the coating changes with the amount of Fe in solution.

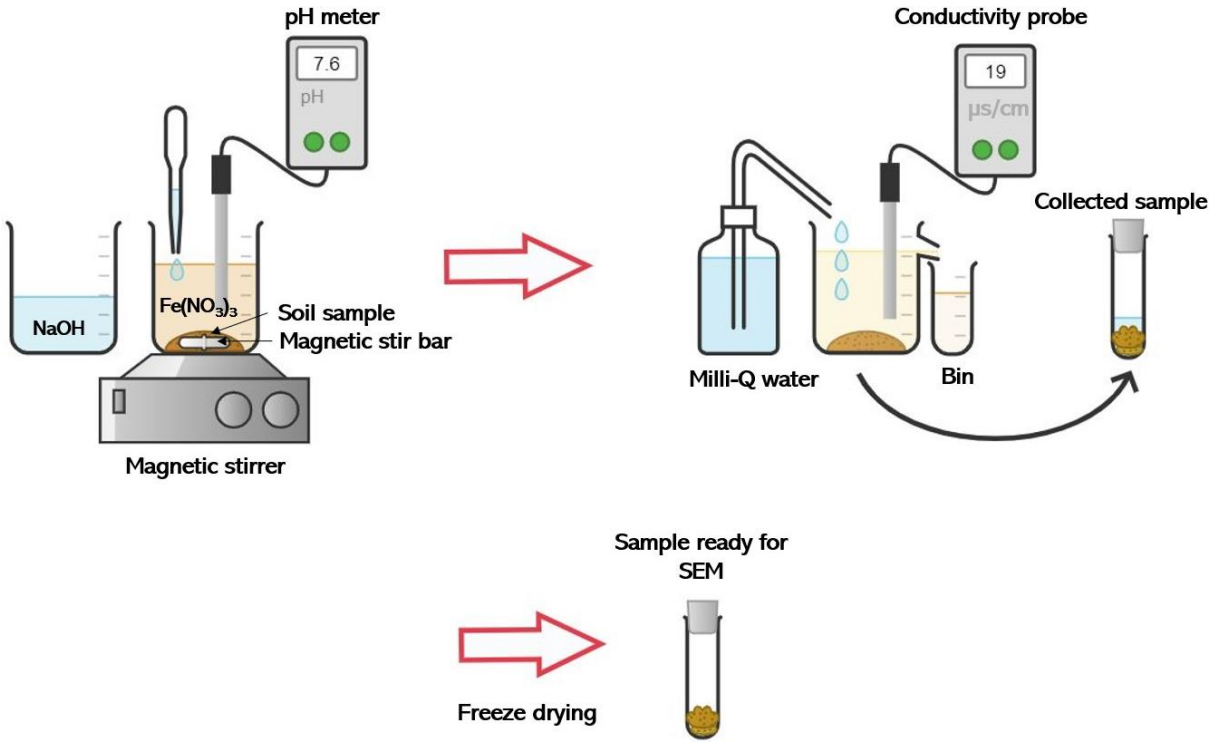

Figure 15: Schematic representation designed to illustrate the setup applied during the ferrihydrite precipitation treatment of the SD and SL sand samples for SEM analysis. In the first step, the iron is precipitated under constant stirring while adding a solution of NaOH to increase the pH of the solution. When a pH range of 7-8 is obtained the solution is washed with Milli-Q water until a conductivity of 21 µs/cm or less is reached. The samples are freeze dried and analyzed with SEM.

3.2.3. X-ray Diffraction

Principle

X-ray diffraction (XRD) is a non-destructive analytical method to analyze material properties such as mineral structure, phase composition and texture of solid, powder and even liquid samples. It is widely used for the identification of unknown mineral samples (Nesse, 2000; Chauhan & Chauhan, 2014; Bunaciu et al., 2015)

The XRD instruments consist of three basic components: An X-ray tube, a sample holder and an X-ray detector (Epp, 2016). X-rays are generated in a cathode ray tube where electrons are produced. The latter are used to bombard the sample material and the diffracted X-ray intensity is recorded by the detector which will convert the X-ray signal into a count rate. To achieve phase identification, the X-ray diffraction pattern is compared with the patterns of a reference database (Nesse, 2000; Epp, 2016).

Sample preparation

Sample preparation for XRD requires the appropriate sample treatment depending on the type of the sample. Bulk samples for XRD analysis need to be finely grained to obtain a good signal-to-noise ratio and minimize preferred orientation so to avoid intensity fluctuations. The advantage of using bulk or powder X-ray diffraction instead of an individual crystal is the high sensitivity of this method, resolution, the ease of data interpretation and statistical reliability as the beam covers more grains which means more intensity (Chauhan & Chauhan, 2014). The sample for the XRD analysis were prepared in accordance with the following criteria.

a. Dry milling:

This part consists of mechanically crushing the sediment for 2-3 minutes by using a high abrasion puck mill pulverizer. Before the grinding process, quartz is milled for 10 minutes before and after grinding the samples. Six samples, from the different depth intervals, of 10-15 g per samples were milled and stored in bags. Between each sample, the equipment was cleaned with water and ethanol to avoid any contamination.

b. Micronizing mill

The samples were micronized using a McCrone micronizing mill. The mill consists of a Teflon cup with 48 agate pellets (Figure 16) which are loaded into a holder that shakes the pellets at a high speed and reduce the grain size to < 10 µm.

Six samples of 3 g were poured into the Teflon cup and 10 ml of ethanol, a wetting agent, was added to reduce the lattice stain during milling. The samples were milled for 10 minutes then were transferred to a plastic container and placed in the oven at ~50° C to evaporate the ethanol from the sample.

c. Final step

After evaporation, the samples are reduced to powder with an agate mortar and the powder is pressed inside a back-loading sample holder, such as the ones in figure 17. To avoid sample orientation at the surface of the sample holder, the samples were gently pressed and flattened using a small glass plate.

Figure 17: the Teflon cup and agate pellets used during the wet milling of the samples. The sample and ethanol are poured on top of the pellets and the cup is firmly closed before inserting it in the micronizing mill.

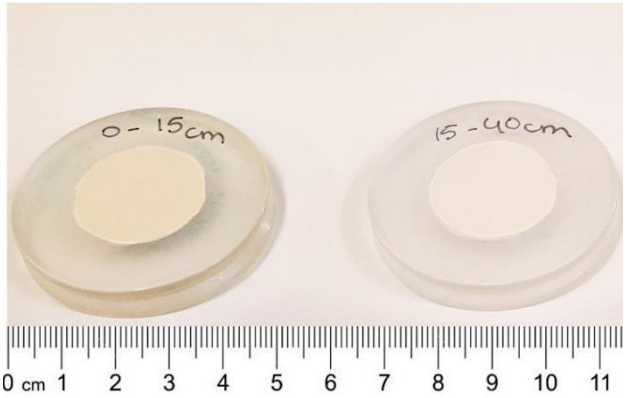

Figure 17: An example of the sample holders used during the XRD analysis. The white circle in the middle represents the sand sample in powder that were softly flattened by a glass plate.

Potential errors

Various potential sources of errors could be introduced during the sample preparation, it is for this reason that a proper sample preparation is crucial for a correct quantitative powder X-ray analysis (Machiels, 2010; Bunaciu et al., 2015). Primarily, if the samples are not correctly prepared the identification of the pattern would be difficult to determine, even impossible. As an example, if the sample is overgrinded the crystallite size decreases which causes an inaccuracy in crystallite size estimations. In the same way, undergrinding the sample may cause a preferred

orientation of the crystallite resulting in an insufficient peak intensity in certain reflections (Buhrke et al., 1998; Bunaciu et al., 2015).

Moreover, a cross contamination between the samples can be caused as a result of the inadequate cleaning of equipment. A small sub-sample from the collected sand in the field was selected for analysis, therefore, the result obtained might not be completely representative of the original sand sample.

The samples (six in total) were prepared with the help of Ibrahim Omar Khaled and the analysis was carried out with a Bruker D8 Advance XRD at the Institute for Geosciences at the University of Oslo, where Lars Riber interpreted the results with the use of Profex and Diffrac.EVA softwares

3.3. Chemical analysis: trace elements analysis

The Quadrupole Inductively Coupled Plasma Mass Spectrometry (ICP-Q-MS) is a highly useful instrument capable of determining trace elements at very low detection limit (Wolf & Tsai, 2005). The ICP-Q-MS uses an inductively coupled Argon plasma as a source of excitement to ionize the atoms in the samples and a quadrupole mass spectrometer to separate the ions by their charge-to-mass ratio. The ions are then directly transferred from the plasma to the detector to be counted and the software quantifies the concentration of each ion based on a reference material (Linge & Jarvis, 2009).

The ICP-Q-MS was used to analyze the concentration of Fe and Mn in the water samples resulting from different experiments explained below.

3.4. Laboratory experiments

From the six sand samples of different depths (0-15 cm, 15-40 cm, 40-50 cm, 50-70 cm, 70-80 cm and 80-100 cm deep) only two of them were considered for the chemical analysis: a sub-sample from the surface 0-15 cm and underneath 40-50 cm which will be named in the rest of the document as SD (dark sample) and SL (light sample) samples respectively.

This selection was made possible through the visual observation of the samples that allowed the detection of a clear change of the soil color pattern with depth. This change of color may indicate the composition of the soil and its horizons and can be the result of possible biological and chemical weathering, in particular redox reactions. The colors of the samples (light and dark) can reflect on the potential presence of Fe and Mn oxides and hydroxides in the soil. **These sand samples (SD and SL) were used as model material for the aquifer material in the in-situ Vyredox system at Grindalsmoen.**

With the purpose of understanding the behavior and sorption properties of Fe and Mn in the aquifer, the following experimental setup was designed:

1) Extraction of iron coating on sand material,
2) Sorption of Mn (II) onto aquifer material
3) Catalytic oxidation of Mn (II) to Mn (IV).

3.4.1. Iron extraction experiments

To estimate the concentration of Fe in soil, two different methods were applied (Darke & Walbridge, 1994):

a. The oxalate extraction method.
b. The Dithionite Citrate Bicarbonate (DCB) procedure.

The ammonium oxalate method was introduced by Tamm (1922,1923) (Rennert et al., 2021) . A mixture of ammonium oxalate and oxalic acid (Van Oorschot & Dekkers, 2001) is used for the removal of non-crystalline and organic matter Fe oxides in soils (Akinbola et al., 2013), and with the exception of magnetite, the crystalline forms are not dissolved (Chao & Zhou, 1983; Golden et al., 1994).

Solution preparation: the extraction solution was prepared as follows:

The extraction solution consists of a mixing 100 ml of 0.2 M ammonium oxalate and 75 ml of 0.2 oxalic acid. 0.4 g of the SD and SL sand sub-samples is added to 40 ml of the prepared mixture then shaked on high speed for 4 h. After a centrifugation that lasted for 12 mn at 4000 rpm, a volume of 2 ml was extracted and acidified with a drop 7 M of nitric acid (HNO_3) before analysis by ICP-MS.

The DCB method enables the dissolution of both organic matter Fe oxides (Akinbola et al., 2013) and the non-crystalline and crystalline iron oxides. Small amounts of Fe-bearing silicates can also be extracted during this procedure.

During this experiment, sodium-dithionite ($Na_2S_2O_4$) is added as a solid instead of a solution and it is used for its powerful reducing effect in order to reduce Fe oxides (III) to Fe (II). The pH is maintained between 7-8 by using a buffer, sodium-bicarbonate ($NaHCO_3$), to avoid important changes in pH. For instance, high pH values decrease the Fe oxide solubility and low pH values result in increased solubility of aluminosilicate (Figure 6). The sodium-citrate ($Na_3C_6H_5O_7$) is

added as a complexing ligand to avoid the reoxidation of Fe (II) after the reduction of Fe (III) (Ryan & Gschwend, 1991). Citrate-bicarbonate was added as a solution with a 4:1 ratio of sodium citrate: sodium bicarbonate.

Solution preparation: the extraction solution was prepared as follows:

0.8 g of 125 µm sieved soil was weighed into a 50 ml centrifuge tube and 0.8 g of $Na_2S_2O_4$ was added to flocculate the sample. A volume of 40 ml of citrate-carbonate solution was added to the sample then put on a shaker on high for 16 h. Centrifugation was carried out for 20 mn at 3500 rpm and the supernatant was decanted and analysed by ICP-MS. Before analysis, a drop of HNO_3 was added to the samples.

The amount of Fe extracted from the DCB method should be equal to or greater than the amount of Fe extracted by the ammonium oxalate method. The difference between the resulting values represents the amount of Fe present in definite crystalline forms (Akinbola et al., 2013).

The Fe activity index (Equation 33) indicates the degree of crystallinity of the soil was calculated for both sub-samples (McFadden & Hendricks, 1985; Jaworska et al., 2015).

$$\text{Iron activity index} = Fe_o / Fe_d \qquad \text{(Eq. 33)}$$

Fe_d and Fe_o represent the Fe extracted by the DCB method and oxalate method, respectively.

3.4.2. Manganese batch sorption experiments :

The sorption experiments were conducted on the sand sub-samples SD and SL only. The experiment was repeated two times for the purpose of comparing the results and to verify if the outcome of the experiments is consistent.

To conduct the experiments, two solutions were prepared: a background and a batch solution. The background solution consists of a 0.01 mol/l of sodium bicarbonate $NaHCO_3$ solution and is used to adjust the ionic strength and to stabilize the pH. The batch solution consists of a solution of manganese nitrate tetrahydrate ($Mn(NO_3)_2*(H_2O)_4$). For the first sorption experiment (Sorption 1), concentration of 0.1 g/l and 0.01 g/l of a solution of $Mn(NO_3)_2*(H_2O)_4$ were used for the first and second sorption experiments, respectively.

The volume of the $NaHCO_3$ solution used is fixed for all the prepared samples, while the volumes of $Mn(NO_3)_2*(H_2O)_4$ increase gradually in order to monitor the sorption of Mn with different initial Mn amounts in solution. The sorption experiments were carried out in a batch of 50 ml centrifuge tubes all containing 40 ml of the background solution and different volumes of Mn $(NO_3)_2*(H_2O)_4$ solution (10, 20, 50, 80, 100, 200, 300, 500, and 800 µl). To these tubes were

added 1 g of the sand sub-samples. Likewise, the higher volumes of Mn $(NO_3)_2$*$(H_2O)_4$ solution (1, 2, 5, and 10 ml) were added to 40 ml of the background solution but with higher sand mass (2 g). A higher amount of sand was added to increase the surface area as there is higher Mn nitrate solution in the sample.

The samples were centrifuged for 2 hours at 2500 rpm and 2 ml of the solutions were collected to which a drop of HNO_3 was added before analysis. The experimental setup for the sorption experiment is illustrated in figure 18.

Blank samples containing only the background and batch solutions were prepared for both sorption experiments and replicates were also realized for different samples. In total, 94 batch experiments samples were prepared for both sorption experiments for SD and SL sub-samples then analyzed by ICP-MS (Table 2 and Appendix III and IV).

Table 2: An example for the sample's preparation method for the manganese sorption experiments. The numbers in SD10, SL20, B80 and so on, represent the volume of $MnNO_3$ used during the preparation in µl. B represents the blank while SD and SL reflects respectively on the dark and light sand sample.

Sample	V_{NaHCO_3} (ml)	V_{MnNO_3} (µl)	Sand sub-sample (g)
SD10	40	10	1.0002
SD80	40	80	1.0005
SD800	40	800	1.0001
SD5000	40	5000	2.0003
SL20 (1)	40	20	1.0002
SL20 (2)	40	20	1.0001
SL100	40	100	1.0001
SL500	40	500	1.0003
B10	40	10	/
B80	40	80	/
B100	40	100	/
B500	40	500	/

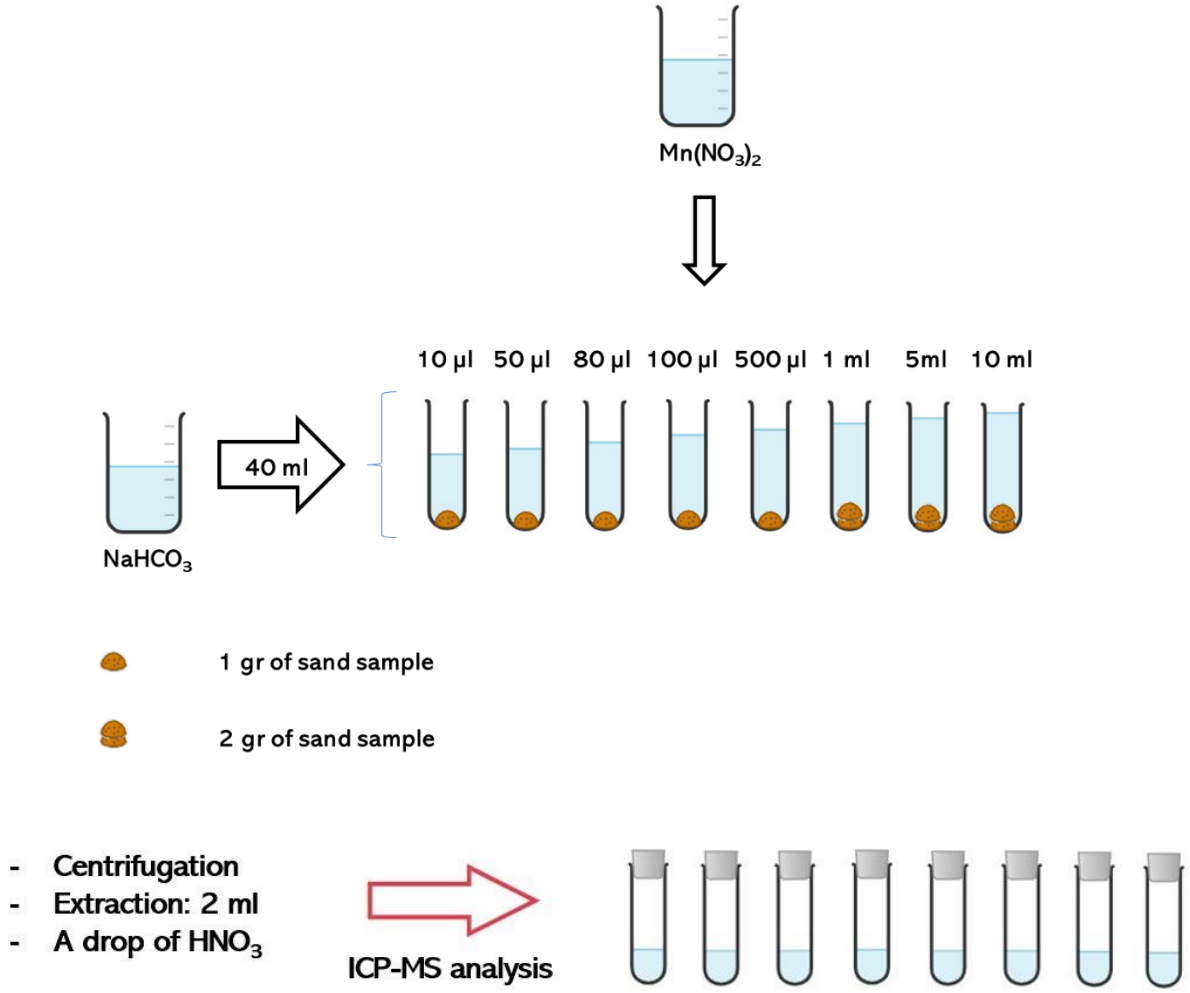

Figure 18: Sorption experimental setup designed for the sorption experiments carried out in the laboratory. The sample are prepared by adding a volume of a solution of $NaHCO_3$ to which is added 1 gr (or 2 gr) of the sand sample and a volume of a solution of $(MnNO_3)_2$. The samples then are centrifuged and analyzed by ICP-MS.

3.4.3. Mn catalytic aerobic oxidation

Mn oxidation experiments were conducted for both samples SD and SL at 2 different pH levels. The first experiment was conducted at a pH ranging between 8-10 while the second experiment was conducted at a lower pH value between 6-7. The decrease of pH was achieved by the addition of hydrochloric acid (HCl).

The oxidation of Mn performed in the laboratory is explained below in figure 19. For the experiment, two beakers are needed, one containing a mixture between a solution of $Mn(NO_3)_2$, a solution of $NaHCO_3$ and a solution of sodium azide (NaN_3). This sample is called later on the blank. The second beaker contains, in addition to the 3 solutions above-mentioned, the sand sub-

sample (either the SD or SL). The two beakers are connected to an air pump generator to maintain oxic conditions during the oxidation of Mn which assures a constant atmospheric partial pressure of oxygen during the experiments.

The solution of $NaHCO_3$ is used as background solution while the $Mn(NO_3)_2$ solution is the batch solution containing the Mn (II) ions intended to be oxidized. The NaN_3 solution is a biological inhibitor added to the preparation to achieve abiotic oxidation conditions.

The experiments were run for 3 to 5 days and sampled periodically to determine the residual concentration of Mn (II). The pH in both beakers is also monitored. The collected samples are acidified with HNO_3 before analysis with ICP-MS.

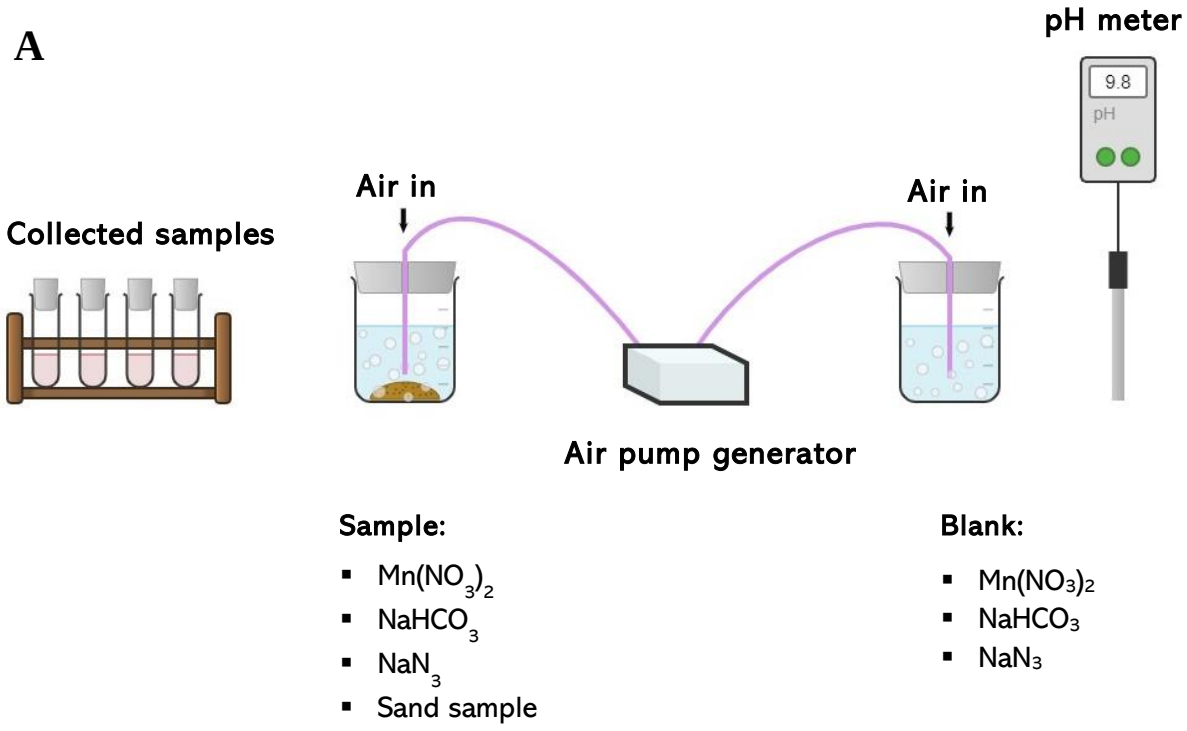

B

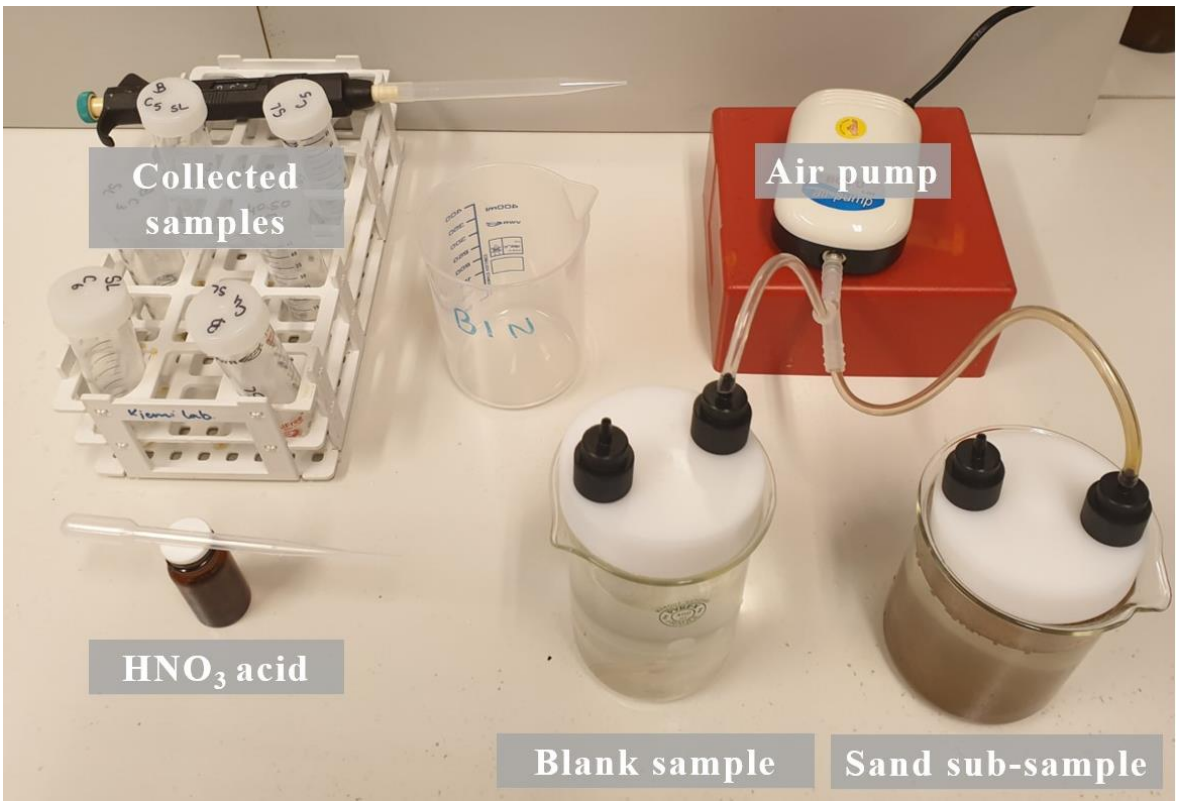

Figure 19: A) A model set-up for the catalytic oxidation of manganese. B) the experimental set-up for the oxidation experiments. The sample containing the sand sub-samples and the blank are connected to the air pump by tubes during the whole period of oxidation.

pH range 8-10

In terms of the oxidation experiments, 7.5 gr of soil sample was added to 300 ml of 0.01 mol/l $NaHCO_3$ and 10 ml of 10 mg/l of $Mn(NO_3)_2$. Moreover, NaN3 was added so that the final solution contains 2% of the biological inhibitor.

A blank sample was also prepared, which contained the same amount of $NaHCO_3$, $Mn(NO_3)_2$ solution, minus the sand sample.

pH range 6-7

The experiments at this pH range were carried out in the same manner as explained above, the only difference consists in the addition of 5.21 ml of 0.5% hydrochloric acid HCl to decrease the pH in solution. This part of the experiment is sensitive as the solution of $NaHCO_3$ is unstable at

this pH range. This means that the pH is not stable at one value but has been observed to vary between 6 and 7.

3.5. Geochemical modelling with PHREEQC

The geochemical modelling of Mn sorption and oxidation was performed with PHREEQC interactive version 3 for this study. PHREEQC is a numerical simulation code, written in the C and C+ languages broadly used for several aqueous geochemical modelling calculations. This program is based on equilibrium chemistry of aqueous solutions interacting with minerals, gases, solid solutions, and sorption surfaces. This program is also able to perform kinetic reactions modelling with rate equations. These kinetically controlled reactions can be defined by using Basic interpreter and the rate expressions are included in the input file where the Basic interpreter calculates the rates (Parkhurst & Appelo, 1999).

PHREEQC is provided with databases files such as *phreeqc.dat* and *wateq4f.dat* that contains different functions necessary for modelling kinetic reactions like Solution_Master_Species, Surface_Species and Phases. For instance, the *phreeqc.dat* database contains thermodynamic data for various chemical elements including Fe and Mn. The data is extracted from literature and is based on the element's chemical reactions and their equilibrium constant (Parkhurst & Appelo, 2013).

PHREEEQC scripts are organized as follows: data blocks start with a keyword followed by supplementary lines containing the data related to the keyword. At the beginning of a simulation, the keyword and the data lines are read by a database file in order to define the elements, reactions, mineral phases, gas phases etc. (Parkhurst & Appelo, 1999).

The output data file is created with the keyword data block "selected_output" which produces a file able to be processed by spreadsheets and other data-management software such as Microsoft Excel. Selected entities from the compositions of solution, exchange assemblage, gas phase and others, can be printed after the end of each type of calculation (Parkhurst & Appelo, 1999).

The modelling performed with PHREEQC consists of:

- Sorption of Mn (II) on sand using the Freundlich isotherm.
- Sorption of Mn (II) modelled as surface complexation on hydrous ferric oxide (Hfo) and organic matter in order to estimate its influence on the sorption process.
- Catalytic oxidation of Mn (II).

The PHREEQC script written for the modelling investigations are provided in the Appendices (Appendix VIIII, X and XI).

4. Results

4.1. Solid material characterisation

4.1.1. Grain size analysis and soil description

Grain size analysis was performed for each sample, the results are presented in figure 19 (A & B). The entire sediment column displays nearly a homogenous sediment distribution. Overall, the samples feature slight gravelly-sand characteristics with thinner material on the surface and coarser towards the bottom with an average content of 95.2 % sand, 2.8 % gravel and 2 % silt. Indeed, sand is the dominant grain size ranging from 93 to 96 %. The sand content increases slightly from the surface to the bottom where it reaches its maximum value (96.8 %) at 70-80 cm before decreasing around 100 cm (93.5 %).

The gravel content is more important in the deepest part of the column (between 80 and 100 cm) with 6 % while in the surface it reaches 1.9 %. The mud content exhibits the opposite trend with a higher percentage at the surface (0-15 cm) with 4.4 % and minimum at the bottom part (80-100 cm) with 0.5 %. The details of the grain size distribution are given in Appendix I and II.

A

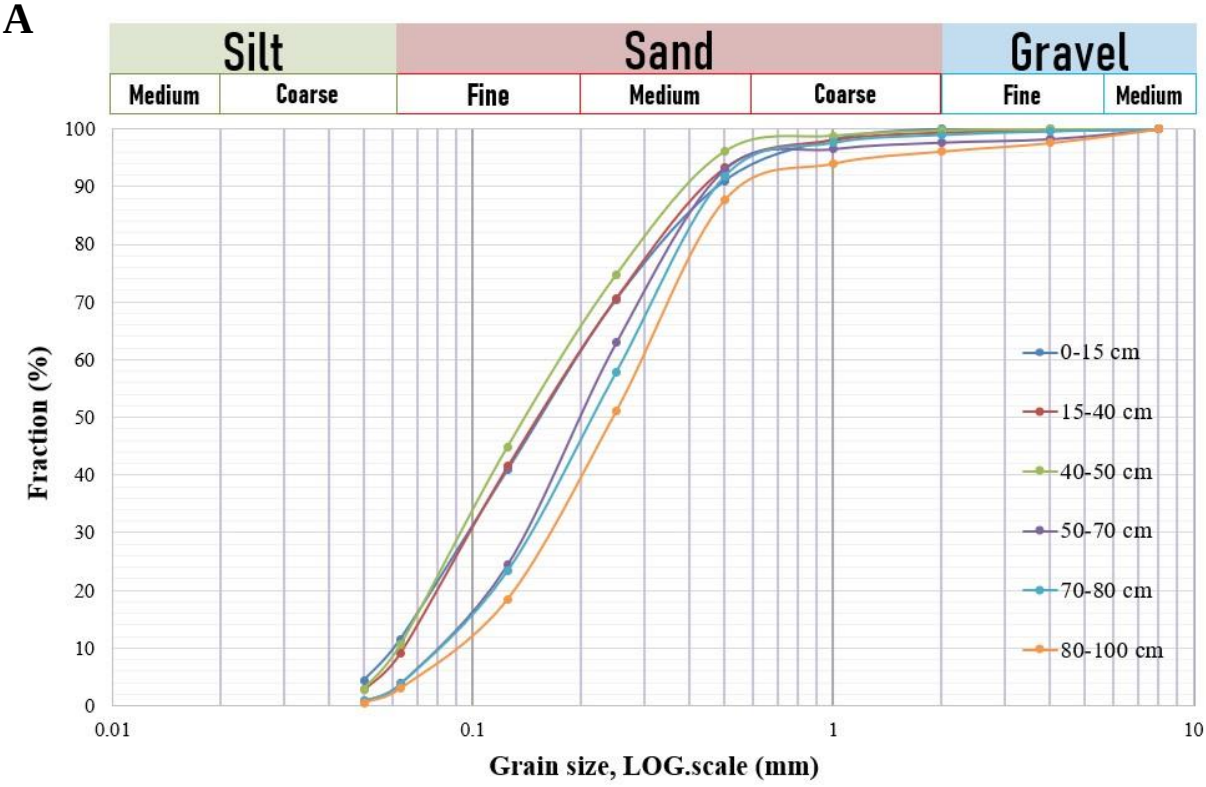

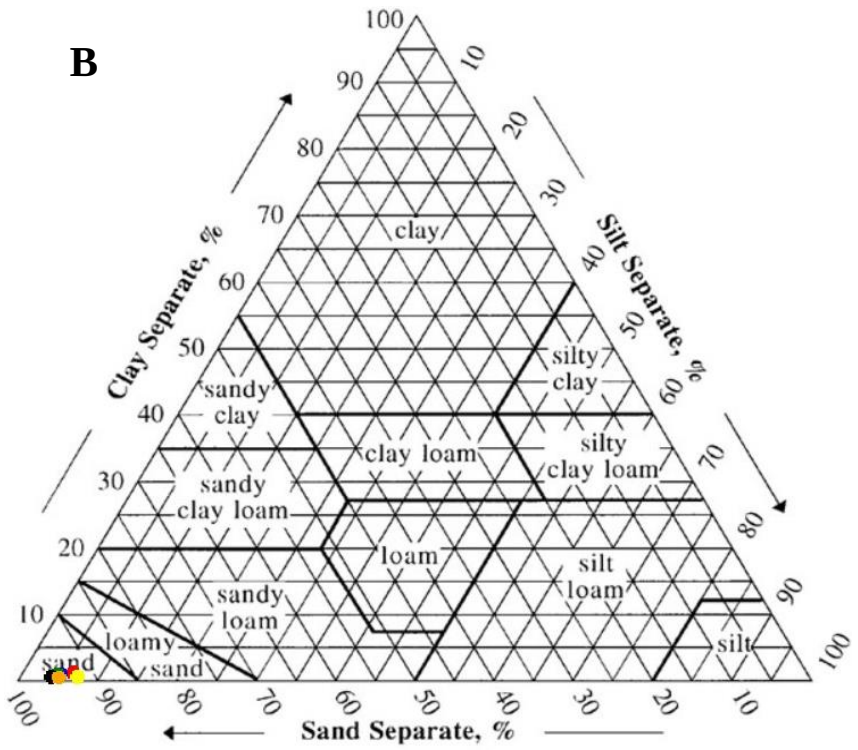

Figure 20: A- Grain size distribution for the collected samples. B- Soil textural triangle for the collected samples. The colored circles dots represent the different soil depth: Red for 0-15 cm, blue for 15-40 cm, green for 40-50 cm, orange for 50-70 cm, black for 70-80 cm and yellow dot for 80-100 cm.

The results from the grain size analysis are shown in table 3. The soil column presents 2 types of sediments, slightly gravelly sand for most of the column and gravelly sand for the bottom part. The results obtained from calculating the coefficient of uniformity and the coefficient of curvature are also presented in table 3. Generally, the soil samples can be summarized as well graded sand with minor gravel and silt fractions.

Table 3: Soil characteristics resulting from the grain size analysis of the sand samples collected in Elverum.

Soil depth (cm)	Sediment type	Coefficient of Uniformity Cu	Coefficient of Curvature Cc
0-15	Slightly gravelly sand	3.4	0.84
15-40		3.2	0.8
40-50		3.03	0.82
50-70		3	1.04
70-80		3.2	1.01
80-100	Gravelly sand	3.4	1.01

4.1.2. Mineral characteristics

a. Scanning Electron Microscopy SEM

Non treated samples

The Scanning Electron Microscopy investigations combined with an EDS spectroscopy conducted on all the sand sub-samples show Fe and Mn coating on the grain surfaces (Figure 21).

Figure 21 shows a backscatter SEM image of all the samples. The analysis showed the presence of different minerals such as quartz, chlorite, albite, ilmenite, titanomagnetite, apatite and amphiboles. The elemental composition analysis carried out on the samples shows a higher presence of Fe compared to Mn. However, the darkest and lightest samples (SD and SL respectively) did not show a notable difference in terms of Fe and Mn content in the samples. The Fe and Mn present in the samples does not consist in a uniform layer, but it is rather present as spots or grains. Phosphoric and aluminium coating were also observed.

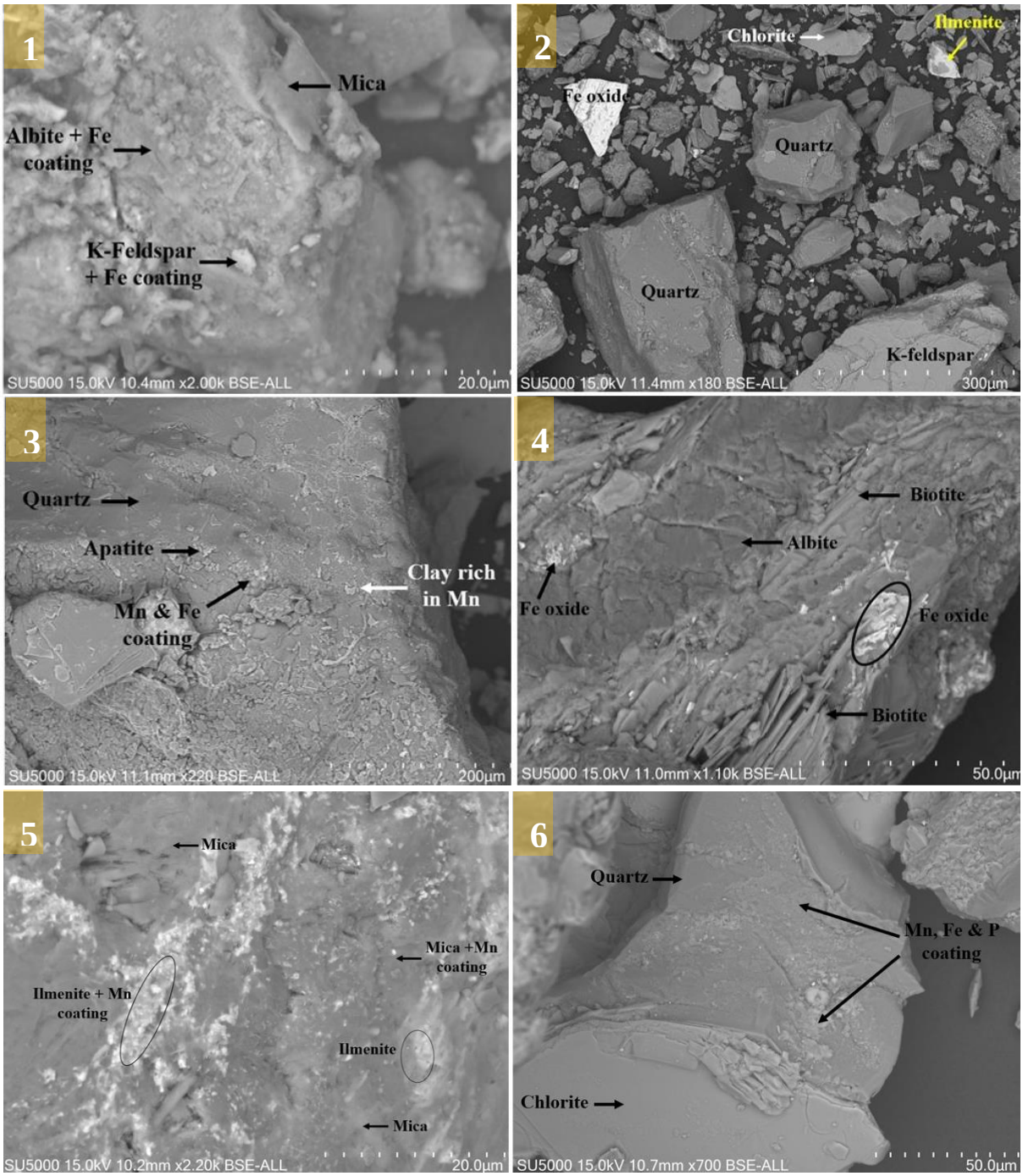

Figure 21: A representative backscatter image of all the samples: 0-15 cm (1), 15-40 cm (2), 40-50 cm (3), 50-70 cm (4), 70-80 cm (5) and 80-100 cm (6). Some of the main minerals are highlighted in the images.

Other minerals such as titanomagnetite (Fe^{3+}, $Ti)_2O_4$ and titanite ($CaTiSiO_5$) were observed in some samples (40-50 cm and 50-70 cm), in addition to amphiboles (Figure 22).

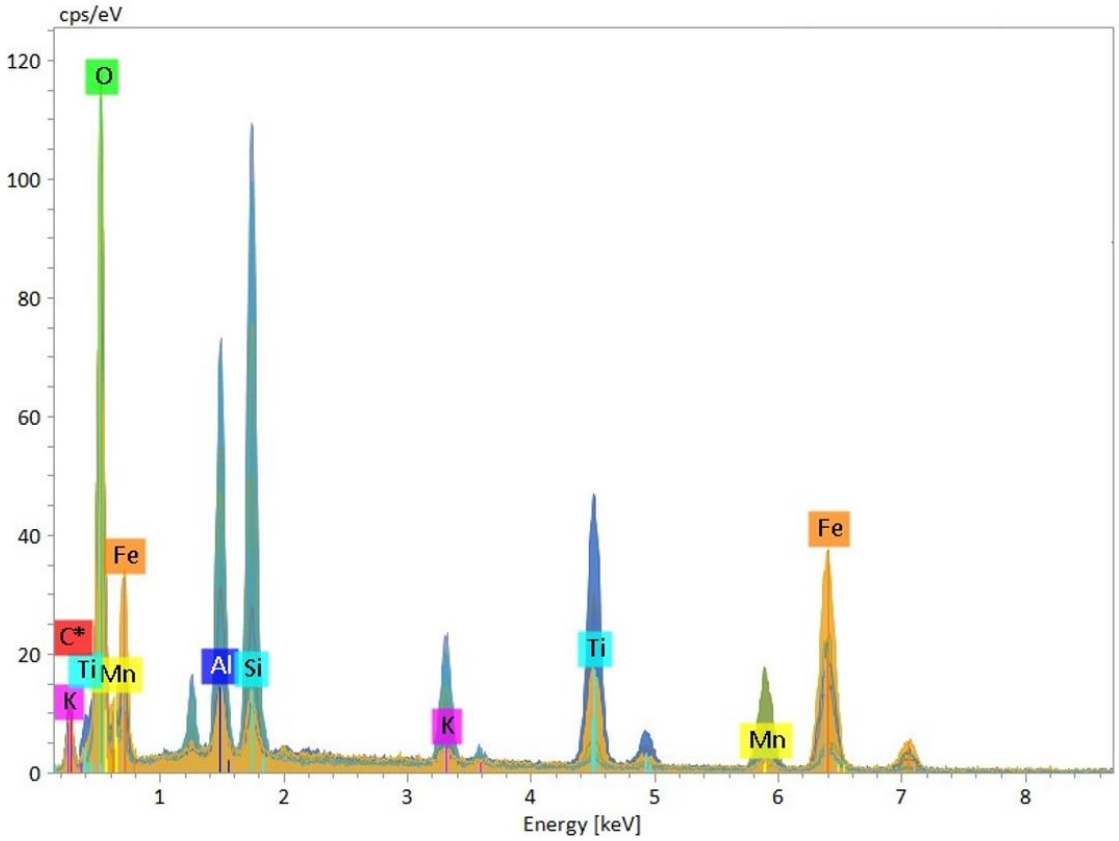

Figure 22: Cumulative element spectra for sample 70-80 cm. Different minerals can be deduced from the graph such as ilmenite ($FeTiO_3$) and titanomagnetite ($Fe^{2+}(Fe^{3+}, Ti)_2O_4$). Mn is also present in this sample as coating on top of mica and ilmenite.

Treated samples

Two SD and SL sub-samples underwent an Fe precipitation experiment with 2 different concentrations of $Fe(NO_3)_3$ solution, 0.01 and 0.001 M, the results are summarized in table 4.

Table 4: Description of the treated SD and SL samples with a solution of 0.01 M and 0.001 M of $Fe(NO_3)_3$.

SL 0.001 M	SL 0.01 M
➢ Dominant minerals: K-feldspar and quartz.	➢ Dominant minerals: quartz. albite, feldspar and kaolinite.
➢ Fe coating is observed but sporadically.	➢ Presence of organic material and a considerable amount of Fe coating.
➢ Fe and P always observed together.	➢ Some brown-coloured grains were observed: rich in Fe

SD 0.001 M	SD 0.01 M
➢ Dominant minerals: quartz, kaolinite, and albite.	➢ Dominant minerals: quartz, chlorite, and albite.
➢ The observed, brown-coloured grains were rich in organic material covered in Fe.	➢ The type of mineral was hard to detect as most of the grains were highly covered with organic material.
➢ The examined colourless grains seldom contained Fe.	➢ Very high amounts of Fe and P were observed in all the examined grains.

The analysis showed that both samples (SD and SL) contain kaolinite and chlorite, but they mainly consist of quartz, k-feldspar and albite. The analysis also showed the presence of clay minerals and organic material. These 2 samples were chosen depending on their colour. Thereby, colourless and brownish-reddish grains were explored during the SEM analysis. The numerous coloured grains were found to be covered by organic material rich in Fe while the colourless grains were cleaner and not much material were observed.

The detailed analysis of the SD and SL samples showed that the dark coloured sample contains more Fe and Mn compared to the light-coloured sample. In the same way, the experiments realized with the highest concentration of $Fe(NO_3)_3$ resulted in more Fe coating on top of the grains, as the solution contained higher amount of Fe.

A mapping of different element's distribution such as Fe, P and Si for the SD and SL samples is shown in Figures 23 and 24. Areas with high Na and K amount probably represents albite and K-feldspar respectively. While the distribution of Si and Fe likely represents quartz and Fe oxides. The mapping for P was also added to compare the distribution of both Fe and P.

The SEM investigations conducted on the surface of the grains in the SL sample showed a very limited and irregular coating on the grain surfaces. It also indicated that the part of the surface covered with coating was mainly Fe and P (Figure 23).

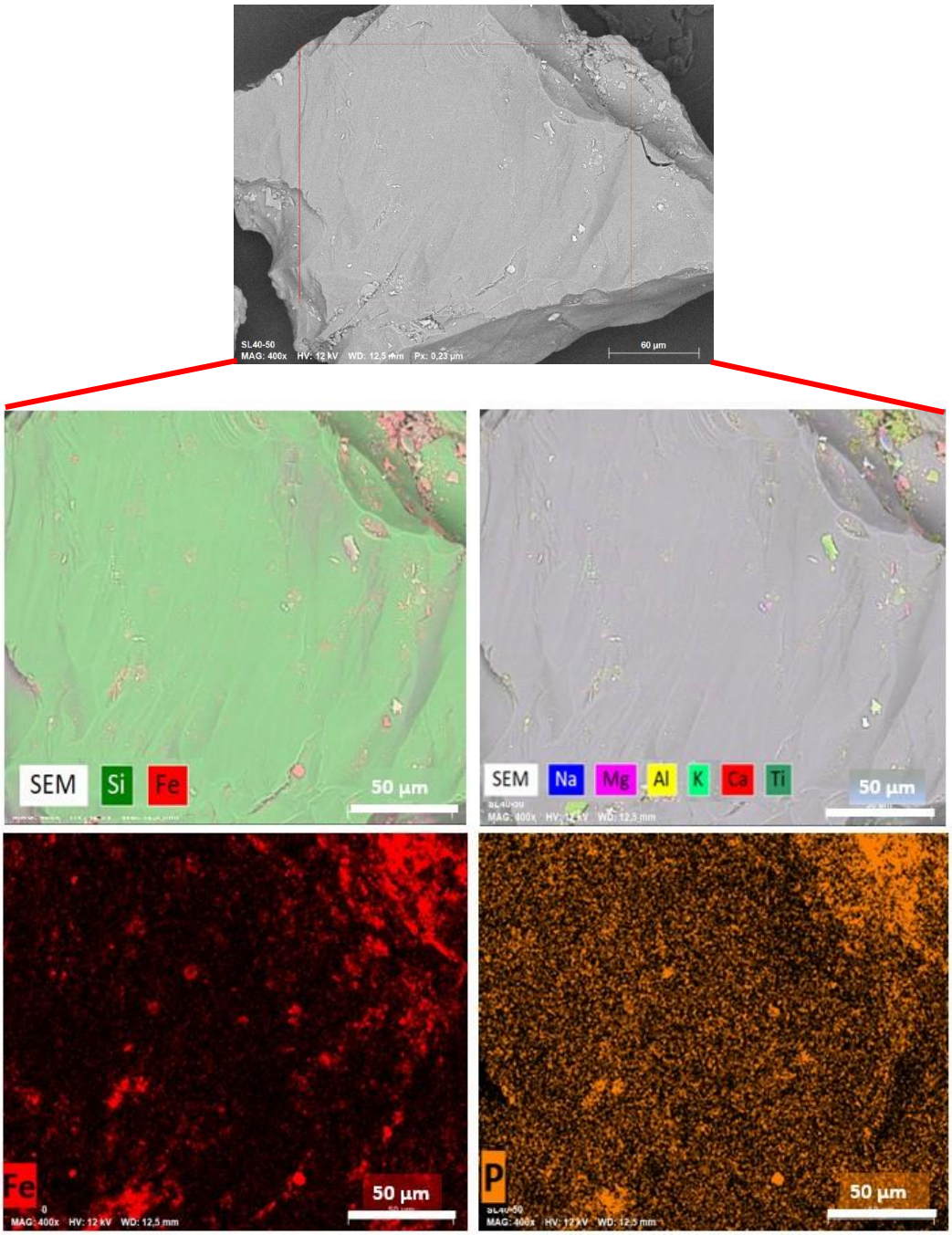

Figure 23: Mapping of the SL sample, showing the distribution of Si, Fe, P, Na, Mg, Al, K, Ca and Ti. Top left: Si and Fe. Top right: mix of different elements: Na, Mg, Al, K, Ca and Ti. Bottom left: Fe. Bottom right: P.

More materials were covering the grains surfaces for the SD sample (Figure 24). All the examined grains for this sample exhibited high amount of Fe coating and P. Most grains were highly covered with organic material and coating which made the identification of the mineral underneath impossible. The grain image used in figure 24 represents one of the few exceptions where the grain surface was clear.

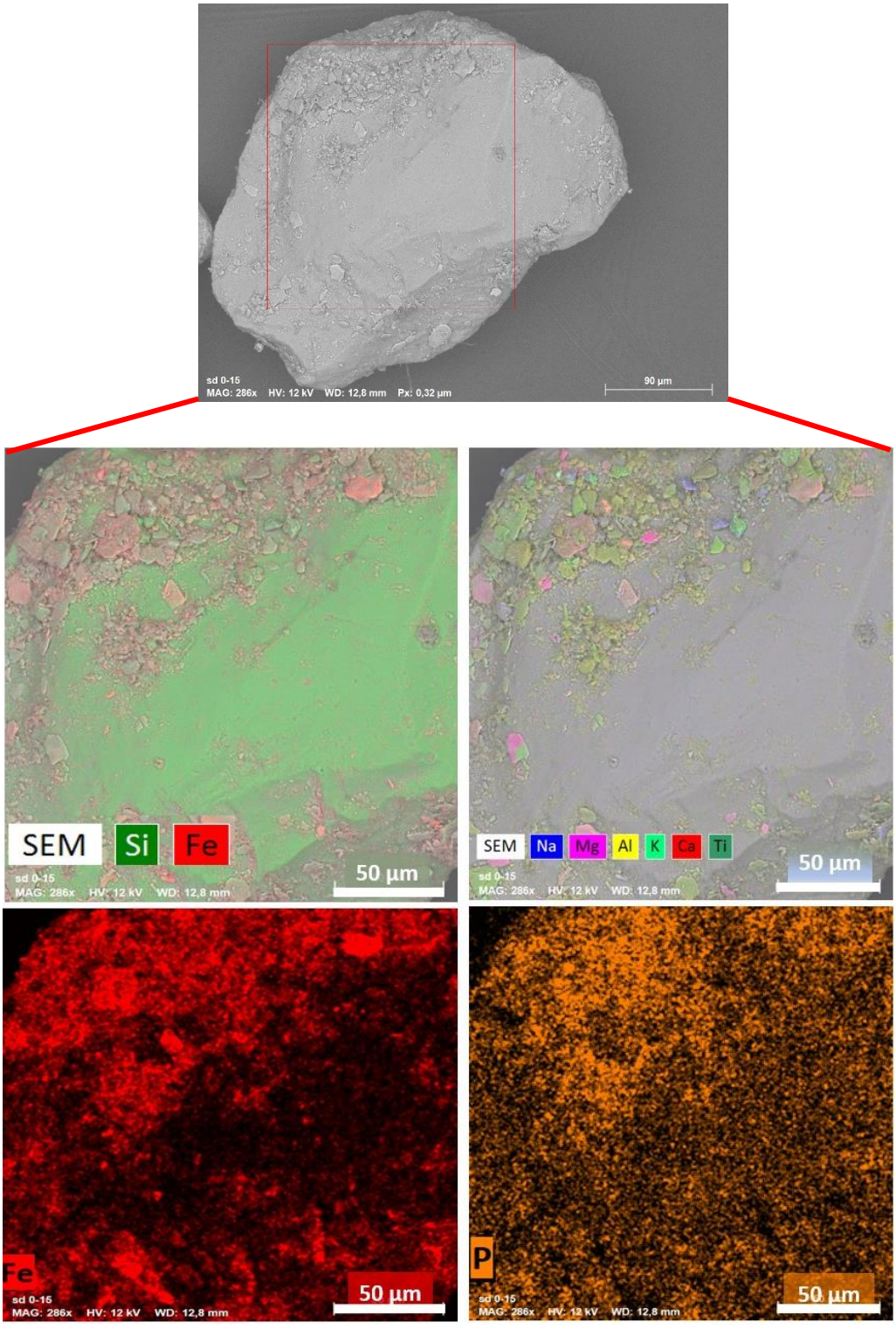

Figure 24: Mapping of the SD sample, showing the distribution of different elements as Si, Fe, P, Na, Mg, Al, K, Ca and Ti.

b. X-ray Diffraction

Six samples representing the soil profile were analysed for bulk composition to identify the minerals present in the soil.

In general, the XRD patterns of the 6 samples are highly similar and the peaks for the different minerals observed are overlapping. Some of the minerals observed during the Scanning Microscopy with SEM are confirmed by the XRD analysis, such as quartz, chlorite, plagioclase, and amphiboles (Figure 25).

Mostly, the samples show a high content of quartz that makes up to 68 % for most samples, followed by microcline 12 %, then plagioclase 10 %, muscovite 5 % and the rest consists mainly of chlorite and at a lesser extent hornblende. Interestingly, sample 70-80 cm has the lowest content of quartz 62 % but a higher content in muscovite 13% and in chlorite 3.9 %. The muscovite content in this sample is more than a double compared to the other samples.

The SD and SL samples have nearly the same composition, the small difference lies in the amount of chlorite and where the SL sample contains slightly more chlorite than the SD sample.

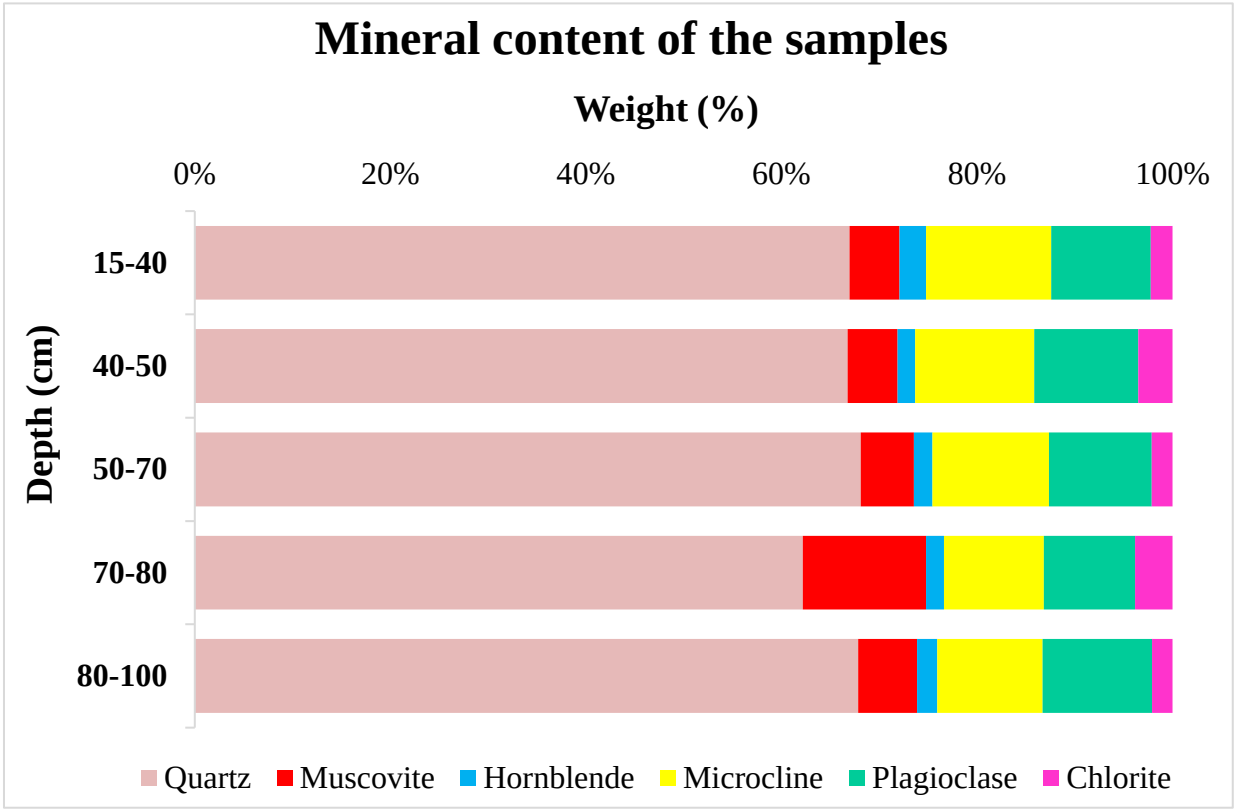

Figure 25: The mineral content detected by XRD for all the samples. The mineral content in percentage is given in the x axis. The Y axis represents the depth at which the samples were collected.

4.2. Iron extraction

The results of the Fe and Mn extracted through the dithionite citrate bicarbonate and the ammonium oxalate methods are given in table 5. The amount of Fe extracted by the DCB method is higher than the amount extracted by the oxalate method. This observation is also valid for Mn. Fe was more extracted from the SD sample compared to the SL sample while for Mn, the extraction exhibited opposite trend. Indeed, more Mn is extracted from the light sample compared to the dark one. For instance, the extracted Fe with the DCB method was ten times higher (69 mg) compared to the oxalate method (6.5 mg) in the SD sample and 24 times more in the SL sample.

Table 5: Results of the iron and manganese extraction experiments. Mn_d and Fe_o reflect to the manganese and iron extracted by the DCB method, while Mn_o and Fe_o express the extraction by oxalate.

Method-Sample	[Mn] (mg/l)	[Fe] (mg/l)	Relation
DCB-SD	0.2	69.4	**Mn_d >> Mno**
Oxalate-SD	0.008	6.5	**Fe_d >> Fe_o**
DCB-SL	1.5	10.6	**Mn_{SL} >> Mn_{SD}**
Oxalate-SL	0.1	0.4	**Fe_{SD} >>Fe_{SL}**

The Fe activity index (Fe_o/Fe_d) for the SD and SL samples are given in table 6. The results show that the SD sample ratio is two times more important than the ratio for the SL sample. The p-value for the ratio between the SD and SL sample is equal to 0.056.

Table 6: The iron activity index (indicates the degree of crystallinity of the soil) for SD and SL samples.

Sample	Fe_o/Fe_d	Average Fe_o/Fe_d
SD	Replicas 1: 0.08 Replicas 2: 0.11	0.09
SL	Replica 1: 0.04 Replica 2: 0.04	0.04

4.3. Manganese sorption experiments

Results from ICP-MS provided information regarding the concentration of Mn in solution and adsorbed into the soil. The adsorbed concentrations of Mn ranges from 0.002 to 4.16 mmol/kg. The results show that the adsorbed Mn is higher in the SD sample compared to the SL samples, which means there is more Mn left in solution in the SL sample. This was observed in both experiments. The results are summarised in table 7 and 8 while the complete data is given in Appendix III and IV.

Table 7: Sorption results for the SD and SL samples for sorption experiment 1. The [Mn] solution represents the concentration of Mn (II) left in solution after sorption and [Mn] sorbed represents the sorbed Mn (II).

Experiment: Sorption 1					
Sample	**[Mn] solution (µmol/l)**	**[Mn] sorbed (µmol/kg)**	**Sample**	**[Mn] solution (µmol/l)**	**[Mn] sorbed (µmol/kg)**
SD10	0.28	53.19	SL10	0.81	25.00
SD20	0.50	65.51	SL20	1.23	36.30
SD50	0.94	92.13	SL50	1.52	68.93
SD80	1.22	229.63	SL80	3.96	119.69
SD100	2.94	385.76	SL100	6.78	231.69
SD200	6.43	633.91	SL200	14.81	296.91
SD300	10.98	775.67	SL300	22.19	324.36
SD500	19.93	1406.25	SL500	38.69	647.07
SD800	32.77	1859.74	SL800	58.63	804.70
SD1000	43.16	1196.60	SL1000	63.12	787.43
SD2000	92.97	2026.10	SL2000	143.78	959.25
SD5000	301.82	4089.39	SL5000	312.38	3852.14
SD10000	656.51	4159.67	SL10000	722.24	2516.65

Table 8: Sorption results for the SD and SL samples for sorption experiment 2. The [Mn] solution represents the concentration of Mn (II) left in solution after sorption and [Mn] sorbed represents the sorbed Mn (II).

Experiment: Sorption 2					
Sample	**[Mn] solution (µmol/l)**	**[Mn] sorbed (µmol/kg)**	**Sample**	**[Mn] solution (µmol/l)**	**[Mn] sorbed (µmol/kg)**
SD10	2.00E-05	4.00E-03	SL10	5.10E-05	2.00E-03
SD20	2.70E-05	3.60E-03	SL20	6.40E-05	1.90E-03
SD50	4.10E-05	4.00E-03	SL50	8.20E-05	3.70E-03
SD80	6.20E-05	1.30E-02	SL80	1.30E-04	4.10E-03
SD100	8.00E-05	1.10E-02	SL100	2.10E-04	7.00E-03
SD300	3.30E-04	2.40E-02	SL300	8.20E-04	1.20E-02
SD500	6.70E-04	5.20E-02	SL500	1.50E-03	2.60E-02
SD800	1.30E-03	6.20E-02	SL800	1.40E-03	1.90E-02
SD1000	1.30E-03	1.10E-01	SL1000	3.60E-03	8.90E-02
SD2000	/	/	SL2000	7.00E-03	9.20E-02

The results of both sorption experiments for the SD and SL sand sub-samples are portrayed in figure 26.

From the graphs, it is clear that more sorption is occurring in the sample containing the SD sand sub-samples compared with the SL sample. The comparison between the concentrations in the two samples showed that sorption is up to two times more important in the solution containing the SD sand sub-samples than in the solution containing the SL sand sub-samples. This is observed for both sorption experiments.

In general, the amount of Mn sorbed increases with the increase of Mn concentration in the initial solution. However, the sorption percentage from the lowest to the highest Mn concentration in solution decreases slightly from 99 % to 86 % for the SD sample and even more for the SL sample, from 98 % to 77 % of Mn removed from solution.

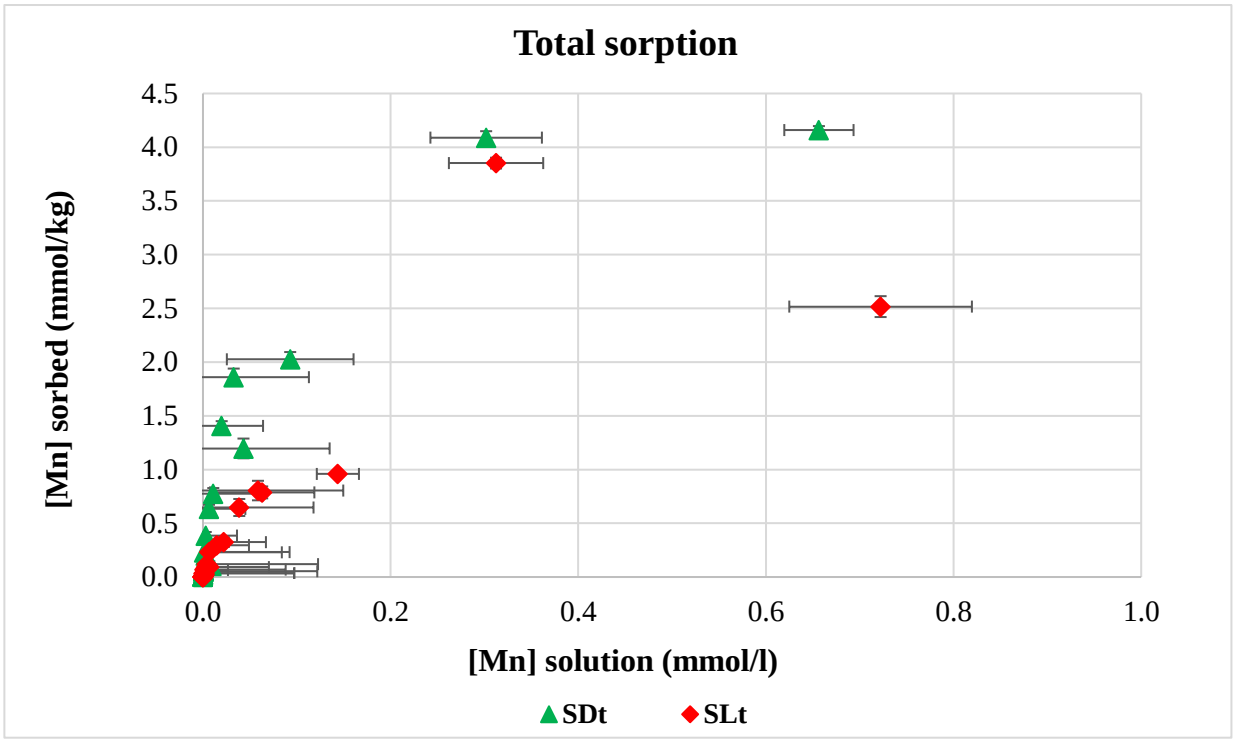

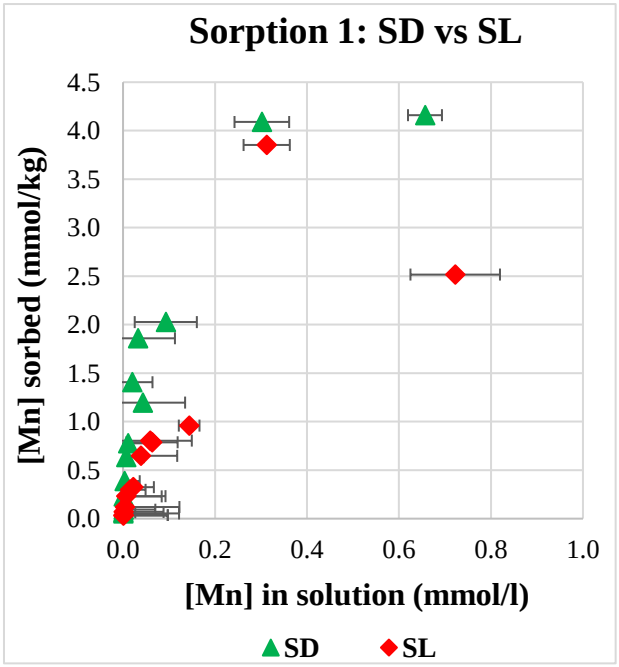

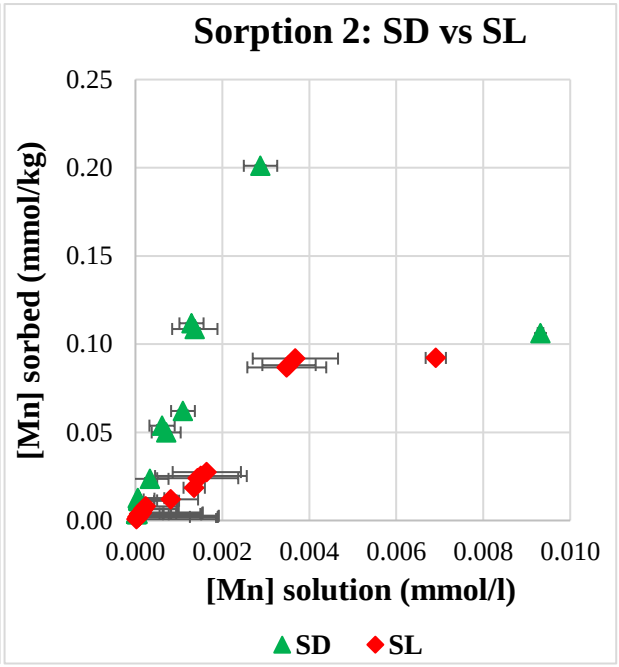

Figure 26: Results of the Manganese sorption experiments. Top: the total distribution for Mn sorption experiments 1 and 2 where both data sets were combined. Bottom Left represents the results of the first sorption experiments and the figure on the right represents the results of the second experiment. [Mn] solution is the concentration of Mn left in solution after sorption while [Mn] sorbed is the concentration of Mn sorbed onto the soil. The green and red markers represent the SD and SL samples, respectively.

The total sorption isotherm for the SD and SL samples is shown in figure 27.

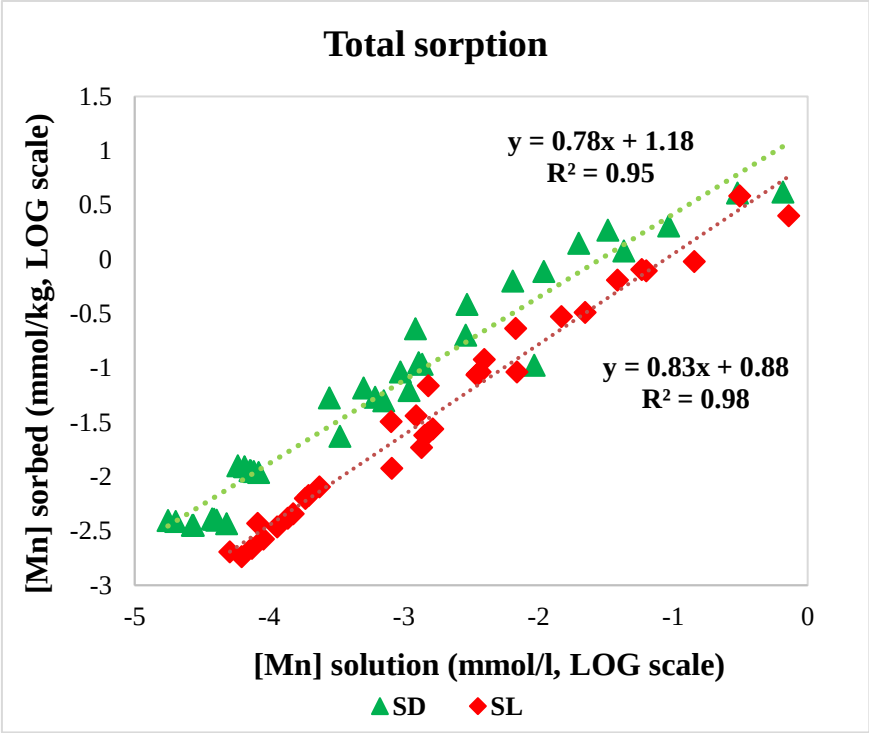

Figure 27: The Freundlich isotherm for the total manganese sorption experiments. The data of the first and second sorptions are combined in one graph. The replicas are also plotted instead of the average of the replicas results. The green and red markers represent the SD and SL samples, respectively.

The generated linear equations show that the exponent n for both data set seems to be similar, while the Freundlich constant is larger for the SD sample compared to the SL sample (15.1 against 7.6). The sorption data for both samples show good fit to the Freundlich sorption isotherm with a better presentation for the SL sample as depicted by the regression coefficient for these two samples (Table 9).

Table 9: The Freundlich isotherm properties for the total sorption experiment for the SD and SL samples. K_F is Freundlich coefficient, n is a measure of the adsorption intensity and reflects on the slope of the curve and R^2 is the regression coefficient.

Total Sorption	K_F	n	R^2	Freundlich isotherm
SD	15.1	0.78	0.95	$\text{Log } X = \text{Log } K_F + n \text{ Log } C$
SL	7.6	0.83	0.98	

4.4. Catalytic oxidation of Mn (II)

4.4.1. High pH: 8-9

The results of Mn oxidation experiments performed under oxic conditions at pH level raging between 8-10 for SD and SL samples are shown in figures 28, 29 and 30. Table 10 displays part of the oxidation results, more detailed tables are provided in Appendix V and VI.

Table 10: Results of the manganese oxidation at high pH levels for the SD and SL samples.

Mn oxidation: pH 8-10			
Sample	**[Mn] (mg/l)**	**pH**	**Time (hours)**
SD0	7.62	9.18	0.0
SD1	6.35	8.94	1.0
SD2	5.07	8.92	2.0
SD3	4.27	8.93	3.5
SD4	4.08	8.93	4.5
SD5	2.80	9.00	7.5
SD6	1.43	9.00	22.5
SD7	1.44	8.99	27.0
SD8	1.16	9.09	47.0
SL0	8.86	9.29	0.0
SL1	5.63	9.15	1.0
SL2	4.24	9.11	2.0
SL3	3.37	9.11	3.0
SL4	3.50	8.98	4.0
SL5	3.20	8.98	5.0
SL6	2.87	9.08	6.0
SL7	2.15	9.08	23.0
SL8	2.21	9.08	25.5
SL9	2.14	9.08	27.5
SL10	2.23	9.07	28.5
SL11	2.49	9.12	45.0

The evolution of the concentration of Mn (II) during the oxidation process is presented in figure 28 for the SD sample. The Mn (II) concentration in the sample decreases from 8 mg/l until reaching its minimum concentration at 1.2 mg/l. In the blank sample, the concentration is approximately stable and varies between 9.8 to 8.6 mg/l. The figure shows a rapid drop in Mn (II) in the sample solution during the first 20 hours of the experiment followed by a slow to nearly

constant concentration of Mn (II) for the rest of the experiment (up to 45 hours). From the graph, it is clear that the concentration of Mn (II) is decreasing with time in the sample while the concentration in the blank is relatively stable.

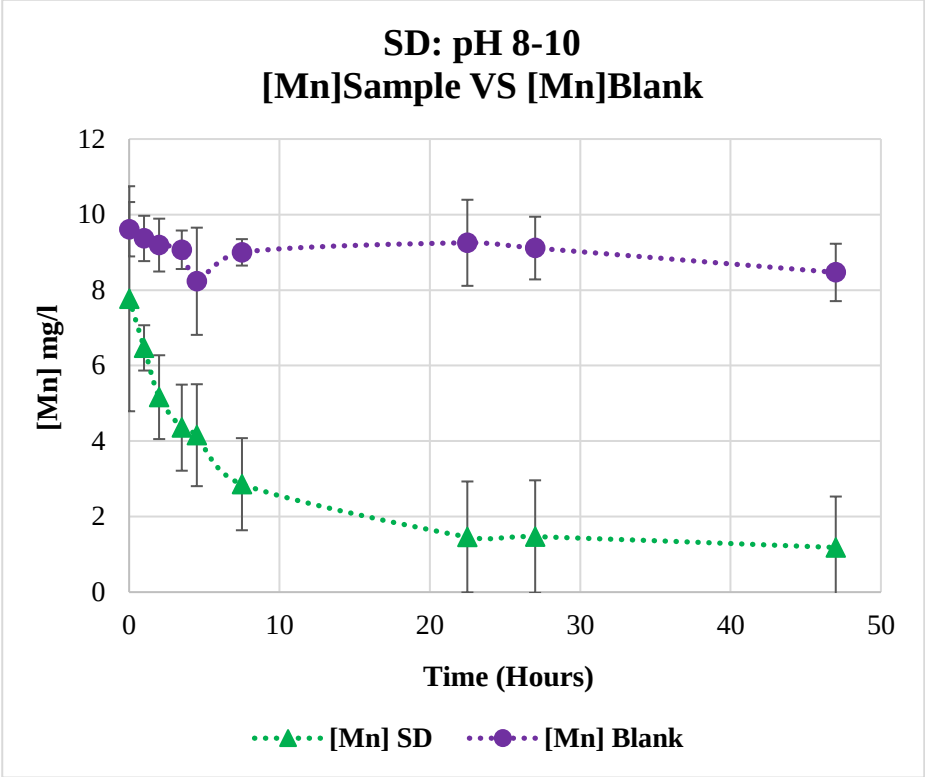

Figure 28: Evolution of the manganese (II) concentration in solution in the SD sample and in the blank for high pH values over time. The marker in green represents the sample containing the SD sand sub-sample while the purple marker is the blank sample free of sand sub-sample.

In comparison to the SL sample, the Mn (II) concentration in the sample decreases from 10.25 mg/l until reaching its minimum concentration at 2.6 mg/l. In the blank sample, the concentration varies between 9.6 to 9.2 mg/l.

As per the previous sample, the Mn (II) concentration in the SL sample decreases rapidly during the first hours of the experiment before reaching equilibrium. After the equilibrium is reached, the Mn (II) concentration remains relatively stable in solution regardless of how long the experiment is run. The Mn (II) concentration in the blank remains relatively constant during the whole experiment.

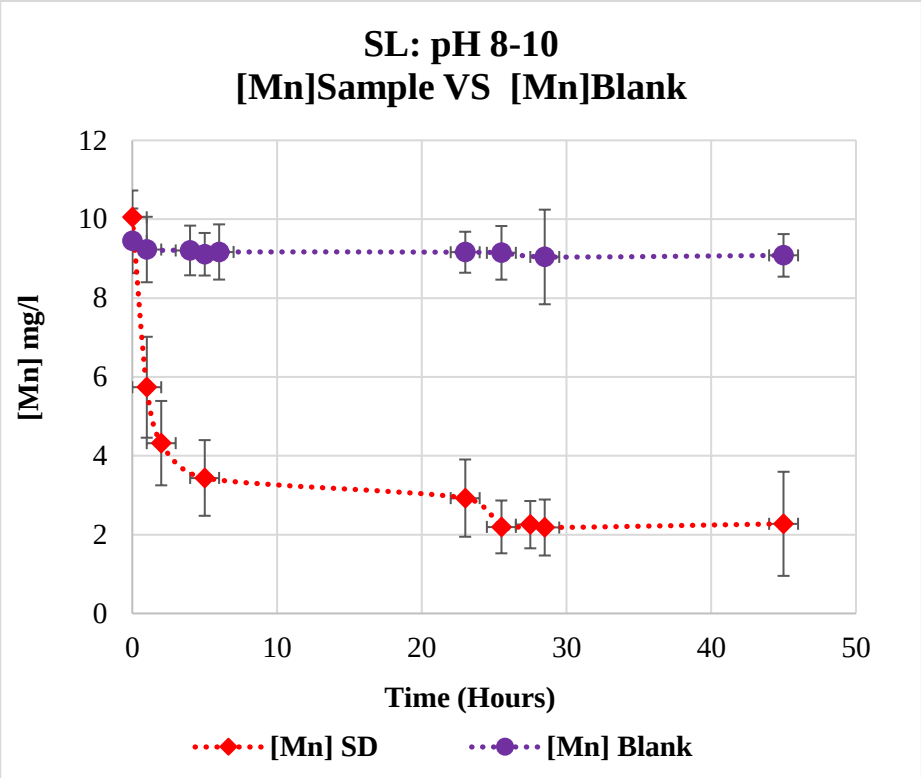

Figure 29: Evolution of manganese (II) concentration in the SL sample and the blank at high pH value over time. Left: concentrations of Mn (II) and right represents the pH. The marker in red represents the sample containing the SL sand sub-sample while the purple marker is the blank sample free of sand sub-sample.

The change of pH in solution was also monitored during the oxidation experiments as showed in figure 30. In both the SD and SL sample, the pH in solution and in the blank decreases slightly during the first hours of the experiments then stabilise until the end. Both graphs show a high similarity in pH evolution with the only difference of a higher pH values for the blank in comparison with the SD sample. The decreases in pH coincides with the decrease in Mn (II) concentration in solution. The pH distribution in the SL sample and blank is highly similar and the two graphs are in most parts overlapping each other.

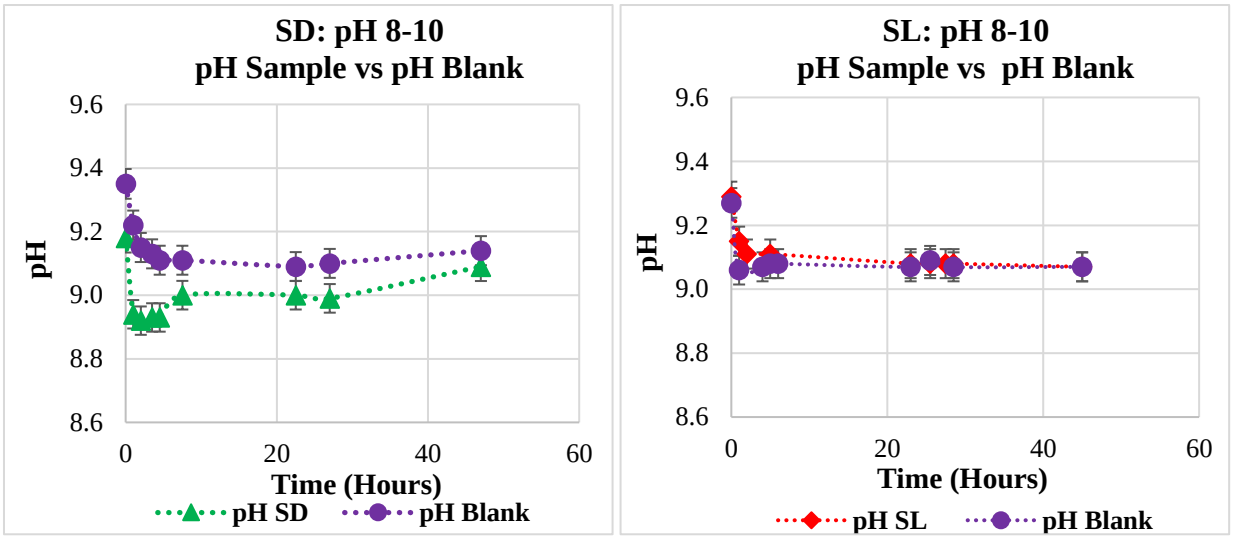

Figure 30: pH evolution in the SD and SL samples during the manganese (II) oxidation experiments over time. Left: the pH in the SD sample. Right: the pH in the SL sample for high pH levels (8-10). The marker in green represents the sample containing the SD sand sub-sample, the red markers represent the sample containing the SL sand sub-samples and the purple markers are used for the blank sample free of sand sub-sample.

4.4.2. Low pH value: 6-7

The same oxidation experiments were run under more acidic conditions compared to the previous experiment. The results are shown in figures 31, 32 and 33. Table 11 displays part of the oxidation results, more detailed tables are provided in Appendix VII and VIII.

Table 11: Manganese oxidation results for the SD and SL samples at low pH values.

Mn oxidation: pH 6-7			
Sample	**[Mn] (mg/l)**	**pH**	**Time (hours)**
SD0	9.50	6.54	0.0
SD1	5.01	7.74	5.0
SD2	2.40	7.90	22.0
SD3	2.14	8.16	27.0
SD4	2.26	7.52	50.0
SD5	2.26	7.94	75.0
SD6	2.03	7.94	93.0
SD7	1.80	7.96	98.0
SL0	12.20	6.41	0.0

SL1	6.88	/	23.0
SL2	5.08	7.51	64.0
SL3	5.06	7.51	69.0
SL4	5.29	7.71	74.0
SL5	4.59	7.77	92.0
SL6	3.40	7.46	121.0
SL7	3.65	7.46	122.0

The evolution of Mn (II) concentration in the SD sample over time at low pH levels is presented in figure 31. As per the previous results, the concentrations of Mn (II) in the sample decreases also with time and reaches a nearly constant concentration after 23 hours. However, in the blank sample, the concentration of Mn (II) increases gradually with time until reaching a concentration of more than 14 mg/l at the end of the experiment.

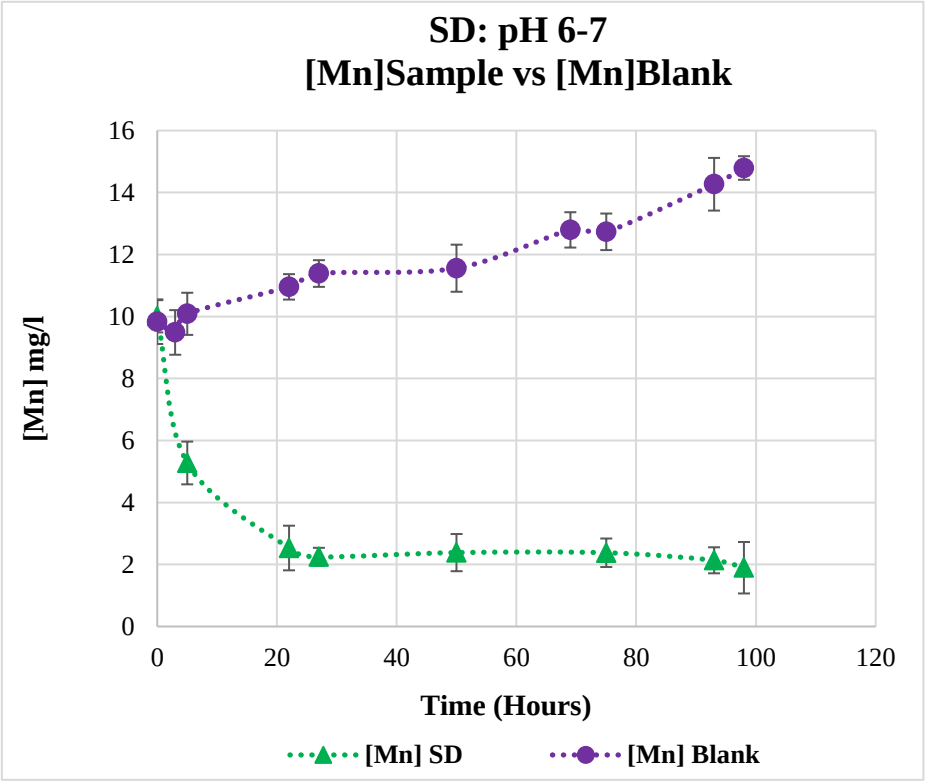

Figure 31: Evolution of manganese (II) concentration in the SD sample and the blank at low pH value over time. The marker in green represents the sample containing the SD sand sub-sample while the purple marker is the blank sample free of sand sub-sample.

In terms of the SL sample, a relatively different tendency is observed for the evolution of the Mn (II) concentration in solution (Figure 32). Indeed, the concentrations keep decreasing with time and do not stabilize like it was observed in the previous results. The concentrations in the blank are relatively stable but start increasing towards the end of the experiment.

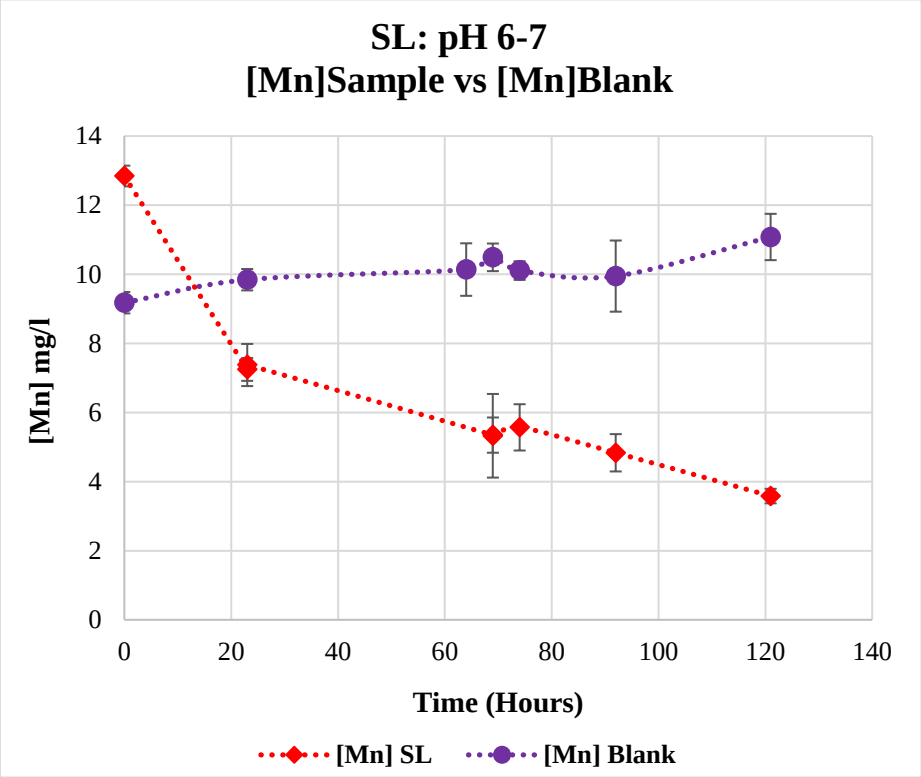

Figure 32: Evolution of mnganese (II) concentration in the SL sample and the blank at low pH value. The red and purple markers represent the SL and blank samples, respectively.

When it comes to the pH evolution in solution, it seems like the pH increases at the very start of the experiment then stabilizes for the rest of the experiment for both the blank and the SD sample. The pH value is however slightly higher in the SD sample compared to the blank. In the SL sample, the pH curves are overlapping each other (blank and sample) as opposed to what was observed for the pH in the SD sample.

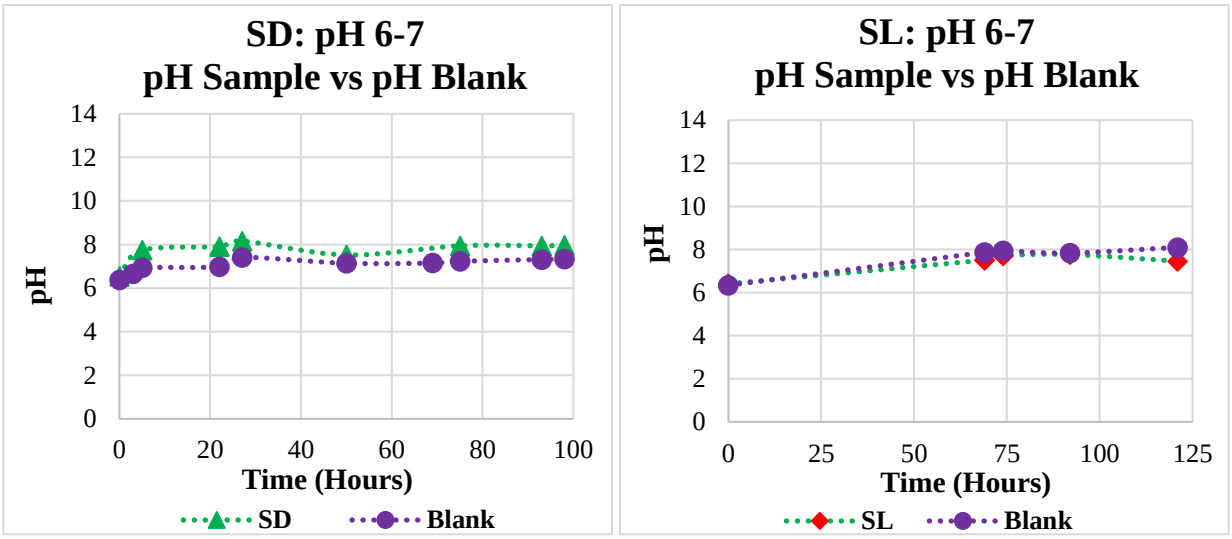

Figure 33: pH evolution in the SD and SL samples during the manganese (II) oxidation experiments over time. Left: the pH in the SD sample. Right: the pH in the SL sample for high pH levels (8-10). The marker in green represents the sample containing the SD sand sub-sample, the red marker represents the sample containing the SL sand sub-samples and the purple marker is the blank sample free of sand sub-sample.

4.5. Geochemical modelling with PHREEQC

4.5.1. Manganese sorption

Freundlich Isotherm

The Mn sorption modelling was performed through the use of Freundlich isotherm that can be calculated by PHREEQC program. In order to achieve a closer modelling of the Mn sorption compared to the sorption results obtained from the experimental study, the equilibrium constant, n, resulted from the laboratory experiments for the SD and SL sand sub-samples and for sorption 1 and 2, was used (Table 9).

The results of the model runs are presented below in figure 34. The profiles show an increase of Mn (II) sorption with the increase of Mn (II) in solution. This tendency is observed in both sorption conditions.

In relation to both sorption experiments (1 and 2) and in accordance with the hypothesis formulated on the basis of the sand sub-samples color, the SD sample exhibits the highest sorption concentrations, followed by the SL sample. The sorption profiles indicate a very similar pattern, where the curves (modelled Mn sorption concentrations) and markers (measured Mn

sorption concentrations) overlap each other for the lowest concentrations of Mn (II) in solution. At higher Mn in solution, the measured sorption is higher compared to what was modelled.

In accordance with the experimental results, the modelling results do not show maximum sorption neither.

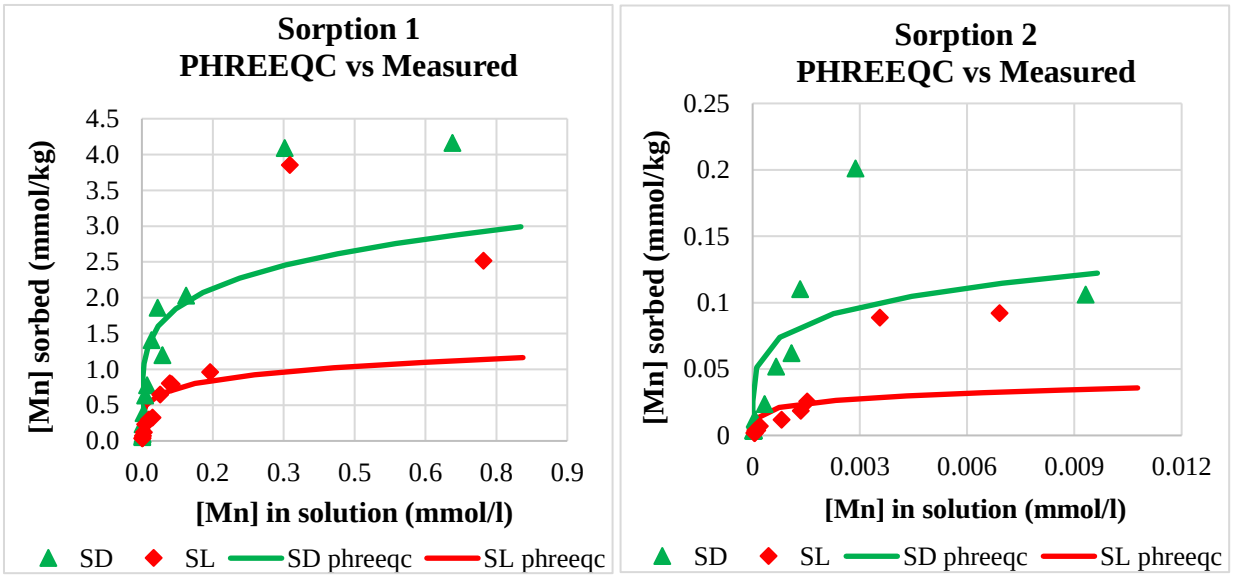

Figure 34: Results of the sorption experiments (1 and 2) compared to the sorption modelling with PHREEQC. [Mn] sorbed reflects on the Mn (II) sorbed onto the sand sub-samples and [Mn] solution reflects on the concentration of Mn (II) remaining in solution. The markers (in green and red) represent the measured sorption results while the solid lines (in green and red) represent the sorption of manganese resulting from PHREEQC.

The Mn sorption isotherms for the SD and SL samples as computed by PHREEQC are shown in figure 35. The generated linear equations show a similar exponent n for both data sets, while the Freundlich constant is larger for the SD sample compared to the SL sample. The sorption data for both samples show good fit to the Freundlich sorption isotherm as depicted by the regression coefficient for these two samples (Table 12).

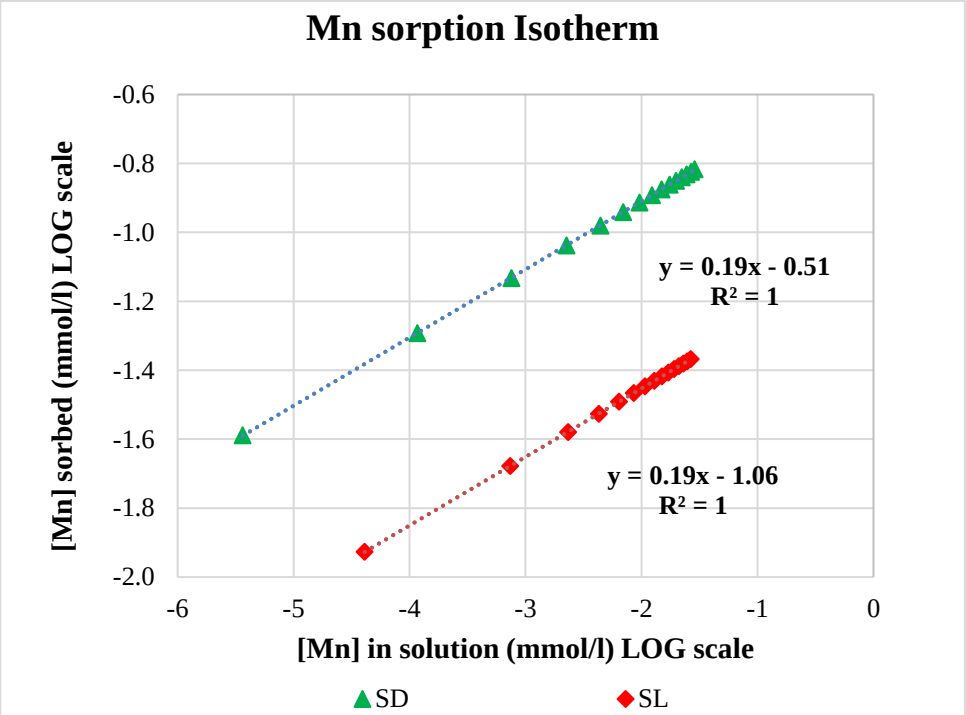

Figure 35: The Freundlich isotherm for the computed manganese sorption. The green and red markers represent the SD and SL samples respectively.

Table 12: Freundlich Isotherm parameters resulting from the modelling investigation. K_F is Freundlich coefficient, n is a measure of the adsorption intensity and reflects on the slope of the curve and R^2 is the regression coefficient.

PHREEQC	K_F	n	R^2	Freundlich isotherm
SD	0.30	0.19	1	$\text{Log } X = \text{Log } K_F + n \text{ Log } C$
SL	0.08	0.19	1	

Surface complexation

Mn sorption was also computed with the surface complexation model on hydrous ferric oxide that includes two types of sites, weak and strong, available on the surface of the oxide. In addition, the complexation on organic matter was considered as a result of the effect that have this one on the sorption of Mn (II). The results are shown in figure 36.

The results obtained first show an increase of the sorption with Mn (II) in solution. The distribution of sorbed Mn on hydrous ferric oxides and bound to organic matter clearly indicate

that Mn (II) is mainly sorbed on the ferrihydrite. The organic matter affects the Mn (II) to a lesser extent with a contribution of about 10% of the total sorption.

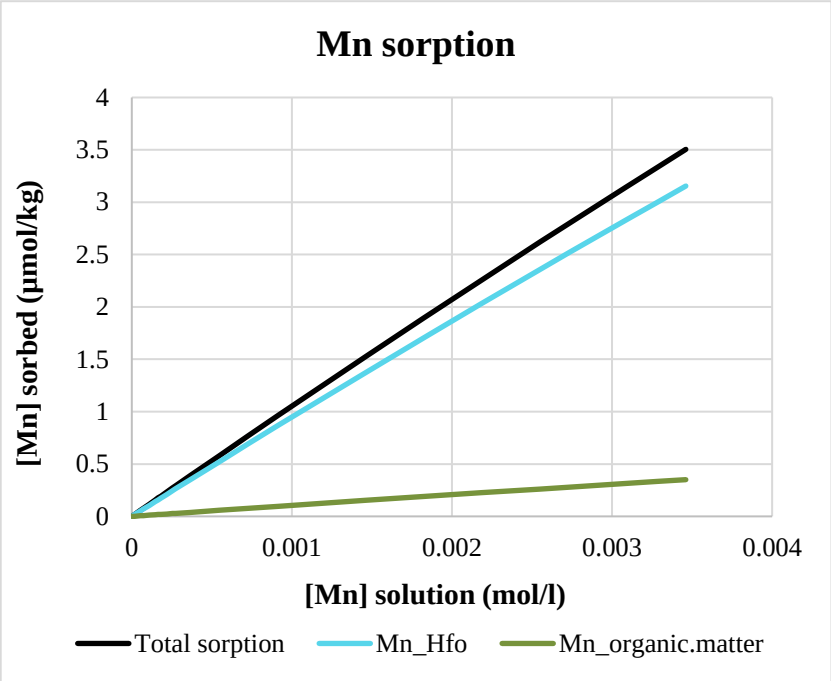

Figure 36: Results of manganese sorption on hydrous ferric oxide and organic matter resulting from PHREEQC modelling. The Mn_Hfo represents the part of Mn sorbed on Fe oxides (blue line) and Mn_organic.matter represents the Mn sorbed onto the organic matter (green line). The Total sorption (black line) is the sum of both Mn_Hfo and Mn_organic.matter.

4.5.2. Manganese oxidation

The Mn oxidation was modelled in PHREEQC with respect to the conditions followed during the laboratory experiments. The Mn reaction rate equation used for the PHREEQC model was obtained from literature (Equation 29). The values of K_1 and K_2, which represents the homogeneous and heterogeneous reaction rate constant respectively, are extracted from the experimental results for both the 1st and 2nd order reaction rates. Thus, the results portrayed in figures 37 shows the simulated Mn (II) concentrations during the oxidation with the 1st and 2nd order reaction rates constants at high pH levels. and the comparison with the measured values. The comparison between the measured and simulated results is illustrated in figure 38.

The PHREEQC results shows that the Mn (II) concentrations decrease in a different trend when simulated with the K_1 and K_2 values of the 1st and 2nd order reaction rates. It is evident from figure 37 that the oxidation of Mn occurs faster with the 2nd order reaction rates compared to the

1st order reaction rates. The concentrations of Mn (II), obtained from the simulations with the 2nd order reaction rate constants, decrease quickly during the first 20 hours of run to stabilize at very low concentrations. The concentrations of Mn (II), obtained from the simulations with the 1st order reaction rate constants, decreases gradually but never reaching as low concentrations values as was observed with the 2nd order reaction rate simulation. The curves for both rates are in accordance with the shape of the curves expected for a 1st and 2nd order reaction rate (Figure 9).

The pH also decreases during the oxidation of Mn (II) and follows the Mn (II) concentrations trend. The pH values are higher for the simulation performed with the 1st order reaction rates compared to the 2nd order reaction rates.

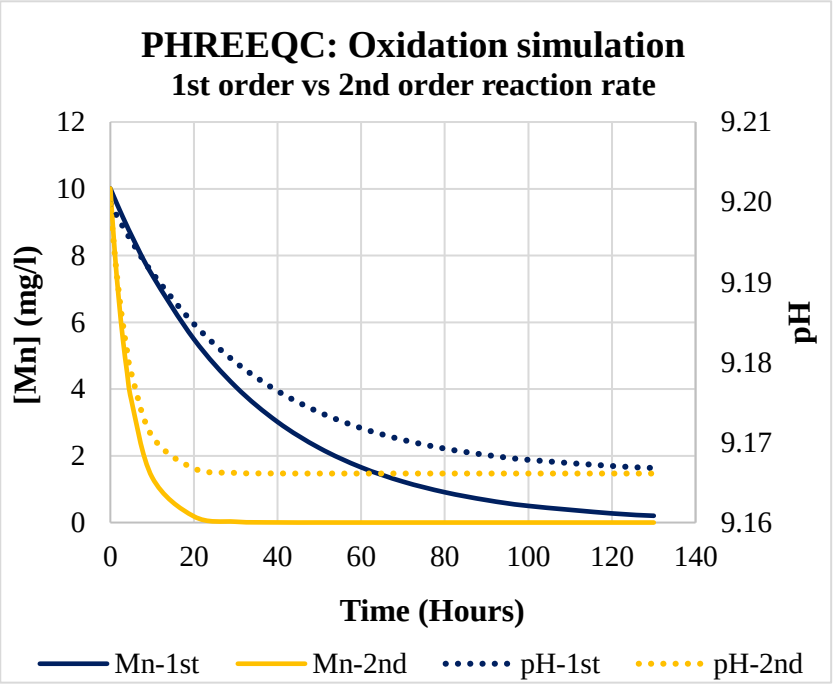

Figure 37: Evolution of manganese (II) and pH during the modelling of the oxidation reaction with PHREEQC at high pH range. Mn-1st (blue solid line) represents the manganese (II) concentrations obtained from the oxidation reaction simulated with the 1st order reaction rate constants resulting from the laboratory experiments (same for Mn-2nd, orange solid line). pH-1st represents the pH values obtained from the oxidation reaction simulated with the 1st order reaction rate constants resulting from the laboratory experiments (same for pH-2nd). The pH is shown in dotted lines and the concentrations of manganese (II) in a solid line.

The comparison between the modelling and the experimental results is shown in figure 38. As depicted in the figure, the Mn (II) concentrations obtained from the simulation performed with the 2nd order reaction rate constants have the same evolution trend as was observed for the experimental results (SD and SL Mn (II) oxidation results). The main difference is that the remaining Mn in solution is higher in the experiments compared to what was obtained by PHREEQC. For High concentrations of Mn (II) in solution, the experimental and the modelled results (2nd order reaction rate) exhibit the same trend. The Mn (II) concentrations obtained from the simulation performed with the 1st order reaction rate constants are higher to what was observed for the SD and SL sand sub-samples in the laboratory for the first 60 hours of run. The modelled concentrations reach lower values after afterwards.

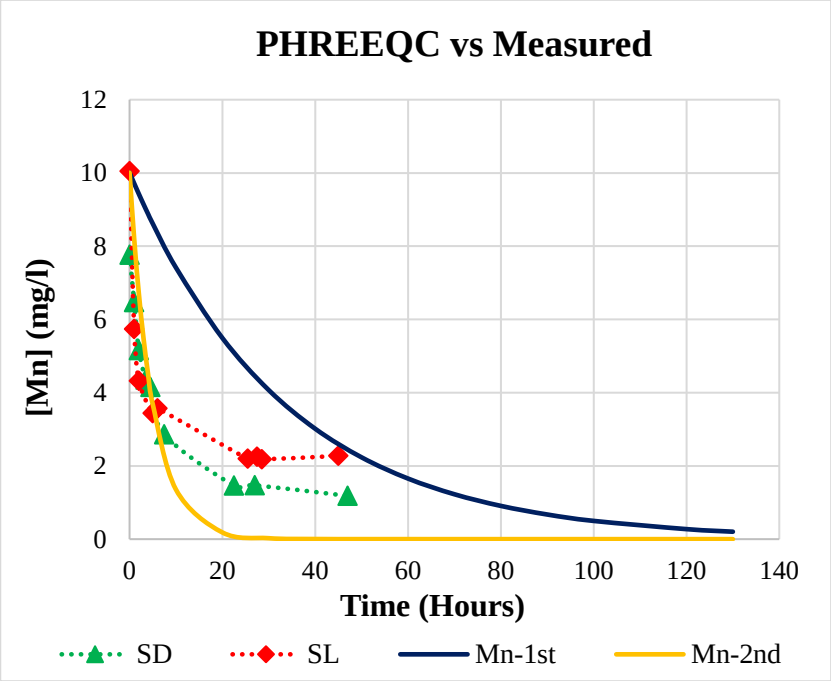

Figure 38: A comparison between the modelling and the experimental results obtained for the oxidation of manganese (II) for high pH levels. The experimental results are represented by the SD (green markers) and SL (red markers) samples. The modelling results are presented in a solid line. Mn-1st (blue solid line) represents the manganese (II) concentrations obtained from the oxidation reaction simulated with the 1st order reaction rate constants resulting from the laboratory experiments (same for Mn-2nd, orange solid line).

5. Discussion

This discussion chapter focuses on explaining and evaluating the importance and relevance of the obtained results presented earlier. This part is necessary as it seeks to understand the behaviour of Fe and Mn observed during the different experiments especially since the mechanism for Fe and Mn removal are still largely unknown. The knowledge that can be extracted from this study in addition to future studies might help answering some main questions such as what kind of minerals precipitates during the oxidation of Fe and Mn? What are the clogging risks? Are there preferential precipitations surfaces depending on the type of solid phase present?

However, this Master study focuses on investigating the Mn adsorption capacities in different Fe-coated sand samples and on determining the effect of pH on the oxidation of Mn with or without Fe-coated sand samples.

5.1. Iron extraction

The amount of Fe and Mn extracted by the DCB and oxalate method varied greatly between the two methods but also between the two sand sub-samples, SD and SL. These differences in the amount of extractable Fe may suggest that the extractant were successful in differentiating the extractable forms of Fe which agrees with the suggestion of McKeague et al. (1971) that the oxalate method dissolves the non-crystalline and organically bound forms of Fe and the DCB method dissolves the crystalline and non-crystalline forms of Fe.

As mentioned in McKeague et al., (1971), The DCB method extracts more Fe and Mn compared to the oxalate method. This indicates that the soil may contain higher amount of crystalline Fe and Mn than the non-crystalline forms. This is probably the result of the preferential behaviour of microorganisms that favour less crystalline phases for iron reduction (Munch & Ottow, 1983; Lovely & Phillips, 1986) as microbial reduction of amorphous Fe-oxide phases is thermodynamically more favourable than the crystalline phases (Weber et al., 2006). The total extractable Fe and the non-crystalline Fe decrease with depth from the SD (0-15 cm) to the SL sample (40-50 cm) (decreased by 7 times for the DCB method and 14 times for the oxalate method). This vertical distribution is likely due to the remobilization and leaching of iron oxides in the soil.

This confirms the theory behind the colour code given to the 2 samples where SD was selected for the darkest sample and SL for the lightest sample. Indeed, it was expected that the SD sample would contain more Fe as its soil colour had a more intense reddish-orangish colour compared

to the duller soil colour of the SL sample. In their article, Schwertmann et al (1993) confirmed the role of the different Fe-oxides in colouring the soil. It was based on this principle that the SD sample was expected to contain more Fe compared to the SL sample.

The Feo/Fed values for the two replicas for the SD sample are equal to 0.08 and 0.11 with an average ratio of 0.09. For the SL sample, the ratios are equal to 0.04 for the two replicas with an average value of 0.04. It is important to note that the sample size (4 values in total) is not important enough to conclude on the age or degree of development of the soil, but in general a smaller Feo/Fed ratio leads to the assumption that the soil is relatively older or / and is more developed. In this case, it is moderately possible to describe the soil at medium depth (SL sample) as older or more developed than the soil at the surface (SD sample).

5.2. Manganese sorption

The experimental results showed an increase of Mn sorption with higher initial Mn concentration in solution (Figure 26). This implies that the sorption process is mostly dependent on the initial concentration of Mn in solution. The fact that the sorption of Mn still increases with the initial amount of Mn may indicates that the availability of surface areas for Mn sorption is not a limiting factor, which coincides perfectly with the Freundlich isotherm as the results do not show a limit in in sorption (Figure 8 left).

The sorption percentage is the highest for low initial Mn concentrations in solution and declines gradually with increasing Mn concentration in solution (Figure 39). Although, the sorption at these high concentrations is still important (up to 86 %), this slight decreasing tendency might also reflect on the efficiency of the sorption process. This decline is highly likely due to the initial sorption of Mn ions on the favourable sorption sites, which render additional Mn sorption increasingly difficult. This also agrees with the Freundlich equation which assumes that the affinity of the sorbent surface decreases exponentially as the sorption of an element progresses (Barrow, 1978).

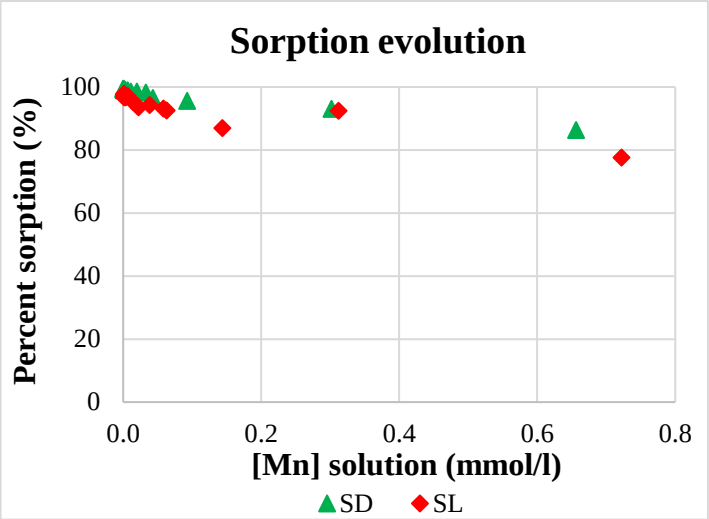

Figure 39: Percentage of manganese sorption for various manganese concentrations in solution for the SD and SL samples in the first sorption experiment.

In the logarithmic scale for Mn (II) sorption evolution (Figure 27), the amount of adsorbed Mn (II) does not seem different between the dark sand sup-samples rich in Fe coating (SD) and the less coated sand sub-sample (SL). However, when a linear distribution is established (Figure 26) it becomes clear that Mn is slightly more absorbed in the SD than in the SL samples. This observation is true for both experiments carried out. As mentioned above, the SEM analysis showed that the SD soil has more coating compared to the SL soil sample.

In addition, the Fe extraction experiments revealed that the SD sample is found to contain more crystalline and non-crystalline forms of Fe compared to the SL sample. The presence of more crystalline and non-crystalline forms of Fe in the SD sample might have influenced the Mn sorption. Indeed, more Mn (II) could have been trapped in the loose porous structure of the non-crystalline Fe and then incorporated into the more crystalline forms of Fe resulting in more Mn sorption in the SD sample compared to the SL sample as was observed in other studies (Detournay et al., 1975; Krishnamurti & Huang, 1989, Ren et al., 2013). Similarly, SD sand sup-sample might have also enhanced the sorption of Mn (II) as more Fe coating was observed in the SD than in the SL sample. In a sorption–oxidation situation, if the sorbed Mn (II) is oxidised then it can form coating with a high sorption capacity which can work in favour of more Mn (II) sorption. In this case, the more coating the more Mn is sorbed.

Sorption simulations with PHREEQC

The sorption results obtained from modelling with PHREEQC and from laboratory experiments showed the same trend in terms of evolution of sorption with higher concentrations of Mn (II) in solution. Similarly, the SD sample also shows higher sorption capacity than the SL sample and the reference sorption computed with the n value from literature.

The results obtained by PHREEQ, modelled with the same solution characteristics as in the experiments, showed a very similar sorption concentrations for low Mn concentrations in solution. However, for high Mn concentrations in solution, the experiments results showed higher Mn sorption concentrations. This difference might be the results of modelling the sorption with the Freundlich isotherm that considers soil as the main sorbent and may sorb most of the Mn at low concentrations in solution. At higher Mn concentrations in solution, the soil might not be sufficient for high sorption capacity. In the laboratory experiment, the used sand sub-sample contains iron oxyhydroxides and organic matter which also plays an important role in Mn sorption. Therefore, this difference between the modelled and measured sorption at high Mn concentrations is probably due to the composition of the used sand sub-sample.

The sorption of Mn (II) on ferrihydrite and on organic matter was also investigated in order to approximate the influence of each of these components on the sorption of Mn (II) (Figure 35). The results showed that 90 % of the sorbed Mn (II) was bound on hydrous ferric oxides and 10 % on organic matter. This might be explained by the fact that Mn shares a higher sorption affinity with metal oxides than with organic matter, therefore more Mn (II) is bound to Fe oxides compared to organic material. This also validates the results obtained in the sorption modelling with the Freundlich Isotherm that only consider soil for the sorption.

5.3. Manganese oxidation

When comparing the evolution on Mn concentration in solution in the SD and SL samples at pH range 8-10 (Figure 33, left), it appears that both samples have an almost identical trend. However, it seems like more Mn (II) is oxidized in the dark sample compared to the light sample.

After 18 h in solution, the oxidation of Mn stabilizes in the SL samples until the end of the experiment at around 47 h. This probably means that the Mn is not further oxidized.

In relation to the pH evolution for the SD and SL samples (Figure 30), the pH follows the same change as the Mn (II) concentration in solution. The drop in pH, during the first 20 h of the

experiment corresponds also to the time where the oxidation is occurring and is probably due to the formation of H^+ when Mn (II) is oxidized which will decrease the pH. At the end of the oxidation experiment, the slight increase of Mn (II) in solution is followed by higher pH value. The reduction of Mn (II) is responsible for this change as it uses H^+ to reduce Mn oxides to Mn (II), which affects the pH in solution.

At a lower pH in the range of 6-7, the oxidation is still occurring although, the amount of Mn (II) oxidized is slightly less compared to the oxidation at higher pH. The SD sample exhibits the same evolution with time at both pH values (6-7 and 8-10) whereas in the SL sample, the oxidation of Mn (II) seems more affected by the drop of pH (Figure 33).

The pH monitoring for this experiment showed an increase of pH during the first few hours of the oxidation then stabilizes at pH levels ranging between 7.4 and 7.9. This pattern might be the result of the HCl that was added in the solution mixture to decrease the pH so that Mn (II) is oxidized in more acidic conditions compared to the first experiment. Many attempts were made to observe how the pH evolves when adding HCl to 300 ml of $NaHCO_3$. Achieving a stable pH between 6 and 7 seemed hardly possible as the pH kept changing (pH values higher than 7) due to the buffer effect of the bicarbonate. Once the pH was deemed relatively stable (value less than 6.5), initial Mn solution was added. The pH increases again before finally stabilizing. This change can be either due to the buffering behavior of HCO_3 that was probably not completely neutralized and which over time increases the pH value in the solution or to the possible precipitation of manganese bicarbonate that could have increased the pH.

The oxidation of Mn (II) was also monitored in a blank sample that does not contain sand material (blank reference sample) for both SD and SL samples. Contrary to the samples with soil, the oxidation in the blanks is highly limited and the concentration of Mn (II) remains relatively stable in most blanks. Thus, the concentration of Mn (II) in the blanks is more important compared to the samples, as it is not oxidized as in the samples. This tendency is due to the absence of a solid phase (the sand sub-samples) which provides minerals or more specifically the surfaces of minerals that are known to accelerate the oxidation of Mn (II) through adsorption-oxidation reactions (Luo et al., 2018). This was confirmed by numerous previous studies (Diem & Stumm, 1984; Davies &Morgan, 1989; Junta & Hochella, 1994).

An exception is observed for one of the blanks oxidation experiments. Indeed, the blank sample for the SD at low pH (6-7) exhibits an increasing concentration of Mn in solution contrary to the other blanks. A possible contamination during sample preparation is not excluded although the

other samples were all prepared in the same way and by observing the same degree of care. Another possibility is a cross-contamination between analytical run when analysing by ICP-MS especially if the blank samples were analysed right after a sample with high Mn (II) concentration.

Another observation was made during data analysis of the results: when analysing the concentration of Mn (II) at t = 0, the concentration observed for the SL sample is always 2 mg/l higher than the concentration found in the SD sample. This discrepancy was initially thought to be due to an error in the analysis by ICP-MS. However, this difference is not observed between the blanks but only between the samples that contains the SD and SL soil which may reflect on the role of the soil in causing this result. Therefore, it is inferred that this difference of Mn (II) concentration at time zero is due to the instant and rapid sorption of Mn (II) present in solution when the soil is added into the solutions mixture. In addition, the fact that it is the SD sample that has lower Mn (II) concentration supports this theory, as the SD contains more Fe oxides and hydroxides compared to the SL sample.

The effect of pH on the Mn (II) oxidation in the SD and SL samples is depicted in figure 40. From the results obtained (Figure 40), there is no doubt that the pH has affected the oxidation process of Mn (II) no matter the type of sand sub-sample (SD or SL) as pH is the only factor that has changed between the two experiments. It is also important to note that more Mn (II) is oxidized either for low or high pH values. The results indicate that the oxidation of Mn (II) increases with increasing pH. However, the extent of oxidation decreases when it reaches its maximum. This oxidation behaviour is in line with expected soil Mn (II) oxidation process in abiotic conditions (Sparrow & Uren, 2014). Low pH values have a negative impact on the abiotic Mn oxidation (as well as biotic oxidation) because the oxidation of Mn at lower pH is considered thermodynamically unfavourable for the initiation of Mn oxides formation when O_2 is the terminal electron acceptor (Sparrow & Uren, 2014) which is the case of this study. Furthermore, low pH values greatly reduce the negatively charged sites which will then inhibit Mn (II) sorption by competition (Gadde & Laitinen, 1974). The oxidation is also relatively faster at high pH value. Diem and Stumm (1984) demonstrated that the oxidation of Mn by O_2 at pH below 8.5 is kinetically very slow, this matches with the results obtained.

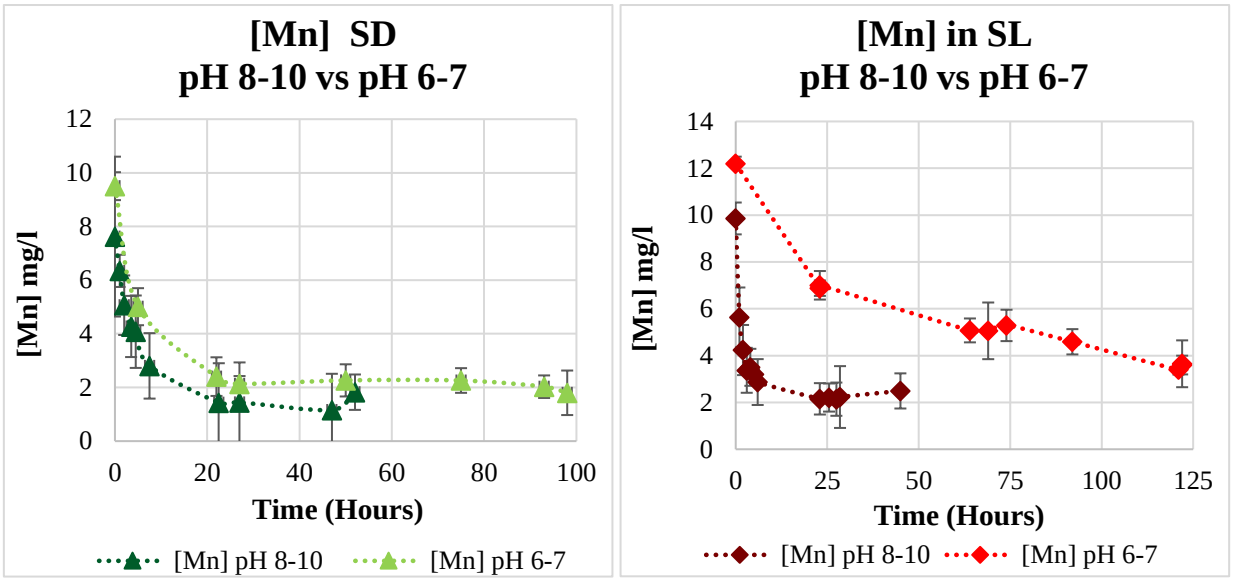

Figure 40: The effect of pH on the oxidation of manganese with time in the SD and SL samples. The figure on the left represents the results of the oxidation experiment for the SD sample for high pH level (dark green markers) and low pH level (light green markers). The results of the oxidation experiments run on the SL sample is represented in the figure on the right. The dark red markers reflect on the experiments at high pH levels and the light red markers reflect on the experiments run at low pH levels.

In addition to the observed pH control (Figure 40), the presence of Fe oxides and hydroxides in the soils could also have affected the amount of Mn oxidized. As the SD sample has higher amount of Fe oxides and hydroxides, it could have played a role in Mn oxidation which resulted in more Mn removal from solution than in SL sample. Numerous studies proved that Fe oxides and hydroxides had the capacity to catalyse the abiotic oxidation of Mn (II) in oxic environment (Davis & Morgan, 1989; Junta & Hochella, 1994; Sung &Morgan 1981; Ren et al., 2013) which matches perfectly with the conditions of the experiments carried out in this study. It was observed by Sung and Morgan (1981) that the surfaces of minerals can accelerate the oxidation of Mn (II) to a certain degree. Thus, it is possible that the adsorbed Mn (II) can be catalytically oxidized to form a thin layer of Mn oxides (Luo et al., 2018) which may result in more Mn (II) oxidation in the SD compared to the SL sample.

Furthermore, the difference in oxidation for both sand sub-samples might be due to the organic matter content in soil. The SD sample was collected near the surface (at 0-15 cm deep) where there is more organic matter present, and it could have been observed as well when sieving the soils after returning from the field. Indeed, there was way more dead leaves and roots in the SD

soil than in the SL soil. However, the organic content of these two samples was not measured, it is considered mainly as a theory which could explain why more Mn was oxidized in the SD than in the SL. Organic matter can donate electrons to Mn (II) and enhance the loss of electrons to O_2 and other electrons acceptors so Mn (II) oxidation can occur at lower pH value. Consequently, if the SD sample has higher organic content in the soil, than more Mn would have been oxidized compared to the SL sample (Luther et al., 1992, 2009, Duckworth & Sposito 2005). The modelling of the effect of the hydrous ferric oxides and organic matter's influence on the sorption of Mn has shown that the organic matter sorbes up to 10 % of the Mn in solution. This proportion is small, but it still can play a valuable role in the sorption of Mn in solution. Additionally, considering that SD hypothetically contains more organic, the latter might also have increased the sorption capacity of this sand samples compared to the SL sand sample.

Even for longer time (more than 100 hours), the Mn in solution is not completely removed or oxidised in solution. The experiments that were run during this project were abiotic oxidation of Mn (II) with constant O_2 flux. This is due to the fact that O_2 is not competent as an oxidant of Mn (II) in abiotic conditions as it is hard for O_2 to accept a single electron from Mn (II) due to the O_2 molecular structure (Sparrow & Uren, 2014).

5.4. Oxidation kinetics

The oxidation kinetics from the Mn oxidation experiments at both pH levels 8-10 and 6-7 are shown in the figures below (Figure 41,42).

During the oxidation at high pH levels, the Mn in solution oxidized faster (less than 10 h) before reaching approximately a stable concentration compared to the oxidation at low pH levels that requires a longer period (around 20 hours for the SD sample and more than 120 hours for the SL sample) (Figure 41).

The relation between Ln [Mn (II)] and time as shown in figure 41 (top), which represents the 1^{st} order rate, is almost linear throughout the first part of the oxidation process (dashed line bracket). The same is observed for the 2^{nd} order reaction rate (Figure 41, bottom). This may suggest that the oxidation is a first-order reaction that might depend mostly on the availability of Mn (II) in solution as the pH has remained nearly constant in solution.

In the second part of the reaction, it seems like the rate increases as the reaction proceeds for longer time. This is reflected by the increasing slope values (solid line bracket) and which is probably caused by the heterogeneous reactions occurring in solution that autocatalyzes further adsorption-oxidation of Mn (II) due to the presence of Fe or Mn oxides, or other oxides.

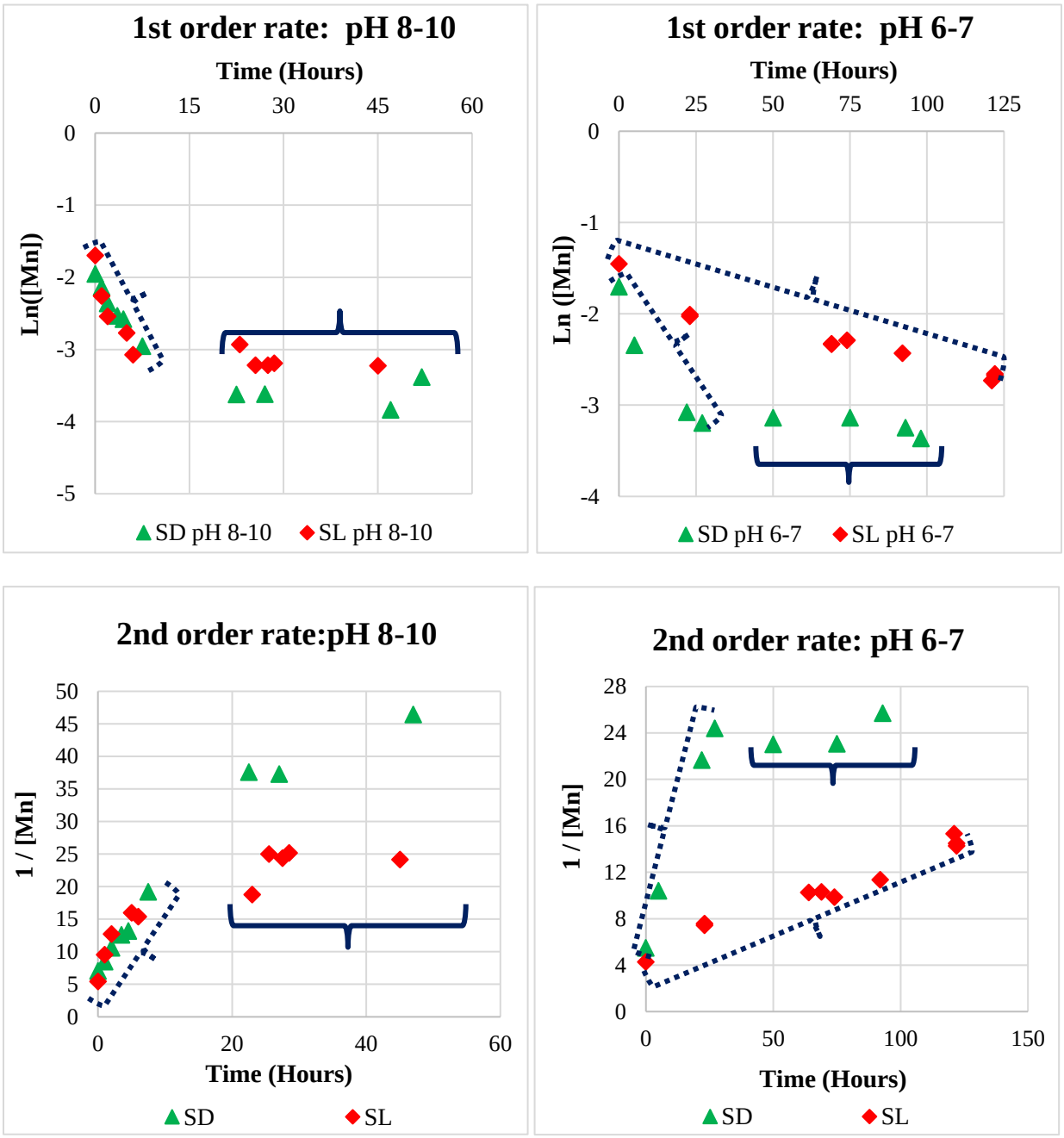

Figure 41: Manganese (II) oxidation kinetics on the SD and SL sand sub-samples at high (left) and low pH (right) ranges. The figures on the top represents the 1st order kinetics and the figures in the bottom represents the 2nd order kinetics. The profiles are divided into two parts: the parts highlighted with a dashed-line bracket where the oxidation rate decreases, and the part highlighted with a solid-line bracket and representing heterogenous reactions occurring in solution.

With the purpose of investigating which kinetic rate order better fits the Mn (II) oxidation reactions, a 1st and 2nd order reaction rates were calculated and are presented in figure 42.

The rates presented below represent only the part where the oxidation of Mn (II) was still occurring in solution (portrayed in figure 42 by a dashed line bracket). The SL sample at low pH levels is not divided into two segments as the oxidation did not reach equilibrium, thus the rate considered for this sample is for the whole duration of the experiment.

The comparison of the regression coefficients shows a better correlation for the oxidation at high pH level than at low pH level with a first order rate contrarily to what was observed with a second order rate. Indeed, with the second order rate the regression coefficients showed a better fit for low pH level oxidation compared to the oxidation at high pH levels.

Furthermore, steeper slopes between the SD and SL sand sub-samples at low pH values are observed compared to high pH values. For instance, the curves at high pH levels are nearly overlapping each other for the 1st and 2nd order rate, as opposed to the curves at low pH levels. This difference is highly likely due to the change of pH in solution during the oxidation process.

The regression coefficients resulting from the 1st order rate show a good to very good fit for all 4 cases (SD and SL samples at both pH ranges) although the 2nd order rate gives slightly better regressions. It is also worth noting that the regression coefficients improve for low pH values for both 1st and 2nd order rate, at the exception of the SD sample when the 1st rate order is considered.

The improved regression coefficients obtained for Mn oxidation at low pH levels compared to the high pH levels are probably due to the influence of pH on the oxidation rate of Mn (II) as there is less variation in terms of Mn (II) concentrations in solution.

The simulation results obtained with PHREEQC showed that the 2nd order reaction rate fits better the experimental results for the oxidation of Mn (II) when the concentrations of Mn (II) are high in solution.

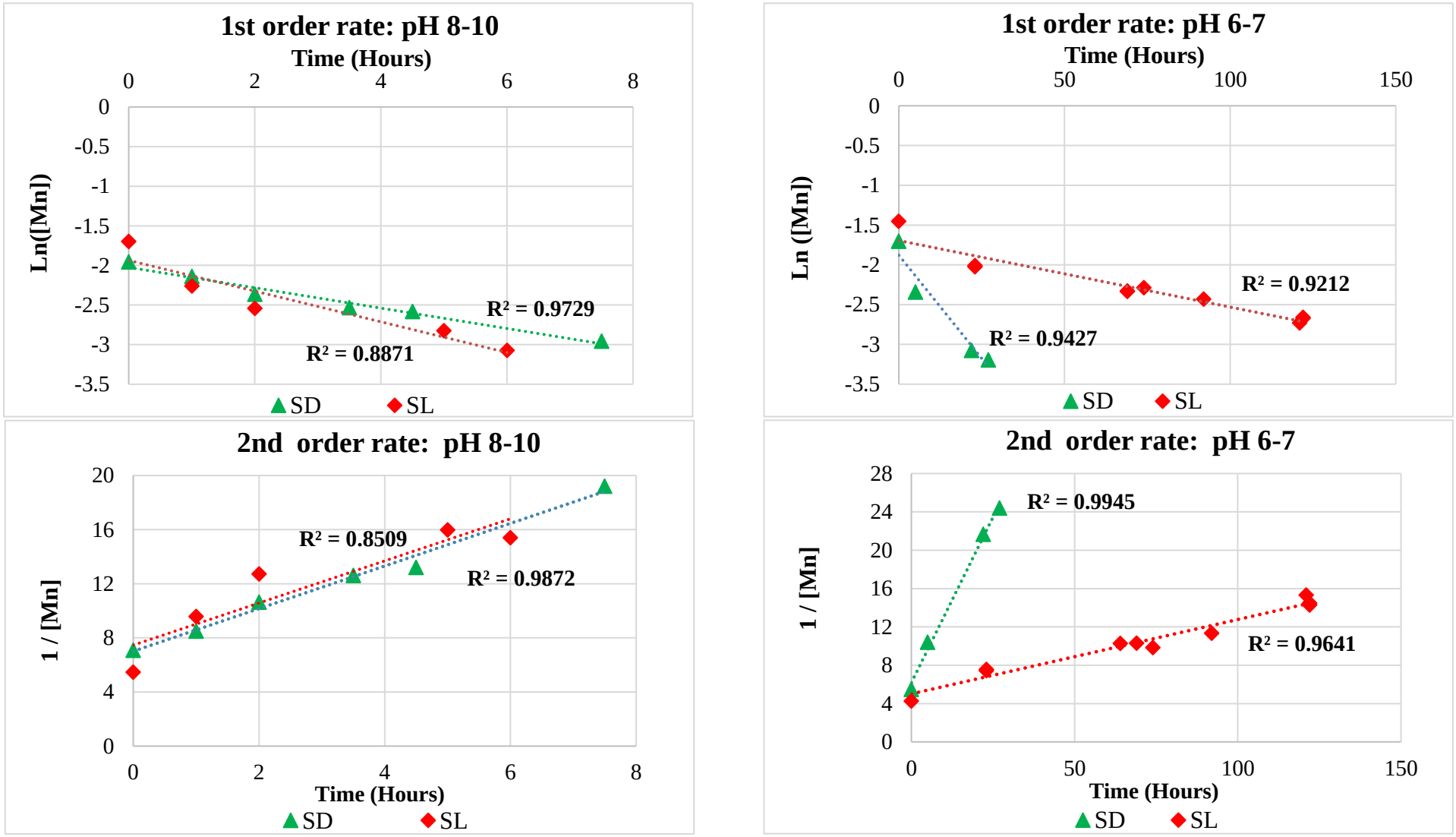

Figure 422: Oxidation kinetics resulting from the manganese (II) oxidation experiments. The figure on the top represents the 1st order reaction rate for high pH (left) and low pH (right) levels. The figures in the bottom represents the 2nd order reaction rate at high pH level (left) and low pH level (right). The green triangle markers and the red lozenge markers represents the SD and SL sand sub-samples, respectively.

5.5. Solid material characterisation

The SEM and XRD results for all the samples, including the SD and SL samples, indicate that the mineralogical composition is similar for all of them with muscovite, hornblende, plagioclase, microcline, chlorite, and quartz being the most abundant. The XRD analysis also correlates with the grain size distribution as the soil is mainly constituted of quartz and to a lesser extent of plagioclase and microcline (Figure 25). These are the common igneous rock-forming minerals found in most sandy soils (Hillel, 2008) which also corresponds to the Holocene deposits of eastern Norway (Høgaas & Longva, 2016).

In addition, the mineral composition at the sampling location coincides with the type of bedrock in Elverum area (Figure 42), which is granite gneiss and known to be composed of quartz, K-feldspar, plagioclase, and hornblende (Rutland & Sutherland, 1967; Campbell, 1997). Moreover, the mineral composition might also reflect on the glaciofluvial sediments deposited along the Glomma River and may originate from upstream the study area.

The mineralogy of the sample indicates that physical processes dominated the pedogenesis of the soil, especially when considering the location of the sampling zone and situated barely few meters from Glomma River which could have played a major role in the formation of the obtained minerals.

From the grain size distribution analysis, it appears that the clay composition of the soil sample is less than 10 %, which may reflect on a soil that has not underwent extensive chemical alterations that make the clay minerals. This was shown during the XRD analysis and where no clay minerals were detected, this may also be due to the difficulties encountered during the quantification of clay minerals when using XRD (Zhou et al., 2018).

5.6. Validity of the results

Sorption and oxidation experiments were run in order to study the behaviour of Fe and Mn. However, a remaining question is whether the experimental results reflect the geochemical processes in the aquifer?

First and foremost, analogue sand, collected close to where the waterworks are located, was used instead of the aquifer material as it was impossible to collect the latter. The solid material used for laboratory purposes was restricted to the grain size interval 125-250 µm so that the grain sizes would be as close as possible to the grain sizes around the wells depth (approximately 19 m). It was also assumed that the analogue material might share the aquifer material characteristics (Figure 3). The sand samples were collected at shallower depth (between 1-100 cm) and the SD

sample was collected at the surface (between 0-15 cm). The collected samples could be either of fluvial origins or a mix between glaciofluvial and fluvial sediments, as fluvial sediments near Glomma river cover the glaciofluvial sediments (Bargel, 1983; Høgaas & Longva, 2016; Olsen et al., 2017). The SEM analysis has showed that most of the observed sand sub-samples portrayed angular, irregular and flaky grains which reflects on the glaciofluvial origin of the deposits, in contrast to more rounded fluvial deposits.

In terms of Fe and Mn coating, the assumption that the analogue samples and the aquifer material have similar sorption properties might not be fully accurate as different types of Fe and Mn oxides and hydroxides can be observed at various depths and can play an important role during the adsorption-oxidation reactions (Detournay et al., 1975; Ren et al., 2013). Nonetheless, the recent findings of Piasecki et al. (2019) indicates that the mineral composition of soils or rocks does not control the fate of Fe (II). Indeed, the latter is mostly dependent on the solution properties such as pH, temperature, redox potential and aerobic or anaerobic conditions. Consequently, the assumption considered when using the analogue sand instead of the in-situ aquifer material might be reasonable and interpolating the results from the analogue sand to the aquifer material is plausible.

Secondly, all the experiments were conducted at room temperature, ca. 21-25° C (the solutions used were also at room temperature), whereas the average temperature in the aquifer is much lower than the one in the laboratory (Average measured groundwater temperatures in Elverum are between 4.8 to 8.0° C). The Mn (II) oxidation experiments in abiotic conditions are expected to increase with increasing pH in solution, increasing temperatures and increasing oxygen activity (Sparrow & Uren, 2014). Although, the oxidation decreases after a maximum is reached (Uren, 2003). The optimum temperature for the oxidation of Mn (II) was found to be 21° C by Thompson et al. (2005) which corresponds to the temperatures during the experiments. Therefore, the results obtained reflects oxidation occurring at optimum temperature conditions. However, these temperatures are higher compared to what is observed in groundwater. In consequence, the oxidation of Mn (II) would probably take longer compared to what was observed during the experiment, as cold temperatures might inhibit or decrease the oxidation rates (Thompson et al., 2005).

Given the fact that the groundwater system is more complex than the setting of the laboratory experiments, the oxidation of Mn (II) is microbially mediated by Mn-oxidising microbes (biotic oxidation) at rates thousand times faster than abiotic oxidation (Diem & Stumm, 1984; Tipping

& Thompson, 1984; Davies & Morgan, 1989; Morgan, 2005; Sparrow & Uren, 2014). Therefore, the obtained experimental results reflect only on abiotic oxidation of Mn.

The sorption and oxidation experimental results were assessed using PHREEQC. The same experiments conditions were respected when writing the scripts in order to compare the modelling results with the laboratory results. Both data sets are comparable, which validates the experimental approach. The modelling investigation were performed in respect to the different geochemical conditions observed in Elverum. It is still possible to follow this approach in other sites where the Vyredox method is applied even if different redox conditions, different Fe and Mn species, pH, and aerobic conditions are observed. Indeed, the laboratory and models set up designed during this study could be easily applied in order to produce site specific parameters. In addition, the results generated from the laboratory experiments could be used as a guide for methodology development for future research studies. For instance, the type of sorption isotherms to select for sorption experiments and the different conditions for oxidation experiments.

The application of the Vyredox method in Elverum has been a great success highly likely due to the characteristics of the aquifer material and where the grain size distribution plays an influential role in controlling the permeability of the material. The latter is permeable enough to deter the pores from clogging, but with sufficient surface area for an optimum sorption of Fe and Mn. Thereupon, laboratory experiments are needed to test the suitability of the Vyredox method in other sites.

6. Conclusions

The Vyredox method has been applied in Grindalsmoen waterworks for more than 30 years and allows the removal of Fe and Mn through aeration. The study focused on studying the sorption and oxidation of Fe and Mn through the use of analogue sand samples and the obtained experimental results were used for geochemical modelling by PHREEQC.

The solid material characterization of the collected samples from Elverum included a grain size analysis and a mineralogy assessment. The grain size distribution showed a homogeneous distribution dominated by sand with minor fractions of silt and gravel. The XRD analysis displayed a similar mineralogy dominated by with varying percentages of quartz, muscovite, plagioclase, hornblende, microcline and chlorite which corresponds to the Holocene deposits of eastern Norway. The use of SEM confirmed the presence of Fe and Mn coating in the form of spots or precipitates on the siliciclastic grain surfaces.

For the chemical characterization of Fe and Mn, two sediment samples were considered and representing the dark (SD) and light (SL) coloured sand. The Fe extraction experiments confirmed the hypothesis that was constructed based on the colour of the sand and where more Fe was extracted from the SD compared to the SL sample.

The influence of more Fe coating in the SD sample was observed when additional laboratory experiments were conducted. Indeed, the Mn sorption experiments showed that Mn was up to 2 times more sorbed in the SD samples compared to the SL samples in both sorption experiments. It was therefore assumed that the presence of more crystalline and non-crystalline form of Fe in the SD sample affected positively the amount of Mn sorbed during the experiments. The sorption data for both samples (SD and SL) showed a very good fit to the Freundlich sorption isotherm with a better regression coefficient for the SL sample. The Freundlich isotherm was preferably used (over the Langmuir isotherm) because it allows to study the sorption on heterogenous formations which is the case of the sand samples used for the laboratory experiments. In general, the Mn sorption capacity was higher on rich Fe-coated sand (SD) compared to less Fe-coated sand (SL).

Oxidation experiments were also carried out in order to determine the effect of pH on the oxidation of Mn with and without Fe-coated sand. The development of these experiments was initially challenging as many trials were needed in order to determine how long the experiments should run, an appropriate concentration of $MnNO_3$ so that the ICP-MS detector are nor saturated, but also the exact volume of HCl that should be added for the oxidation at low pH levels. Every

experiment was at least run for 50 hours in order to monitor the Mn concentration in solution. Based on the results obtained, the oxidation of Mn is more important for high pH ranges (8-10) compared to low pH levels (6-7) as oxidation reactions at low pH values is considered thermodynamically unfavourable when O_2 is the terminal electron receptor. The rates of Mn (II) oxidation are therefore affected by the pH condition in solution and the Mn (II) is oxidized faster at high pH condition than at low pH levels. The oxidation of Mn (II) fits both a 1^{st} and 2^{nd} order reaction rates with slightly better regression coefficients for the 2^{nd} order reaction rate.

The oxidation was observed to be more efficient in the sediment containing more Fe coating (SD sample). Both samples showed a similar trend in terms of the decreasing concentrations of Mn (II) in solution due to its oxidation in the presence of oxygen. The results showed that the oxidation occurs during the first 20 hours of experiment where 80 % of the initial Mn (II) available in solution was lost. For the rest of the experiment, the oxidation reached equilibrium and Mn (II) stopped decreasing in solution. When the oxidation experiments were run in the absence of Fe-coated sand (blank), the Mn (II) concentrations in solution remained stable due to the absence of a solid phase that accelerates the oxidation of Mn (II) through adsorption-oxidation reactions.

6.1. Recommendations for further studies

This study has generated important results with respect to the Mn sorption and oxidation experiments in the area of Grindalsmoen waterworks. These results can be interpolated to the aquifer material from depth around the production wells. It is, however, necessary to carry out further research by using the aquifer material from the production well (or from a nearby drilling aquifer depth) as the mineral composition, biological conditions, groundwater chemistry, pressure and temperature might change over small distance. Using the in-situ aquifer material will ensure more precise and accurate results about the processes occurring exactly where the wells are located.

More extensive oxidation experiments on Fe and Mn at higher and lower pH ranges is imperative as it would shed more light on the Fe and Mn oxidation catalytic rate. Additionally, these experiments need to be conducted in biotic conditions using the aquifer's bacterial composition in order to reproduce as close as possible the same oxidation conditions occurring in the area around the wells. The experimental research would be further complete if the aquifer microbial community would be used for the oxidation experiments as it would enhance our understanding

of the microbial behaviour towards the environmental conditions during the oxidation of Fe and Mn.

Several research articles (e.g. Tronc et al., 1992; Stumm & Sulzberger, 1992; Coughlin & Stone, 1995; Hiemstra & Riemsdijk, 2007) have indicated the role of the mineral composition on the end product of the Fe and Mn oxidation. Consequently, identifying the dominant oxides and hydroxides in the sand aquifer would be a step further towards knowing the fate of the Fe and Mn. More importantly it may give more information on the stability of the formed precipitates and their role in clogging the pores during the Vyredox treatment which might reflect on this method's efficiency.

7. References

Ahmad, M. (2012). *Iron and manganese removal from groundwater: geochemical modeling of the Vyredox method* (Master's thesis, Norway). Oslo: University of Oslo.

Akinbola, G. E. (2013). Dithionite and oxalate extraction of iron and manganese in some basement complex soils of southwestern Nigeria. *Journal of Experimental Sciences*, *4*(2), 22–26. Retrieved from http://jexpsciences.com

Al-Ghouti, M. A., & Da'ana, D. A. (2020). Guidelines for the use and interpretation of adsorption isotherm models: A review. *Journal of Hazardous Materials*, *393*(122383). doi.org/10.1016/j.jhazmat.2020.122383

Allen, D. M., & Suchy, M. (2001). Geochemical evolution of groundwater on Saturna Island, British Columbia. *Canadian Journal of Earth Sciences*, *38*(7), 1059–1080. doi.org/10.1139/e01-007

Appelo, C. A. J., & Postma, D. (2005). *Geochemistry, Groundwater and Pollution, Second Edition* (2nd ed.). The Netherlands: Taylor & Francis.

Appelo, C., & Postma, D. (2005). *Geochemistry, Groundwater and Pollution* (2nd ed.). The Netherlands: CRC Press.

Baker, B. J., & Banfield, J. F. (2003). Microbial communities in acid mine drainage. *FEMS Microbiology Ecology*, *44*(2), 139–152. doi.org/10.1016/s0168-6496(03)00028-x

Ballantine Jr., D. S., White, R. M., Martin, S. J., Ricco, A. J., Zellers, E. T., Frye, G. C., Wohltjen, H., Levy, M., & Stern, R. (1996). *Acoustic Wave Sensors: Theory, Design and Physico-Chemical Applications (Applications of Modern Acoustics)* (1st ed.). San Diego: Academic Press.

Banks, D., Kjersti Midtgård, A., Frengstad, B., Reidar Krog, J., & Strand, T. (1998). The chemistry of Norwegian groundwaters: II. The chemistry of 72 groundwaters from Quaternary sedimentary aquifers. *Science of The Total Environment*, *222*(1–2), 93–105. doi.org/10.1016/s0048-9697(98)00292-7

Bargel, T.H. (1983). Elverum. Quaternary geological map with description 2016 IV, scale 1:50 000. Norges geologiske undersøkelse, 376. Retrieved from https://www.ngu.no

Barloková, D., & Ilavský, J. (2010). Removal of iron and manganese from water using filtration by natural materials. *Polish Journal of Environmental Studies*, *19*(6), 1117–1122. Retrieved from https://www.researchgate.net/publication/285527881_Removal_of_Iron_and_Manganese_from_Water_Using_Filtration_by_Natural_Materials

Barrow, N. J. (1978). The description of phosphate adsorption curve. *Journal of Soil Science*, *29*(4), 447–462. doi.org/10.1111/j.1365-2389.1978.tb00794.x

Bharat, T. V. (2017). Selection and Configuration of Sorption Isotherm Models in Soils Using Artificial Bees Guided by the Particle Swarm. *Advances in Artificial Intelligence*, *2017*, 1–22. doi.org/10.1155/2017/3497652

Bray, A. W., Oelkers, E. H., Bonneville, S., Wolff-Boenisch, D., Potts, N. J., Fones, G., & Benning, L. G. (2015). The effect of pH, grain size, and organic ligands on biotite weathering rates. *Geochimica et Cosmochimica Acta*, *164*, 127–145. doi.org/10.1016/j.gca.2015.04.048

Bricker, O. (1965). Some stability relations in the system Mn-O,-H,O and one atmosphere total pressure. *The American Mineralogist*, *50*, 1296–1354. Retrieved from https://rruff-2.geo.arizona.edu/uploads/AM50_1296.pdf

Brindha, K., Paul, R., Walter, J., Tan, M. L., & Singh, M. K. (2020). Trace metals contamination in groundwater and implications on human health: comprehensive assessment using hydrogeochemical and geostatistical methods. *Environmental Geochemistry and Health*, *42*(11), 3819–3839. doi.org/10.1007/s10653-020-00637-9

Brown, C. J., Coates, J. D., & Schoonen, M. A. (1999). Localized Sulfate-Reducing Zones in a Coastal Plain Aquifer. *Ground Water*, *37*(4), 505–516. doi.org/10.1111/j.1745-6584.1999.tb01136.x

Bruins, J. H., Petrusevski, B., Slokar, Y. M., Huysman, K., Joris, K., Kruithof, J. C., & Kennedy, M. D. (2015). Biological and physico-chemical formation of Birnessite during the ripening of manganese removal filters. *Water Research*, *69*, 154–161. doi.org/10.1016/j.watres.2014.11.019

Buamah, R. (2009). *Adsorptive Removal of Manganese, Arsenic and Iron from Groundwater:* (Doctoral dissertation, UNESCO-IHE Institute for Water Education, Delft & Wageningen University, The Netherlands). The Netherlands: CRC Press.

Buamah, R., Petrusevski, B., de Ridder, D., van de Wetering, T. S. C. M., & Shippers, J. C. (2009). Manganese removal in groundwater treatment: practice, problems and probable solutions. *Water Supply*, *9*(1), 89–98. doi.org/10.2166/ws.2009.009

Buhrke, V. E., Jenkins, R., & Smith, D. K. (1997). *A Practical Guide for the Preparation of Specimens for X-Ray Fluorescence and X-Ray Diffraction Analysis* (1st ed.). New York: Wiley-VCH.

Bunaciu, A. A., Udriştioiu, E. G., & Aboul-Enein, H. Y. (2015). X-Ray Diffraction: Instrumentation and Applications. *Critical Reviews in Analytical Chemistry*, *45*(4), 289–299. doi.org/10.1080/10408347.2014.949616

Burger, M. S., Krentz, C. A., Mercer, S. S., & Gagnon, G. A. (2008a). Manganese removal and occurrence of manganese oxidizing bacteria in full-scale biofilters. *Journal of Water Supply: Research and Technology-Aqua*, *57*(5), 351–359. doi.org/10.2166/aqua.2008.050

Burger, M. S., Mercer, S. S., Shupe, G. D., & Gagnon, G. A. (2008a). Manganese removal during bench-scale biofiltration. *Water Research*, *42*(19), 4733–4742. doi.org/10.1016/j.watres.2008.08.024

Chao, T. T., & Zhou, L. (1983). Extraction Techniques for Selective Dissolution of Amorphous Iron Oxides from Soils and Sediments. *Soil Science Society of America Journal*, *47*(2), 225–232. doi.org/10.2136/sssaj1983.03615995004700020010x

Chauhan, A., & Chauhan, P. (2014). Powder XRD Technique and its Applications in Science and Technology. *Journal of Analytical & Bioanalytical Techniques*, *5*(5), 1–5. doi.org/10.4172/2155-9872.1000212

Chung, H. K., Kim, W. H., Park, J., Cho, J., Jeong, T. Y., & Park, P. K. (2015). Application of Langmuir and Freundlich isotherms to predict adsorbate removal efficiency or required amount of adsorbent. *Journal of Industrial and Engineering Chemistry*, *28*, 241–246. doi.org/10.1016/j.jiec.2015.02.021

Colmer, A. R., & Hinkle, M. E. (1947). The Role of Microorganisms in Acid Mine Drainage: A Preliminary Report. *Science*, *106*(2751), 253–256. doi.org/10.1126/science.106.2751.253

Coughlin, B. R., & Stone, A. T. (1995). Nonreversible Adsorption of Divalent Metal Ions (MnII, CoII, NiII, CuII, and PbII) onto Goethite: Effects of Acidification, FeII Addition, and

Picolinic Acid Addition. *Environmental Science & Technology*, *29*(9), 2445–2455. doi.org/10.1021/es00009a042

Coughlin, R., & Matsui, I. (1976). Catalytic oxidation of aqueous Mn(II). *Journal of Catalysis*, *41*(1), 108–123. doi.org/10.1016/0021-9517(76)90206-2

Darke, A. K., & Walbridge, M. R. (1994). Estimating non-crystalline and crystalline aluminum and iron by selective dissolution in a riparian forest soil. *Communications in Soil Science and Plant Analysis*, *25*(11–12), 2089–2101. doi.org/10.1080/00103629409369174

Davies, S. H., & Morgan, J. J. (1989). Manganese (II) oxidation kinetics on metal oxide surfaces. *Journal of Colloid and Interface Science*, *129*(1), 63–77. doi.org/10.1016/0021-9797(89)90416-5

Davison, W. (1993). Iron and manganese in lakes. *Earth-Science Reviews*, *34*(2), 119–163. doi.org/10.1016/0012-8252(93)90029-7

Detournay, J., de Miranda, L., Derie, R., & Ghodsi, M. (1975). The region of stability of green rust II in the electrochemical potential-pH equilibrium diagram of iron in sulphate medium. *Corrosion Science*, *15*(5), 295–306. doi.org/10.1016/s0010-938x(75)80011-4

Diem, D., & Stumm, W. (1984). Is dissolved Mn2+ being oxidized by O2 in absence of Mn-bacteria or surface catalysts? *Geochimica et Cosmochimica Acta*, *48*(7), 1571–1573. doi.org/10.1016/0016-7037(84)90413-7

Dobson, A. W., Erikson, K. M., & Aschner, M. (2004). Manganese Neurotoxicity. *Annals of the New York Academy of Sciences*, *1012*(1), 115–128. doi.org/10.1196/annals.1306.009

Dove, P. M., & Hochella, M. F. (1993). Compatible real-time rates of mineral dissolution by Atomic Force Microscopy (AFM). *Geochimica et Cosmochimica Acta*, *57*(3), 705–7014. doi.org/10.1016/0016-7037(93)90381-6

Duckworth, O. W., & Sposito, G. (2005). Siderophore−Manganese(III) Interactions. I. Air-Oxidation of Manganese(II) Promoted by Desferrioxamine B. *Environmental Science & Technology*, *39*(16), 6037–6044. doi.org/10.1021/es050275k

Edmunds, M. W., & Shand, P. (2008). *Natural Groundwater Quality* (1st ed.). Oxford: Wiley-Blackwell.

Edmunds, W. M., & Smedley, P. L. (1996). Groundwater geochemistry and health: an overview. *Geological Society, London, Special Publications*, *113*(1), 91–105. doi.org/10.1144/gsl.sp.1996.113.01.08

Ehrlich, H. (1998). Geomicrobiology: its significance for geology. *Earth-Science Reviews*, *45*(1–2), 45–60. doi.org/10.1016/s0012-8252(98)00034-8

Emerick, R. W., Loge, F. J., Ginn, T., & Darby, J. L. (2000). Modeling the Inactivation of Particle-Associated Coliform Bacteria. *Water Environment Research*, *72*(4), 432–438. doi.org/10.2175/106143000x137969

Emerson, D., Fleming, E. J., & McBeth, J. M. (2010). Iron-Oxidizing Bacteria: An Environmental and Genomic Perspective. *Annual Review of Microbiology*, *64*(1), 561–583. doi.org/10.1146/annurev.micro.112408.134208

Epp, J. (2016). X-ray diffraction (XRD) techniques for materials characterization. *Materials Characterization Using Nondestructive Evaluation (NDE) Methods*, 81–124. doi.org/10.1016/b978-0-08-100040-3.00004-3

European Commission. Directorate-General for the Environment. (2008). *Groundwater protection in Europe*. Office for Official Publications of the European Communities. doi.org/10.2779/84304

Faust, S. D., & Aly, O. M. (1998). *Chemistry of Water Treatment, 2nd Edition* (2nd ed.). New York: CRC Press.

Fitsanakis, V. A., Zhang, N., Garcia, S., & Aschner, M. (2009). Manganese (Mn) and Iron (Fe): Interdependency of Transport and Regulation. *Neurotoxicity Research*, *18*(2), 124–131. doi.org/10.1007/s12640-009-9130-1

Gadde, R. R., & Laitinen, H. A. (1974). Heavy metal adsorption by hydrous iron and manganese oxides. *Analytical Chemistry*, *46*(13), 2022–2026. doi.org/10.1021/ac60349a004

Ghiorse, W. C. (1984). Biology of Iron-and Manganese-Depositing Bacteria. *Annual Review of Microbiology*, *38*(1), 515–550. doi.org/10.1146/annurev.mi.38.100184.002503

Goldberg, S., Criscenti, L. J., Turner, D. R., Davis, J. A., & Cantrell, K. J. (2007). Adsorption-Desorption Processes in Subsurface Reactive Transport Modeling. *Vadose Zone Journal*, *6*(3), 407–435. doi.org/10.2136/vzj2006.0085

Golden, D. C. (1994). Acidified Oxalate and Dithionite Solubility and Color of Synthetic, Partially Oxidized Al-Magnetites and their Thermal Oxidation Products. *Clays and Clay Minerals*, *42*(1), 53–62. doi.org/10.1346/ccmn.1994.0420107

Golden, D., Dixon, J., & Kanehiro, Y. (1993). The manganese oxide mineral, lithiophorite, in an oxisol From Hawaii. *Soil Research*, *31*(1), 51. doi.org/10.1071/sr9930051

Gu, H., Chi, B., Li, H., Jiang, J., Qin, W., & Wang, H. (2014). Assessment of groundwater quality and identification of contaminant sources of Liujiang basin in Qinhuangdao, North China. *Environmental Earth Sciences*, *73*(10), 6477–6493. doi.org/10.1007/s12665-014-3870-9

Hallberg, R. O., & Martinell, R. (1976). Vyredox - In Situ Purification of Ground Water. *Ground Water*, *14*(2), 88–93. doi.org/10.1111/j.1745-6584.1976.tb03638.x

Harland, C. (1994). *Ion exchange (RSC Paperbacks)* (2nd ed., Vol. 6). Cambridge: Royal Society of Chemistry

Hem, J. D. (1963). *Chemical equilibria and rates of manganese oxidation* (No. 1667). Water supply paper USGS. doi.org/10.3133/wsp1667A

Hem, J. D. (1972). Chemical Factors that Influence the Availability of Iron and Manganese in Aqueous Systems. *Geological Society of America Bulletin*, *83*(2), 443–450. doi.org/10.1130/SPE140-p17

Hem, J. D. (1989). *Study and Interpretation of the Chemical Characteristics of Natural Water* (No. 2254). US Geological Survey Water Supply Paper. doi.org/10.3133/wsp1473

Hiemstra, T., & van Riemsdijk, W. H. (2007). Adsorption and surface oxidation of Fe(II) on metal (hydr)oxides. *Geochimica et Cosmochimica Acta*, *71*(24), 5913–5933. doi.org/10.1016/j.gca.2007.09.030

Høgaas, F., & Longva, O. (2016). Mega deposits and erosive features related to the glacial lake Nedre Glomsjø outburst flood, southeastern Norway. *Quaternary Science Reviews*, *151*(1), 273–291. doi.org/10.1016/j.quascirev.2016.09.015

Høgaas, F., & Longva, O. (2019). The late-glacial ice-dammed lake Nedre Glomsjø in Mid-Norway: an open lake system succeeding an actively retreating ice sheet. *Norwegian Journal of Geology*. Published. doi.org/10.17850/njg98-4-08

Howe, P., WHO, Malcolm, H., Dobson, S., World Health Organization, WHO, World Health Organization, United Nations Environment Programme, International Labour Organisation, International Program on Chemical Safety, & Inter-Organization Programme for the Sound Management of Chemicals. (2004). *Manganese and Its Compounds: Environmental Aspects*. World Health Organization.

Hoyland, V. W., Knocke, W. R., Falkinham, J. O., Pruden, A., & Singh, G. (2014). Effect of drinking water treatment process parameters on biological removal of manganese from surface water. *Water Research*, *66*, 31–39. doi.org/10.1016/j.watres.2014.08.006

Huang, B., Li, Z., Chen, Z., Chen, G., Zhang, C., Huang, J., Nie, X., Xiong, W., & Zeng, G. (2015). Study and health risk assessment of the occurrence of iron and manganese in groundwater at the terminal of the Xiangjiang River. *Environmental Science and Pollution Research*, *22*(24), 19912–19921. doi.org/10.1007/s11356-015-5230-z

Huang, J., & Zhang, H. (2020). Redox reactions of iron and manganese oxides in complex systems. *Frontiers of Environmental Science & Engineering*, *14*(5), 1–12. doi.org/10.1007/s11783-020-1255-8

Jacobs, P. M., West, L. T., & Shaw, J. N. (2002). Redoximorphic Features as Indicators of Seasonal Saturation, Lowndes County, Georgia. *Soil Science Society of America Journal*, *66*(1), 315–323. doi.org/10.2136/sssaj2002.0315

Jaudon, P., Massiani, C., Galea, J., Rey, J., & Vacelet, E. (1989). Groundwater pollution by manganese. Manganese speciation: Application to the selection and discussion of an in situ groundwater treatment. *Science of The Total Environment*, *84*, 169–183. doi.org/10.1016/0048-9697(89)90381-1

Jin, Q., Huang, L., Li, A., & Shan, A. (2017). Quantification of the limitation of Langmuir model used in adsorption research on sediments via site energy heterogeneity. *Chemosphere*, *185*, 518–528. doi.org/10.1016/j.chemosphere.2017.07.051

Jolis, D., Lam, C., & Pitt, P. (2001). Particle Effects on Ultraviolet Disinfection of Coliform Bacteria in Recycled Water. *Water Environment Research*, *73*(2), 233–236. doi.org/10.2175/106143001x139218

Junta, J. L., & Hochella, M. F. (1994). Manganese (II) oxidation at mineral surfaces: A microscopic and spectroscopic study. *Geochimica et Cosmochimica Acta*, *58*(22), 4985–4999. doi.org/10.1016/0016-7037(94)90226-7

Khatri, N., Tyagi, S., & Rawtani, D. (2017). Recent strategies for the removal of iron from water: A review. *Journal of Water Process Engineering*, *19*, 291–304. doi.org/10.1016/j.jwpe.2017.08.015

Khozyem, H., Hamdan, A., Tantawy, A. A., Emam, A., & Elbadry, E. (2019). Distribution and origin of iron and manganese in groundwater: case study, Balat-Teneida area, El-Dakhla

Basin, Egypt. *Arabian Journal of Geosciences*, *12*(16), 1–16. doi.org/10.1007/s12517-019-4689-1

Klemsdal, T. (2010). The eolian landforms and sediment in the valley of River Jømna, east of Elverum, south-east Norway. *Norsk Geografisk Tidsskrift - Norwegian Journal of Geography*, *64*(2), 94–104. doi.org/10.1080/00291951.2010.481138

Kløve, B., Kvitsand, H. M. L., Pitkänen, T., Gunnarsdottir, M. J., Gaut, S., Gardarsson, S. M., Rossi, P. M., & Miettinen, I. (2017). Overview of groundwater sources and water-supply systems, and associated microbial pollution, in Finland, Norway and Iceland. *Hydrogeology Journal*, *25*(4), 1033–1044. doi.org/10.1007/s10040-017-1552-x

Krishnamurti, G. S. R., & Huang, P. M. (1989). Influence of Mn2+ and pH on the Formation of Iron Oxides from Ferrous Chloride and Ferrous Sulfate Solutions1. *Clays and Clay Minerals*, *37*(5), 451–458. doi.org/10.1346/ccmn.1989.0370509

Kundu, S., & Gupta, A. (2006). Arsenic adsorption onto iron oxide-coated cement (IOCC): Regression analysis of equilibrium data with several isotherm models and their optimization. *Chemical Engineering Journal*, *122*(1–2), 93–106. doi.org/10.1016/j.cej.2006.06.002

Lambe, W. T. (1969). *Soil Mechanics (Series in Soil Engineering)* (1st ed.). John Wiley & Sons.

LaZerte, B. D., & Burling, K. (1990). Manganese speciation in dilute waters of the Precambrian shield, Canada. *Water Research*, *24*(9), 1097–1101. doi.org/10.1016/0043-1354(90)90172-3

Linge, K. L., & Jarvis, K. E. (2009). Quadrupole ICP-MS: Introduction to Instrumentation, Measurement Techniques and Analytical Capabilities. *Geostandards and Geoanalytical Research*, *33*(4), 445–467. doi.org/10.1111/j.1751-908x.2009.00039.x

Liu, L., Luo, X. B., Ding, L., & Luo, S. L. (2019). Application of Nanotechnology in the Removal of Heavy Metal From Water. *Nanomaterials for the Removal of Pollutants and Resource Reutilization*, 83–147. doi.org/10.1016/b978-0-12-814837-2.00004-4

Longva, O. (1994). *Flood deposits and erosional features from the catastrophic drainage of Preboreal glacial lake Nedre Glåmsjø, SE Norway*. Bergen: University of Bergen.

Lovley, D. R., & Phillips, E. J. P. (1986). Organic Matter Mineralization with Reduction of Ferric Iron in Anaerobic Sediments. *Applied and Environmental Microbiology*, *51*(4), 683–689. doi.org/10.1128/aem.51.4.683-689.1986

Luo, Y., Ding, J., Shen, Y., Tan, W., Qiu, G., & Liu, F. (2018). Symbiosis mechanism of iron and manganese oxides in oxic aqueous systems. *Chemical Geology*, *488*, 162–170. doi.org/10.1016/j.chemgeo.2018.04.030

Luther, G. W. (2009). The Role of One- and Two-Electron Transfer Reactions in Forming Thermodynamically Unstable Intermediates as Barriers in Multi-Electron Redox Reactions. *Aquatic Geochemistry*, *16*(3), 395–420. doi.org/10.1007/s10498-009-

Luther, G. W., Kostka, J. E., Church, T. M., Sulzberger, B., & Stumm, W. (1992). Seasonal iron cycling in the salt-marsh sedimentary environment: the importance of ligand complexes with Fe(II) and Fe(III) in the dissolution of Fe(III) minerals and pyrite, respectively. *Marine Chemistry*, *40*(1–2), 81–103. doi.org/10.1016/0304-4203(92)90049-g

Luzati, S., Beqiraj, A., Goga, E. B., & Jaupaj, O. (2016). Iron and Manganese in Groundwater of Rrogozhina Aquifer, Western Albania. *Journal of Environmental Science and Engineering B*, *5*(6). doi.org/10.17265/2162-5263/2016.06.002

Machiels, L., Garcés, D., Snellings, R., Vilema, W., Morante, F., Paredes, C., & Elsen, J. (2014). Zeolite occurrence and genesis in the Late-Cretaceous Cayo arc of Coastal Ecuador: Evidence for zeolite formation in cooling marine pyroclastic flow deposits. *Applied Clay Science*, *87*, 108–119. doi.org/10.1016/j.clay.2013.10.018

Malard, F., & Hervant, F. (1999). Oxygen supply and the adaptations of animals in groundwater. *Freshwater Biology*, *41*(1), 1–30. doi.org/10.1046/j.1365-2427.1999.00379.x

McKeague, J. A., Brydon, J. E., & Miles, N. M. (1971). Differentiation of Forms of Extractable Iron and Aluminum in Soils. *Soil Science Society of America Journal*, *35*(1), 33–38. doi.org/10.2136/sssaj1971.03615995003500010016x

Martin, S. T. (2005). Precipitation and dissolution of iron and manganese oxides. *Environmental Catalysis*, *1*, 61–82. Retrieved https://www.researchgate.net

Mergler, D., Baldwin, M., Belanger, S., Larribe, F., Beuter, A., Bowler, R., Panisset, M., Edwards, R., de Geoffroy, A., Sassine, M. P., & Hudnell, K. (1999). Manganese neurotoxicity, a continuum of dysfunction: results from a community-based study. *Neurotoxicology*, *20*(2–3), 327–342.

Mettler, S. (2002). *In situ removal of iron from ground water Fe(II) oxygenation, and precipitation products in a calcareous aquifer* (Doctoral dissertation). ETH: Zürich.

Millero, F. J. (1985). The effect of ionic interactions on the oxidation of metals in natural waters. *Geochimica et Cosmochimica Acta*, *49*(2), 547–553. doi.org/10.1016/0016-7037(85)90046-8

Millero, F. J. (1990). Marine solution chemistry and ionic interactions. *Marine Chemistry*, *30*, 205–229. doi.org/10.1016/0304-4203(90)90071-j

Millero, F. J., & Hawke, D. J. (1992). Ionic interactions of divalent metals in natural waters. *Marine Chemistry*, *40*(1–2), 19–48. doi.org/10.1016/0304-4203(92)90046-d

Millero, F. J., Sotolongo, S., & Izaguirre, M. (1987). The oxidation kinetics of Fe(II) in seawater. *Geochimica et Cosmochimica Acta*, *51*(4), 793–801. doi.org/10.1016/0016-7037(87)90093-7

Moen, A. (1998). *Atlas: vegetation*. Norway: the Norwegian Geographical Survey.

Montes, S., Riojas-Rodríguez, H., Sabido-Pedraza, E., & Ríos, C. (2008). Biomarkers of manganese exposure in a population living close to a mine and mineral processing plant in Mexico. *Environmental Research*, *106*(1), 89–95. doi.org/10.1016/j.envres.2007.08.008

Morgan, B., & Lahav, O. (2007). The effect of pH on the kinetics of spontaneous Fe(II) oxidation by O2 in aqueous solution – basic principles and a simple heuristic description. *Chemosphere*, *68*(11), 2080–2084. doi.org/10.1016/j.chemosphere.2007.02.015

Morgan, J. J. (2005). Kinetics of reaction between O2 and Mn(II) species in aqueous solutions. *Geochimica et Cosmochimica Acta*, *69*(1), 35–48. doi.org/10.1016/j.gca.2004.06.013

Morgan, J. J., & Stumm, W. (1964). Colloid-chemical properties of manganese dioxide. *Journal of Colloid Science*, *19*(4), 347–359. doi.org/10.1016/0095-8522(64)90036-4

Mouchet, P. (1992). From Conventional to Biological Removal of Iron and Manganese in France. *Journal - American Water Works Association*, *84*(4), 158–167. doi.org/10.1002/j.1551-8833.1992.tb07342.x

Mukhopadhyay, S. M. (2003). Sample Preparation for Microscopic and Spectroscopic Characterization of Solid Surfaces and Films. *Sample Preparation Techniques in Analytical Chemistry*, 377–411. doi.org/10.1002/0471457817.ch9

Munch, J. C., & Ottow, J. C. G. (1983b). Reductive Transformation Mechanism of Ferric Oxides in Hydromorphic Soils. *Environmental Biogeochemistry*, *35*. Retrieved from https://www.jstor.org/stable/20112874?seq=1#metadata_info_tab_contents

Nesse, W. D. (2000). *Introduction to Mineralogy*. New York: Oxford University Press.

Ngah, S. A., & Nwankoala, H. O. (2013). Iron (Fe 2+) occurrence and distribution in groundwater sources in different geomorphologic zones of Eastern Niger Delta. *Archives of Applied Science Research*, *5*(2), 266–272. Retrieved from https://www.scholarsresearchlibrary.com/abstract/iron-fe2-occurrence-and-distribution-in-groundwater-sources-in-different-geomorphologic-zones-of-eastern-niger-delta-922.html

Novak, M., Zemanova, L., Voldrichova, P., Stepanova, M., Adamova, M., Pacherova, P., Komarek, A., Krachler, M., & Prechova, E. (2011). Experimental Evidence for Mobility/Immobility of Metals in Peat. *Environmental Science & Technology*, *45*(17), 7180–7187. doi.org/10.1021/es201086v

Parkhurst, D. L., & Appelo, C. A. J. (1999). User's guide to PHREEQC (Version 2): A computer program for speciation, batch-reaction, one-dimensional transport, and inverse geochemical calculations. *Water Resources Investigations Report*, *99*(4259), 312. doi.org/10.3133/wri994259

Penrose, R. A. F. (1893). The Chemical Relation of Iron and Manganese in Sedimentary Rocks. *The Journal of Geology*, *1*(4), 356–370. doi.org/10.1086/606194

Piasecki, W., Szymanek, K., & Charmas, R. (2019). Fe^{2+} adsorption on iron oxide: the importance of the redox potential of the adsorption system. *Adsorption*, *25*(3), 613–619. doi.org/10.1007/s10450-019-00054-0

Pillans, B., & Gibbard, P. (2012). The Quaternary Period. *The Geologic Time Scale*, *2*, 979–1010. doi.org/10.1016/b978-0-444-59425-9.00030-5

Post, J. E. (1999). Manganese oxide minerals: Crystal structures and economic and environmental significance. *Proceedings of the National Academy of Sciences*, *96*(7), 3447–3454. doi.org/10.1073/pnas.96.7.3447

Postawa, A., Hayes, C., Criscuoli, A., Macedonio, F., Angelakis, A. N., Rose, J. B., Maier, A., & McAvoy, D. C. (2013). *Best Practice Guide on the Control of Iron and Manganese in Water Supply*. Van Haren Publishing.

Postma, D. (1985). Concentration of Mn and separation from Fe in sediments—I. Kinetics and stoichiometry of the reaction between birnessite and dissolved Fe(II) at 10°C. *Geochimica et Cosmochimica Acta*, *49*(4), 1023–1033. doi.org/10.1016/0016-7037(85)90316-3

Ren, H. T., Jia, S. Y., Wu, S. H., Liu, Y., Hua, C., & Han, X. (2013). Abiotic oxidation of Mn(II) induced oxidation and mobilization of As(III) in the presence of magnetite and hematite. *Journal of Hazardous Materials*, *254-255–255*, 89–97. doi.org/10.1016/j.jhazmat.2013.03.022

Rennert, T., Dietel, J., Heilek, S., Dohrmann, R., & Mansfeldt, T. (2021). Assessing poorly crystalline and mineral-organic species by extracting Al, Fe, Mn, and Si using (citrate-) ascorbate and oxalate. *Geoderma*, *397*, 115095. doi.org/10.1016/j.geoderma.2021.115095

Rezakazemi, M., & Zhang, Z. (2018). 2.29 Desulfurization Materials. *Comprehensive Energy Systems*, 944–979. doi.org/10.1016/b978-0-12-809597-3.00263-7

Rosecrans, C. Z., Nolan, B. T., & Gronberg, J. M. (2017). Prediction and visualization of redox conditions in the groundwater of Central Valley, California. *Journal of Hydrology*, *546*, 341–356. doi.org/10.1016/j.jhydrol.2017.01.014

Rutland, R. W., & Sutherland, D. S. (1967). The chemical composition of granitic gneisses and sparagmitic metasediments in the Glomfjord region. *Norwegian Journal of Geology*, *47*(4), 359–374. Retrieved from https://njg.geologi.no

Ryan, J. N., & Gschwend, P. M. (1991). Extraction of Iron Oxides from Sediments Using Reductive Dissolution by Titanium(III). *Clays and Clay Minerals*, *39*(5), 509–518. doi.org/10.1346/ccmn.1991.0390506

Sarikaya, H. Z. (1990). Contact aeration for iron removal—A theoretical assessment. *Water Research*, *24*(3), 329–331. doi.org/10.1016/0043-1354(90)90008-T

Schwartz, J. (1985). Alkane activation by oxide-bound organorhodium complexes. *Accounts of Chemical Research*, *18*(10), 302–308. doi.org/10.1021/ar00118a004

Schwertmann, U. (1959). Die fraktionierte Extraktion der freien Eisenoxyde in Böden, ihre mineralogischen Formen und ihre Entstehungsweisen. *Zeitschrift Für Pflanzenernährung, Düngung, Bodenkunde*, *84*(1–3), 194–204. doi.org/10.1002/jpln.19590840131

Schwertmann, U. (1964). Differenzierung der Eisenoxide des Bodens durch Extraktion mit Ammoniumoxalat-Lösung. *Zeitschrift Für Pflanzenernährung, Düngung, Bodenkunde*, *105*(3), 194–202. doi.org/10.1002/jpln.3591050303

Schwertmann, U. (1993). *Relations Between Iron Oxides, Soil Color, and Soil Formation* (1st ed., Vol. 31). Ciolkosz.

Schwertmann, U., & Cornell, R. M. (2000a). *Iron Oxides in the Laboratory*. Weinheim: Wiley-VCH

Schwertmann, U., & Cornell, R. M. (2000b). *Iron Oxides in the Laboratory: Preparation and Characterization* (2nd ed.). Weinheim: Wiley-VCH.

Seelig, B., Bergsrud, F., & Derickson, R. (1996). Treatment Systems for Household Water Supplies: Iron and Manganese Removal. *Fact Sheets*, *59*, 4–6. Retrieved from https://openprairie.sdstate.edu/extension_fact/59/

Seppanen, H. T. (1992). Experiences of Biological Iron and Manganese Removal in Finland. *Water and Environment Journal*, *6*(3), 333–340. doi.org/10.1111/j.1747-6593.1992.tb00757.x

Singer, P. C., & Stumm, W. (1970). Acidic Mine Drainage: The Rate-Determining Step. *Science*, *167*(3921), 1121–1123. doi.org/10.1126/science.167.3921.1121

Sparrow, L. A., & Uren, N. C. (2014). Manganese oxidation and reduction in soils: effects of temperature, water potential, pH and their interactions. *Soil Research*, *52*(5), 483–494. doi.org/10.1071/sr13159

Steefel, C. I., & van Cappellen, P. (1990). A new kinetic approach to modeling water-rock interaction: The role of nucleation, precursors, and Ostwald ripening. *Geochimica et Cosmochimica Acta*, *54*(10), 2657–2677. doi.org/10.1016/0016-7037(90)90003-4

Stumm, W., & Lee, G. F. (1961). Oxygenation of Ferrous Iron. *Industrial & Engineering Chemistry*, *53*(2), 143–146. doi.org/10.1021/ie50614a030

Stumm, W., & Morgan, J. J. (1996a). *Aquatic Chemistry: Chemical Equilibria and Rates in Natural Waters* (3rd ed.). New York: Wiley-Interscience.

Stumm, W., & Morgan, J. J. (1996b). *Aquatic Chemistry: Chemical Equilibria and Rates in Natural Waters* (3rd ed.). New York: Wiley-Interscience.

Stumm, W., & Sulzberger, B. (1992). The cycling of iron in natural environments: Considerations based on laboratory studies of heterogeneous redox processes.

Geochimica et Cosmochimica Acta, *56*(8), 3233–3257. doi.org/10.1016/0016-7037(92)90301-x

Sunda, W. G., Huntsman, S. A., & Harvey, G. R. (1983). Photoreduction of manganese oxides in seawater and its geochemical and biological implications. *Nature*, *301*(5897), 234–236. doi.org/10.1038/301234a0

Sung, W., & Morgan, J. J. (1980). Kinetics and product of ferrous iron oxygenation in aqueous systems. *Environmental Science & Technology*, *14*(5), 561–568. doi.org/10.1021/es60165a006

Sung, W., & Morgan, J. J. (1981). Oxidative removal of Mn(II) from solution catalysed by the γ-FeOOH (lepidocrocite) surface. *Geochimica et Cosmochimica Acta*, *45*(12), 2377–2383. doi.org/10.1016/0016-7037(81)90091-0

Suzuki, M. (1990). *Adsorption Engineering (Chemical Engineering Monographs)* (Vol. 25). Tokyo: Elsevier Science.

Tamm, O. (1922). Eine Methode zur Bestimmung des anorganischen Gelkomplexes im Boden. *Meddelanden Från Statens Skogsförsöksanstalt*, *19*, 385–404.

Tamura, H., Goto, K., & Nagayama, M. (1976). The effect of ferric hydroxide on the oxygenation of ferrous ions in neutral solutions. *Corrosion Science*, *16*(4), 197–207. doi.org/10.1016/0010-938x(76)90046-9

Taylor, R. M., McKenzie, R. M., & Norrish, K. (1964). The mineralogy and chemistry of manganese in some Australian soils. *Soil Research*, *2*(2), 235–248. doi.org/10.1071/sr9640235

Taylor, S. (1964). Trace element abundances and the chondritic Earth model. *Geochimica et Cosmochimica Acta*, *28*(12), 1989–1998. doi.org/10.1016/0016-7037(64)90142-5

Templeton, M., Andrews, R., & Hofmann, R. (2006). Impact of iron particles in groundwater on the UV inactivation of bacteriophages MS2 and T4. *Journal of Applied Microbiology*, *101*(3), 732–741. doi.org/10.1111/j.1365-2672.2006.02980.x

Theis, T. L., & Singer, P. C. (1974). Complexation of iron(II) by organic matter and its effect on iron(II) oxygenation. *Environmental Science & Technology*, *8*(6), 569–573. doi.org/10.1021/es60091a008

Thompson, A., & Goyne, K. W. (2012). Introduction to the Sorption of Chemical Constituents in Soils. *Nature Education Knowledge*, *4*(4), 7. Retrieved from https://www.nature.com/scitable/knowledge/library/introduction-to-the-sorption-of-chemical-constituents-94841002/

Tipping, E., Thompson, D., & Davison, W. (1984). Oxidation products of Mn(II) in lake waters. *Chemical Geology*, *44*(4), 359–383. doi.org/10.1016/0009-2541(84)90149-9

Tronc, E., Belleville, P., Jolivet, J. P., & Livage, J. (1992). Transformation of ferric hydroxide into spinel by iron(II) adsorption. *Langmuir*, *8*(1), 313–319. doi.org/10.1021/la00037a057

Tufekci, N., & Sarikaya, H. Z. (1996). Catalytic effects of high fe(iii) concentrations on Fe (II) oxidation. *Water Science and Technology*, *34*(7–8), 389–396. doi.org/10.1016/s0273-1223(96)00770-6

U.S. EPA. (2006). *Provisional Peer Reviewed Toxicity Values for Iron and Compounds (CASRN 7439–89-6)*. U.S. Environmental Protection Agency. Retrieved from https://cfpub.epa.gov/ncea/pprtv/documents/IronandCompounds.pdf

Van der Bruggen, B. (2014). Freundlich Isotherm. *Encyclopedia of Membranes*, 1–2. doi.org/10.1007/978-3-642-40872-4_254-3

Van Oorschot, I. H. M., & Dekkers, M. J. (2001). Selective dissolution of magnetic iron oxides in the acid-ammonium oxalate/ferrous iron extraction method-I. Synthetic samples. *Geophysical Journal International*, *145*(3), 740–748. doi.org/10.1046/j.0956-540x.2001.01420.x

Villacís García, M., Ugalde Arzate, M., Vaca Escobar, K., Villalobos, M., Zanella, R., & Martínez Villegas, N. (2015). Laboratory synthesis of goethite and ferrihydrite of controlled particle sizes. *Boletín de La Sociedad Geológica Mexicana*, *67*(3), 433–446. doi.org/10.18268/bsgm2015v67n3a7

Vodyanitskii, Y. N., & Savichev, A. T. (2017). The influence of organic matter on soil color using the regression equations of optical parameters in the system CIE- L*a*b*. *Annals of Agrarian Science*, *15*(3), 380–385. doi.org/10.1016/j.aasci.2017.05.023

Vos, K., Vandenberghe, N., & Elsen, J. (2014). Surface textural analysis of quartz grains by scanning electron microscopy (SEM): From sample preparation to environmental

interpretation. *Earth-Science Reviews*, *128*, 93–104. doi.org/10.1016/j.earscirev.2013.10.013

Weber, K. A., Achenbach, L. A., & Coates, J. D. (2006). Microorganisms pumping iron: anaerobic microbial iron oxidation and reduction. *Nature Reviews Microbiology*, *4*(10), 752–764. doi.org/10.1038/nrmicro1490

Weng, H. X., Qin, Y. C., & Chen, X. H. (2007). Elevated iron and manganese concentrations in groundwater derived from the Holocene transgression in the Hang-Jia-Hu Plain, China. *Hydrogeology Journal*, *15*(4), 715–726. doi.org/10.1007/s10040-006-0119-z

White, A. F., & Peterson, M. L. (1990). Role of Reactive-Surface-Area Characterization in Geochemical Kinetic Models. *ACS Symposium Series*, 461–475. doi.org/10.1021/bk-1990-0416.ch035

WHO. (2007). *pH in Drinking-water. Background document for development of WHO Guidelines for Drinking-water Quality* (No. 17). World Health Organization. Retrieved from https://www.who.int

Winograd, I. J., & Robertson, F. N. (1982). Deep Oxygenated Ground Water: Anomaly or Common Occurrence? *Science*, *216*(4551), 1227–1230. doi.org/10.1126/science.216.4551.1227

Wolf, S. F., & Tsai, Y. (2005). Application of ICP-MS and HR-ICP-MS for the characterization of solutions generated from corrosion testing of spent nuclear fuel. *Journal of Radioanalytical and Nuclear Chemistry*, *263*(3), 575–579. doi.org/10.1007/s10967-005-0626-8

Wright, H. B., Mackey, E., Cushing, R., & Tekippe, T. (2002). A comparison of Uv disinfection for drinking water, wastewater, and reclaimed wastewater. *Proceedings of the Water Environment Federation*, *2002*(16), 662–676. doi.org/10.2175/193864702784246973

Yamaguchi, K. S., & Sawyer, D. T. (1985). The Redox Chemistry of Manganese (III) and -(IV) Complexes. *Israel Journal of Chemistry*, *25*(2), 164–176. doi.org/10.1002/ijch.198500026

Zhang, Z., Xiao, C., Adeyeye, O., Yang, W., & Liang, X. (2020). Source and Mobilization Mechanism of Iron, Manganese and Arsenic in Groundwater of Shuangliao City, Northeast China. *Water*, *12*(2), 534. doi.org/10.3390/w12020534

Zhou, X., Liu, D., Bu, H., Deng, L., Liu, H., Yuan, P., Du, P., & Song, H. (2018b). XRD-based quantitative analysis of clay minerals using reference intensity ratios, mineral intensity factors, Rietveld, and full pattern summation methods: A critical review. *Solid Earth Sciences*, *3*(1), 16–29. doi.org/10.1016/j.sesci.2017.12.002

8. Appendices

Appendix I: Table containing the samples' sediment type by percentage with depth. The results were obtained from the Gradistatv8 excel spread sheet, a USGS tool.

	Sample depth (cm)					
	0 - 15	**15 - 40**	**40 - 50**	**50-70**	**70 - 80**	**80 - 100**
% Gravel	1.9%	1.9%	1.2%	3.4%	2.3%	6.0%
% Sand	93.7%	95.3%	95.9%	95.7%	96.8%	93.5%
% Mud	4.4%	2.8%	2.9%	0.8%	0.8%	0.5%
% Very coarse gravel	0.0%	0.0%	0.0%	0.0%	0.0%	0.0%
% Coarse gravel	0.0%	0.0%	0.0%	0.0%	0.0%	0.0%
% Medium gravel	0.0%	0.3%	0.0%	1.7%	0.3%	2.4%
% Fine gravel	0.0%	0.3%	0.3%	0.6%	0.6%	1.5%
% Very fine gravel	1.9%	1.3%	0.9%	1.1%	1.4%	2.1%
% Very coarse sand	7.1%	4.9%	2.7%	3.6%	5.8%	6.3%
% Coarse sand	20.5%	22.6%	21.4%	30.1%	34.0%	36.7%
% Medium sand	29.58%	29.2%	29.8%	38.5%	34.4%	32.6%
% Fine sand	29.33%	32.4%	34.4%	20.7%	19.7%	15.5%
% Very fine sand	7.1%	6.3%	7.6%	3.0%	2.9%	2.4%
% Very coarse silt	0.7%	0.5%	0.5%	0.8%	0.1%	0.1%
% Coarse silt	0.7%	0.5%	0.5%	0.0%	0.1%	0.1%
% Medium silt	0.7%	0.5%	0.5%	0.0%	0.1%	0.1%
% Fine silt	0.7%	0.5%	0.5%	0.0%	0.1%	0.1%
% Very fine silt	0.7%	0.5%	0.5%	0.0%	0.1%	0.1%
% Clay	0.7%	0.5%	0.5%	0.0%	0.1%	0.1%

Appendix II: Table containing the samples grain size analysis. For each sample, the sieving was repeated twice.

Depth (cm)		0 -15		15 - 40		40 - 50		50 - 70		70 -80		80 - 100	
Nbr sieving		1	2	1	2	1	2	1	2	1	2	1	2
Sieve size (µm)	8000	0.00	0.0	1.78	5.02	0.00	0.00	5.68	4.64	0.00	1.38	5.82	8.50
	4000	0.00	0.09	2.17	2.84	1.00	1.08	1.33	2.18	0.57	1.92	4.62	4.16
	2000	3.37	3.97	9.13	10.52	3.52	3.75	3.28	3.49	3.13	2.34	5.87	6.70
	1000	14.68	13.66	33.68	34.78	10.67	10.80	10.06	11.32	11.55	11.43	18.06	19.68
	500	41.39	40.08	156.78	161.45	85.67	84.63	84.63	95.54	66.64	69.04	108.45	111.11
	250	58.97	58.31	202.54	198.53	119.69	117.77	117.42	112.94	68.22	69.10	97.94	97.15
	125	57.21	59.08	224.68	218.99	136.44	137.40	65.04	58.80	40.80	37.60	48.65	44.14
	63	13.69	14.44	43.70	42.71	29.05	31.41	9.15	8.41	6.62	5.11	8.01	6.48
	< 63	8.90	8.61	19.53	20.13	12.09	11.12	2.69	2.50	1.83	1.40	1.83	1.40

Appendix III: Soprtion-1. Table containing the amount of different compound used for the sorption experiments and also the results of the sorption. The concentration of Mn is referred to as [Mn]. [Mn] ICP-Ms represents the raw data of Mn concentrations analyzed by ICP-MS. [Mn] solution and [Mn] sorbed are the concentrations of Mn in solution and sorbed calculated from the raw concentrations. (1), (2) and so on, represents the replicas realized for different samples. The following slash (/) was used to indicate Mn concentrations too high to be detected by ICP-MS. Vol. refers to volume.

Sample	Vol. $NaHCO_3$	Vol. $MnNO_3$	Total volume	Mass sand	Ratio Solid/solute	Blank	[Mn] ICP-MS	[Mn] solution	[Mn] sorbed	RSD
	ml	µl	ml	g	g/ml	µg/l	µg/l	(*10^{-3}) mmol/l	mmol/kg	%
SD10	40	10	40.01	1.0002	0.025	88.30	15.30	0.29	0.05	1.35
SD20	40	20	40.02	1.0003	0.025	117.40	27.50	0.50	0.07	0.29
SD50	40	50	40.05	1.0001	0.025	178.00	51.70	0.94	0.09	0.77
SD80	40	80	40.08	1.0005	0.025	381.50	66.80	1.21	0.23	0.92
SD100	40	100	40.10	1.0003	0.025	689.70	161.40	2.94	0.39	0.37
SD200	40	200	40.20	1.0001	0.025	1218.60	352.80	6.42	0.63	0.43
SD300	40	300	40.30	1.0003	0.025	1660.00	603.00	10.98	0.78	0.58
SD500	40	500	40.50	1.0006	0.025	3001.40	1094.00	19.93	1.41	0.49
SD800	40	800	40.80	1.0001	0.025	4301.80	1799.10	32.77	1.86	0.89
SD1000	40	1000	41.00	2.0004	0.049	5574.50	2369.30	43.16	1.20	1.02
SD2000	40	2000	42.00	2.0003	0.048	10401.60	5104.00	92.97	2.03	0.75
SD5000	40	5000	45.00	2.0003	0.044	26549.60	16570.00	301.82	4.09	0.66
SD10000	40	10000	50.00	2.0003	0.040	45178.60	36042.60	656.51	4.16	0.41
SL10	40	10	40.01	1.0001	0.025	88.30	44.20	0.81	0.03	0.9
SL20	40	20	40.02	1.0002	0.025	117.40	67.60	1.23	0.04	0.9
SL50	40	50	40.05	1.0001	0.025	178.00	83.50	1.52	0.07	0.81
SL80	40	80	40.08	1.0003	0.025	381.50	217.50	3.96	0.12	1.11

SL100	40	100	40.10	1.0003	0.025	689.70	372.40	6.78	0.23	0.8
SL200	40	200	40.20	1.0003	0.025	1218.60	813.00	14.81	0.30	0.32
SL300	40	300	40.30	1.0003	0.025	1660.00	1218.00	22.19	0.32	0.42
SL500	40	500	40.50	1.0003	0.025	3001.40	2124.00	38.69	0.65	0.74
SL800	40	800	40.80	1.0001	0.025	4301.80	3218.90	58.63	0.80	0.85
SL1000	40	1000	41.00	2.0002	0.049	5574.50	3465.50	63.12	0.79	0.52
SL2000	40	2000	42.00	2.0002	0.048	10401.60	7893.60	143.78	0.96	0.21
SL5000	40	5000	45.00	2.0001	0.044	26549.60	17149.90	312.38	3.85	0.47
SL10000	40	10000	50.00	2.0003	0.040	45178.60	39651.20	722.24	2.52	0.91

Appendix IV: Soprtion-2. Table containing the amount of different compound used for the sorption experiments and also the results of the sorption. The concentration of Mn is referred to as [Mn]. [Mn] ICP-Ms represents the raw data of Mn concentrations analyzed by ICP-MS. [Mn] solution and [Mn] sorbed are the concentrations of Mn in solution and sorbed calculated from the raw concentrations. (1), (2) and so on, represents the replicas realized for different samples. The following slash (/) was used to indicate Mn concentrations too high to be detected by ICP-MS. Vol. refers to volume.

Sample	Vol. $NaHCO_3$	Vol. $MnNO_3$	Total volume	Mass sand	Ratio Solid/solute	Blank	[Mn] ICP-MS	[Mn] solution	[Mn] sorbed	RSD
	ml	µl	ml	g	g/ml	µg/l	µg/l	($*10^{-3}$) mmol/l	mmol/kg	%
SD10 (1)	40	10	40.01	1.0002	0.025	6.40	0.97	0.0176	0.0040	1.26
SD10 (2)	40	10	40.01	1.0003	0.025	6.40	1.11	0.0202	0.0039	2.15
SD20 (1)	40	20	40.02	1.0001	0.025	6.37	1.47	0.0269	0.0036	1.42
SD20 (2)	40	20	40.02	1.0004	0.025	6.37	1.49	0.0272	0.0036	1.73
SD50 (1)	40	50	40.05	1.0003	0.025	7.69	2.64	0.0481	0.0037	1.81
SD50 (2)	40	50	40.05	1.0003	0.025	7.69	2.13	0.0389	0.0040	1.43
SD50 (3)	40	50	40.05	1.0003	0.025	7.69	2.07	0.0376	0.0041	1.81
SD50 (4)	40	50	40.05	1.0005	0.025	7.69	2.23	0.0407	0.0040	1.37
SD80 (1)	40	80	40.08	1.0002	0.025	20.51	3.20	0.0583	0.0126	1.42
SD80 (2)	40	80	40.08	1.0001	0.025	20.51	3.59	0.0654	0.0123	0.87
SD100 (1)	40	100	40.10	1.0002	0.025	19.54	3.95	0.0720	0.0114	1.00
SD100 (2)	40	100	40.10	1.0005	0.025	19.54	4.22	0.0768	0.0112	2.17
SD100 (3)	40	100	40.10	1.0002	0.025	19.54	4.57	0.0833	0.0109	0.81
SD100 (4)	40	100	40.10	1.0001	0.025	19.54	4.01	0.0730	0.0113	2.06
SD300	40	300	40.30	1.0002	0.025	50.51	18.35	0.3342	0.0236	1.00
SD500 (2)	40	500	40.50	1.0005	0.025	106.53	38.84	0.7075	0.0499	0.78
SD500 (3)	40	500	40.50	1.0004	0.025	106.53	33.60	0.6121	0.0538	0.68

SD800	40	800	40.80	1.0003	0.025	143.57	60.04	1.0937	0.0621	0.64
SD1000 (1	40	1000	41.00	1.0002	0.024	220.45	70.79	1.2895	0.1117	0.65
SD1000 (2)	40	1000	41.00	1.0004	0.024	220.45	75.00	1.3661	0.1086	1.22
SD2000	40	2000	42.00	1.0003	0.024	420.88	157.95	2.8770	0.2011	0.90
SD5000 (2)	40	5000	45.00	1.0002	0.022	641.15	511.50	9.3169	0.1063	0.15
SD 10000	40	10000	50.00	1.0004	0.020	/	/	/	/	/
SL10	40	10	40.01	1.0001	0.025	5.59	2.80	0.0509	0.0020	0.98
SL20 (1)	40	20	40.02	1.0002	0.025	8.63	4.97	0.0906	0.0027	1.49
SL20 (2)	40	20	40.02	1.0001	0.025	7.08	4.08	0.0743	0.0022	1.49
SL20 (3)	40	20	40.02	1.0004	0.025	5.94	3.42	0.0623	0.0018	1.49
SL20 (4)	40	20	40.02	1.0003	0.025	2.63	1.51	0.0276	0.0008	1.49
SL50	40	50	40.05	1.0003	0.025	9.58	4.50	0.0819	0.0037	1.15
SL80 (1)	40	80	40.08	1.0002	0.025	13.24	7.55	0.1374	0.0042	1.14
SL80	40	80	40.08	1.0001	0.025	11.02	6.28	0.1145	0.0035	1.14
SL80 (3)	40	80	40.08	1.0005	0.025	14.49	8.26	0.1505	0.0045	1.14
SL100 (1)	40	100	40.1	1.0002	0.025	18.84	10.17	0.1852	0.0063	0.62
SL100 (2)	40	100	40.1	1.0005	0.025	19.92	10.76	0.1959	0.0067	0.62
SL100 (3)	40	100	40.1	1.0001	0.025	24.03	12.97	0.2363	0.0081	0.62
SL300	40	300	40.3	1.0004	0.025	60.98	44.74	0.8150	0.0119	0.51
SL500 (2)	40	500	40.5	1.0002	0.025	111.11	78.63	1.4323	0.0240	0.76
SL500 (3)	40	500	40.5	1.0003	0.025	127.35	90.12	1.6415	0.0275	0.64
SL500 (4)	40	500	40.5	1.0002	0.025	116.87	82.71	1.5065	0.0252	0.86
SL800	40	800	40.8	1.0001	0.025	99.18	74.22	1.3518	0.0186	0.20
SL1000 (1)	40	1000	41	1.0003	0.024	307.42	191.12	3.4812	0.0868	0.74
SL1000 (2)	40	1000	41	1.0001	0.024	324.89	201.98	3.6790	0.0918	0.80
SL1000 (3)	40	1000	41	1.0002	0.024	311.94	193.92	3.5323	0.0881	0.50
SL2000	40	2000	42	1.0003	0.024	499.76	379.26	6.9081	0.0922	0.19
SL5000	40	5000	45	1.0001	0.022	/	/	/	/	/
SL10000	40	10000	50	1.002	0.020	/	/	/	/	/

Appendix V: Mn oxidation pH 8-10 for SD sample. Table containing the data related to the oxidation of Mn at high pH levels. [Mn] refers to the concentration of Mn in µg/l for the result given by ICP-MS and in mg/l for the converted concentration. During the experiment the pH was also monitored. The volume remaining in solution represents the volume of solution after extraction of 2 ml to be analysed. B refers to the blank sample. RSD (in %) represents the relative standard deviation.

SD: Mn oxidation pH 8-10

Sample	[Mn]	RSD	[Mn]	pH	Time	remaining volume in solution
	µg/l	%	mg/l	/	Hours	ml
SD0	245.91	2.98	7.77	9.18	0	314
SD1	204.71	0.60	6.47	8.94	1	312
SD2	163.41	1.11	5.16	8.92	2	310
SD3	137.84	1.14	4.36	8.93	3.5	308
SD4	131.54	1.35	4.16	8.93	4.5	306
SD5	90.46	1.22	2.86	9.00	7.5	304
SD6	46.23	1.47	1.46	9.00	22.5	302
SD7	46.56	1.49	1.47	8.99	27	300
SD8	37.40	1.35	1.18	9.09	47	298
SD9	58.83	0.66	1.86	9.04	52	296
B0	304.15	0.72	9.61	9.35	0	314
B1	296.43	0.60	9.37	9.22	1	312
B2	290.86	0.70	9.19	9.15	2	310
B3	286.96	0.51	9.07	9.13	3.5	308
B4	260.55	1.42	8.23	9.11	4.5	306
B5	284.79	0.35	9.00	9.11	7.5	304
B6	292.80	1.14	9.25	9.09	22.5	302
B7	288.37	0.83	9.11	9.10	27	300
B8	267.95	0.76	8.47	9.14	47	298
B9	280.91	1.57	8.88	9.14	52	296

Appendix VI: Mn oxidation pH 8-10 for SL sample. Table containing the data related to the oxidation of Mn at high pH levels. [Mn] refers to the concentration of Mn in µg/l for the result given by ICP-Ms and in mg/l for the converted concentration. During the experiment the pH was also monitored. The volume remaining in solution represents the volume of solution after extraction of 2 ml to be analysed. B refers to the blank sample. RSD (in %) represents the relative standard deviation.

SL: Mn oxidation pH 8-10

Sample	[Mn]	RSD	[Mn]	pH	Time	remaining volume in solution
	µg/l	%	mg/l	/	Hours	ml
SL0	317.98	0.68	10.05	9.29	0	314
SL1	181.57	1.28	5.74	9.15	1	312
SL2	136.70	1.07	4.32	9.11	2	310
SL3	108.77	0.96	3.44	9.11	5	304
SL4	112.88	0.79	3.57	8.98	6	302
SL5	92.58	0.98	2.93	9.08	23	300
SL6	69.46	0.67	2.19	9.08	25.5	298
SL7	71.27	0.60	2.25	9.08	27.5	296
SL8	68.98	0.71	2.18	9.08	28.5	294
SL9	71.95	1.32	2.27	9.07	45	292
B0	299.09	0.82	9.45	9.27	0	314
B1	292.11	0.83	9.23	9.06	1	312
B2	290.66	0.55	9.18	9.12	2	310
B3	291.36	0.63	9.21	9.07	4	306
B4	288.32	0.54	9.11	9.08	5	304
B5	290.15	0.7	9.17	9.08	6	302
B6	289.94	0.52	9.16	9.07	23	300
B7	289.46	0.68	9.15	9.09	25.5	398
B8	286.14	1.20	9.04	9.07	28.5	294
B9	287.41	0.54	9.08	9.07	45	292

Appendix VII: Mn oxidation pH 6-7 for SD sample. Table containing the data related to the oxidation of Mn at low pH levels. [Mn] refers to the concentration of Mn in µg/l for the result given by ICP-Ms and in mg/l for the converted concentration. During the experiment the pH was also monitored. The volume remaining in solution represents the volume of solution after extraction of 2 ml to be analysed. B refers to the blank sample. RSD (in %) represents the relative standard deviation.

SD: Mn oxidation pH 6-7

Sample	[Mn]	RSD	[Mn]	pH	Time	remaining volume in solution
	µg/l	%	mg/l	/	Hours	ml
SD0	311.58	0.52	10.01	6.54	0	319.2
SD1	3.00	36.44	0.10	/	2	317.2
SD2	164.26	0.69	5.28	7.74	5	315.2
SD3	78.83	0.72	2.53	7.9	22	313.2
SD4	70.00	0.29	2.25	8.16	27	311.2
SD5	74.22	0.60	2.38	7.52	50	309.2
SD6	107.11	0.60	3.44	7.96	69	307.2
SD7	74.07	0.46	2.38	7.94	75	305.2
SD8	66.50	0.42	2.14	7.94	93	303.2
SD9	59.04	0.83	1.90	7.96	98	301.2
B0	306.18	0.72	9.83	6.38	0	319.2
B1	295.38	0.72	9.49	6.65	3	317.2
B2	314.07	0.68	10.09	6.93	5	315.2
B3	341.14	0.41	10.96	6.98	22	313.2
B4	354.55	0.43	11.39	7.41	27	311.2
B5	359.89	0.76	11.56	7.14	50	309.2
B6	398.37	0.57	12.80	7.15	69	307.2
B7	396.45	0.59	12.73	7.23	75	305.2
B8	444.23	0.85	14.27	7.31	93	303.2
B9	460.54	0.38	14.79	7.33	98	301.2

Note 1: the SD1 sample was highlighted in yellow because the RSD (%) obtained from ICP-MS analysis was too high, thus this sample was not considered when plotting the graphs.

Note 2: the SD6 sample was highlighted in orange because there was a problem with the internal standard during ICP-MS analysis.

Appendix VIII: Mn oxidation pH 6-7 for SL sample. Table containing the data related to the oxidation of Mn at low pH levels. [Mn] refers to the concentration of Mn in µg/l for the result given by ICP-Ms and in mg/l for the converted concentration. During the experiment the pH was also monitored. The volume remaining in solution represents the volume of solution after extraction of 2 ml to be analysed. B refers to the blank sample. RSD (in %) represents the relative standard deviation.

SL: Mn oxidation pH 6-7

Sample	[Mn]	RSD	[Mn]	pH	Time	remaining volume in solution
	µg/l	%	mg/l	/	Hours	ml
SL0	399.88	0.30	12.84	6.41	0	319.2
SL1 (1)	225.56	0.33	7.25	/	23	317.2
SL1 (2)	229.58	0.61	7.37	/	23	315.2
SL2	22.34	134.9	0.72	64	313.2	313.2
SL3 (1)	166.42	0.51	5.35	7.51	69	311.2
SL3 (2)	165.82	1.21	5.33	7.51	69	309.2
SL4	173.39	0.67	5.57	7.71	74	307.2
SL5	150.49	0.54	4.83	7.77	92	305.2
SL6	111.48	0.21	3.58	7.455	121	303.2
SL7 (1)	117.94	0.40	3.79	7.455	122	301.2
SL7 (2)	119.69	1.00	3.84	7.455	122	299.2
B0	285.72	0.31	9.18	6.34	0	319.2
B1	306.43	0.31	9.84	/	23	317.2
B2	315.58	0.76	10.14	/	64	315.2
B3	326.59	0.40	10.49	7.87	69	313.2
B4	314.68	0.27	10.11	7.94	74	311.2
B5	309.70	1.03	9.95	7.835	92	309.2
B6	344.93	0.67	11.08	8.1	121	307.2

Note 1: the SL2 sample was highlighted in orange because of the high uncertainty due to a problem with the internal standard during ICP-MS analysis.

Appendix VIIII: PHREEQC code for Mn sorption with Freundlich isotherm.

```
SURFACE_MASTER_SPECIES
   Freundlich    Freundlich

SURFACE_SPECIES
Freundlich = Freundlich
Freundlich + 0.95 Mn+2 = FreundlichMn+2
    log_k     -87.90
   -no_check

   -mole_balance FreundlichMn+2

SURFACE 1
   Freundlich    1e+100  1  1
SOLUTION 1
   temp      25
   pH        8
   units     mol/l
   density   1
   C(4)      0.01 as HCO3-
   Na        0.01
   -water    1 # kg


REACTION 1
   MnNO3     1.0 # 0.0018    0.81  logk 83.93
   0.18 millimoles in 15 steps


SELECTED_OUTPUT 1
   -file               selected_output_1.xls
   -reset              false
   -solution           true
   -molalities     Mn+2    FreundlichMn+2

User_Graph
-headings Freundlich
     -chart_title "Sorption Isotherm"
     -axis_titles "Dissolved Mn,mmol/l" \
                  "Sorbed Mn, mmol/Kg"
  -start
10 x = TOTMOLE("Mn(2)")*1e3
#20 Y = MOL("Mn(+2)")*1e3
20 PLOT_XY x, MOL("FreundlichMn+2")*1e3
  -end
END
```

Appendix X: PHREEQC code for Mn surface complexation.

```
PRINT
       -reset false
       -user_print true
SURFACE_MASTER_SPECIES
# Monodentate 60%
  H_a  H_aH;  H_b  H_bH;  H_c  H_cH;  H_d  H_dH
  H_e  H_eH;  H_f  H_fH;  H_g  H_gH;  H_h  H_hH
# Bidentate 40%
  H_ab H_abH2;  H_ad H_adH2;  H_af H_afH2;  H_ah H_ahH2
  H_bc H_bcH2;  H_be H_beH2;  H_bg H_bgH2;  H_cd H_cdH2
  H_cf H_cfH2;  H_ch H_chH2;  H_de H_deH2;  H_dg H_dgH2
SURFACE_SPECIES
  H_aH = H_aH; log_k 0;  H_bH = H_bH; log_k 0;  H_cH = H_cH; log_k 0;  \
      H_dH = H_dH; log_k 0;
  H_eH = H_eH; log_k 0;  H_fH = H_fH; log_k 0;  H_gH = H_gH; log_k 0;  \
      H_hH = H_hH; log_k 0;

  H_abH2 = H_abH2; log_k 0;  H_adH2 = H_adH2; log_k 0;  H_afH2 = H_afH2; log_k 0;
  H_ahH2 = H_ahH2; log_k 0;  H_bcH2 = H_bcH2; log_k 0;  H_beH2 = H_beH2; log_k 0;
  H_bgH2 = H_bgH2; log_k 0;  H_cdH2 = H_cdH2; log_k 0;  H_cfH2 = H_cfH2; log_k 0;
  H_chH2 = H_chH2; log_k 0;  H_deH2 = H_deH2; log_k 0;  H_dgH2 = H_dgH2; log_k 0;
# Protons
  H_aH = H_a- + H+; log_k  -1.59
  H_bH = H_b- + H+; log_k  -2.70
  H_cH = H_c- + H+; log_k  -3.82
  H_dH = H_d- + H+; log_k  -4.93

  H_eH = H_e- + H+; log_k  -6.88
  H_fH = H_f- + H+; log_k  -8.72
  H_gH = H_g- + H+; log_k  -10.56
  H_hH = H_h- + H+; log_k  -12.40

  H_abH2 = H_abH- + H+; log_k -1.59;  H_abH- = H_ab-2 + H+; log_k -2.70
  H_adH2 = H_adH- + H+; log_k -1.59;  H_adH- = H_ad-2 + H+; log_k -4.93
  H_afH2 = H_afH- + H+; log_k -1.59;  H_afH- = H_af-2 + H+; log_k -8.72
  H_ahH2 = H_ahH- + H+; log_k -1.59;  H_ahH- = H_ah-2 + H+; log_k -12.40
  H_bcH2 = H_bcH- + H+; log_k -2.70;  H_bcH- = H_bc-2 + H+; log_k -3.82
  H_beH2 = H_beH- + H+; log_k -2.70;  H_beH- = H_be-2 + H+; log_k -6.88
  H_bgH2 = H_bgH- + H+; log_k -2.70;  H_bgH- = H_bg-2 + H+; log_k -10.56
  H_cdH2 = H_cdH- + H+; log_k -3.82;  H_cdH- = H_cd-2 + H+; log_k -4.93
  H_cfH2 = H_cfH- + H+; log_k -3.82;  H_cfH- = H_cf-2 + H+; log_k -8.72
  H_chH2 = H_chH- + H+; log_k -3.82;  H_chH- = H_ch-2 + H+; log_k -12.40
  H_deH2 = H_deH- + H+; log_k -4.93;  H_deH- = H_de-2 + H+; log_k -6.88
  H_dgH2 = H_dgH- + H+; log_k -4.93;  H_dgH- = H_dg-2 + H+; log_k -10.56

# Manganese
  H_aH + Mn+2 = H_aMn+ + H+; log_k  -1.7
  H_bH + Mn+2 = H_bMn+ + H+; log_k  -1.7
```

```
  H_cH + Mn+2 = H_cMn+ + H+; log_k  -1.7
  H_dH + Mn+2 = H_dMn+ + H+; log_k  -1.7

  H_eH + Mn+2 = H_eMn+ + H+; log_k  -4.91
  H_fH + Mn+2 = H_fMn+ + H+; log_k  -4.91
  H_gH + Mn+2 = H_gMn+ + H+; log_k  -4.91
  H_hH + Mn+2 = H_hMn+ + H+; log_k  -4.91

  H_abH2 + Mn+2 = H_abMn + 2H+; log_k -3.4
  H_adH2 + Mn+2 = H_adMn + 2H+; log_k -3.4
  H_afH2 + Mn+2 = H_afMn + 2H+; log_k -6.61
  H_ahH2 + Mn+2 = H_ahMn + 2H+; log_k -6.61
  H_bcH2 + Mn+2 = H_bcMn + 2H+; log_k -3.4
  H_beH2 + Mn+2 = H_beMn + 2H+; log_k -6.61
  H_bgH2 + Mn+2 = H_bgMn + 2H+; log_k -6.61
  H_cdH2 + Mn+2 = H_cdMn + 2H+; log_k -3.4
  H_cfH2 + Mn+2 = H_cfMn + 2H+; log_k -6.61
  H_chH2 + Mn+2 = H_chMn + 2H+; log_k -6.61
  H_deH2 + Mn+2 = H_deMn + 2H+; log_k -6.61
  H_dgH2 + Mn+2 = H_dgMn + 2H+; log_k -6.61
END

SURFACE 1
  H_a  2.48e-06 46.5e3 3.50e-03
  H_b  2.48e-06; H_c  2.48e-06; H_d  2.48e-06

# charge on 4 nHB sites: 0.5 * charge on nHA sites
  H_e  1.24e-06; H_f  1.24e-06; H_g  1.24e-06; H_h  1.24e-06

# charge on 12 diprotic sites: -2.84 / 12 * 3.5e-3 / 1e3
  H_ab 8.28e-07; H_ad 8.28e-07; H_af 8.28e-07; H_ah 8.28e-07
  H_bc 8.28e-07; H_be 8.28e-07; H_bg 8.28e-07; H_cd 8.28e-07
  H_cf 8.28e-07; H_ch 8.28e-07; H_de 8.28e-07; H_dg 8.28e-07
       -Donnan

 Hfo_w 2e-5 600 1
 Hfo_s 2e-4
       -equilibrate 1

SOLUTION 1
  temp        25
  pH          8.0
  Na          0.01
  C(+4)       0.01    as HCO3-
  units       mol/l
  density     1


REACTION 1
  MnNO3   0.0018
```

```
  1.8 millimoles   in 30

USER_GRAPH Example 19
        -headings Mn_HumicAcids Mn_Hfo TOTAL
        -chart_title "Deterministic Sorption Model"
        -axis_titles "Dissolved Mn, in micrograms per kilogram water" \
                     "Sorbed Mn, in micrograms per gram soil"
        -initial_solutions true
  -start
10 H_Mn = SURF("Mn", "Hfo") + EDL("Mn", "Hfo")
20 print CHR$(10) + " ug Mn/L =", tot("Mn") * 54.9e6, " ug Mn/g = ", H_Mn * 54.9e6 \
        ," Kd (L/kg) = ", H_Mn*1e3/tot("Mn"), " ug Mn/g in DL =", \
        EDL("Mn", "H") * 54.9e6
50 print "Surface charge      =", EDL("Charge", "Hfo")
55 af_OM = 1 / 9
80 x = TOT("Mn") * 54.9e6
90 H_Mn = H_Mn * 54.9e6 * af_OM
110 Hfo_Mn = (mol("Hfo_wOMn+") + mol("Hfo_sOMn+")) * 54.9e6
120 PLOT_XY x, H_Mn, color = Green, line_width = 2, symbol = None
140 PLOT_XY x, Hfo_Mn, color = Black, line_width = 2, symbol = None
150 PLOT_XY x, H_Mn + Hfo_Mn, color = Red, line_width = 2, symbol = None
  -end

selected_output
        #-reset              true
        -file mohfo.xls
        -selected_out   true
        -user_punch     true
        -molalities     Mn+2    Hfo_wOMn+   Hfo_sOMn+
        -totals         H_Mn  Hfo_Mn
        -reaction       true
        #-activities     H_Mn  Hfo_Mn
        -state          true
        -solution       true
END
```

Appendix XI: PHREEQC code for Mn oxidation

```
SOLUTION_MASTER_SPECIES
Mn_di            Mn_di+2    0.0     Mn_di           54.92

SOLUTION_SPECIES
Mn_di+2 = Mn_di+2
       log_k   0.0

Mn_di+2 + H2O = Mn_diOH+ + H+
       log_k   -10.590
       delta_h 14.00   kcal


SURFACE_SPECIES 1
    Hfo_sOH + Mn+2 = Hfo_sOMn+ + H+
    log_k -0.4
    Hfo_wOH + Mn+2 = Hfo_wOMn+ + H+
    log_k -3.5

SURFACE 1

   Hfo_sOH 5e-4 600 7.5
   Hfo_wOH 2e-3


SOLUTION 1
       pH     6.28
       units       mol/l
       O(0)  1 O2(g) -0.67
       Mn_di  0.000055
       Na  0.01
       C(+4)     0.01 as HCO3-

EQUILIBRIUM_PHASES 1
       O2(g)          -0.67



Rates
Mn_di_ox
  -start
  10 Mn_di = TOT("Mn_di")
  20 if (Mn_di <= 0) then goto 200
```

```
 30  p_o2 = SR("O2(g)")
 40  rate = (0.2 + 1.35 *(ACT("OH-"))^2 * p_O2)*Mn_di
 50  moles = rate * Time
 60  PRINT moles, (0.19 + 1.35 *(ACT("OH-"))^2 * p_O2)* Mn_di* Time
 200 SAVE moles
 -end

KINETICS 1
Mn_di_ox
   -formula  Mn_diO2  -1.0
   -steps     0 1 2 3 4 5 10 20 30 40 50 60 70 80 90 100 120 130

SELECTED_OUTPUT
       -file newoxidation.xls
       -reset false
       -time  true
       -pH true
       -totals Mn_di
       -molalities  Hfo_wOMn+   Hfo_sOMn+
       -user_punch  true


USER_GRAPH

       -headings _time_ Mn(2)           pH
       -chart_title "Oxidation of Manganese"
       -axis_titles "Time, in hours" "Millimole per kilogram water" "pH"

 -start
 10  H_Mn = SURF("Mn", "Hfo") + EDL("Mn", "Hfo")
 20  Hfo_Mn = (mol("Hfo_wOMn+") + mol("Hfo_sOMn+")) * 54.92e6
 30 GRAPH_X TOTAL_TIME
 50 GRAPH_Y TOT("Mn_di")*178.95*1000
 70 GRAPH_SY -LA("H+")
 -end
END
```